To

My Wife

XIANG

THEORY OF SATURABLE ABSORBER LASER MODE-LOCKING

THEORY OF SATURABLE ABSORBER LASER MODE-LOCKING

by

TUAN-KAY LIM, B.Sc.

A Thesis

Submitted to the School of Graduate Studies

In Partial Fulfilment of the Requirements

for the Degree

Doctor of Philosophy

McMaster University

September 1974

DOCTOR OF PHILOSOPHY
(Physics)

McMASTER UNIVERSITY
Hamilton, Ontario

TITLE: Theory of Saturable Absorber Laser Mode-Locking

AUTHOR: Tuan-Kay Lim, B.Sc. (Nanyang University)

SUPERVISOR: Professor B. K. Garside

NUMBER OF PAGES: xi, 217

SCOPE AND CONTENTS:

The major purpose of the work described in this thesis is the development of a theoretical model for the mode-locked continuous (CW) and quasi-continuous lasers using a suitable saturable absorber, and the direct testing of the applicability of this model to some important systems.

In essence, the development of the theoretical model consists of three parts. First, the dynamical equations governing the laser operation are derived employing a semi-classical approach, where both the gain and the absorber media are treated in the density matrix formalism and propagation of the electromagnetic radiation is governed by Maxwell's equations. Second, the possibility of achieving mode-locking is investigated by examining the stability of the time-invariant solutions of the dynamical equations against small perturbations. Finally, a finite difference approximation is employed as a means of solving the laser dynamical equations so that steady-state pulses (SSP) can be generated within the mode-locking regime.

A systematic study of the general behaviour of CW mode-locked lasers is undertaken. Such an investigation helps to provide an overall understanding of the physical mechanisms controlling the mode-locking process. In particular, the atomic coherence effects of the interactions between the radiation field and the active media are studied. Furthermore, the general procedure and techniques employed for the numerical analysis form the basic mathematical tool for handling specific systems.

The behaviour of mode-locked CW and flashlamp-pumped (FLP) dye lasers is investigated. It is verified directly that picosecond pulses can be generated from a CW dye laser with an absorber whose recovery time is several hundred picoseconds. Further, it is shown that under typical experimental conditions, the FLP dye lasers can be operated in the quasi-continuous regime where the output pulses are close to being SSP. Numerical results concerning the build-up process of the SSP are in good agreement with experimental observations.

As an integral part of our work, the interrelation between mode-locking and relaxation oscillations (passive Q-switching) is also discussed. It is shown that the passive Q-switching instability solutions follow as a special case of the analysis employed for saturable absorber mode-locking. The impact of the presence of passive Q-switching instabilities on the prediction of mode-locking instability regions is investigated.

As a particular result of a study of the transition from a mode-locked to a passive Q-switched regime, it is suggested that relaxation oscillations from FLP dye lasers and mode-locking in suitable semiconductor lasers may be obtainable.

Finally, a number of suggestions on further research are proposed.

ACKNOWLEDGMENTS

I am particularly grateful to my thesis supervisor, Dr. B. K. Garside for his helpful guidance and constant encouragement in this work. The financial support from McMaster University and the National Research Council and Defence Research Board of Canada is also acknowledged. Finally, to Mrs. H. Kennelly of the Physics Department go my sincere thanks for her excellent typing of the manuscript.

TABLE OF CONTENTS

LIST OF FIGURES

LIST OF TABLES

CHAPTER 1

INTRODUCTION

1.1 HISTORICAL REVIEW:

Generally speaking, a laser which is forced, in one way or another, to maintain a constant frequency spacing of the oscillating modes and to have well-defined relative mode phases is said to be "phase-locked" or "mode-locked". One of the novel properties of a mode-locked laser is that a frequency modulated (FM) laser oscillation with constant intensity in time or a strongly amplitude modulated (AM) output consisting of a regularly spaced train of pulses can be produced, in contrast with the output from a free-running (unmode-locked) laser which fluctuates in an irregular manner. Therefore, the output of a mode-locked laser is, in a sense, more coherent.

Since the first papers published in 1964 and early 1965, the subject of laser mode-locking has been one of the most active fields in laser research. In the past ten years, numerous experiments have been performed employing different laser materials and various mode-locking techniques. In the meantime, different theoretical approaches aimed towards an understanding of the mechanisms in the mode-locking process have also been undertaken with some success. Recently, several review articles have appeared[1-7] containing extensive and systematic surveys on this subject.

In the present work, we do not attempt to give an extensive and chronological review on the whole subject of laser mode-locking. Rather, in this section, a brief discussion is given concerning the basic principles of the different techniques in achieving mode-locking and the theoretical approaches which have been applied so far. Emphasis will be put on the topic of saturable absorber mode-locking with which this thesis is particularly concerned.

1.1.1 Basic Idea of Laser Mode-Locking

A typical laser consists of an optical resonator formed by two coaxial mirrors with a laser gain medium inside the resonator. It is well known[8] that in general such a laser resonator can support a variety of laser modes some of which may have different field distributions normal to the resonator axis (transverse modes). Each of these transverse modes has an infinite set of eigenfrequencies (longitudinal modes) separated in frequency by an amount c/2L where L is the optical length of the resonator and c is the speed of light. Practically, the frequency band over which laser oscillation can occur is determined by the frequency region over which the gain of the laser medium exceeds the resonator losses. Very often, there are many resonator modes which fall within this oscillation band, and the laser output consists of radiation at a number of closely spaced frequencies*. The total output of such a laser as a function of time depends on the amplitudes, frequencies and relative phases of all the

*The frequencies of the oscillating modes appear to be closely spaced, since the total oscillating bandwith is usually very narrow compared with the optical frequency of the laser light.

oscillating modes. If there is nothing which fixes these parameters, random fluctuations and nonlinear effects in the laser medium will cause them to change with time, and the output will vary in an uncontrolled way, even though the average power may remain relatively constant. On the other hand, if the oscillating modes are somehow forced to maintain equal frequency spacing with a fixed phase relationship to each other, the output will be a well-defined function of time and the laser is said to be "phase-locked". The form of the output depends on which modes are oscillating and what phase relationship is maintained. For example, for a laser operated in a single longitudinal mode, but with a set of simultaneously oscillating transverse modes, it is possible to obtain a spatially scanning laser beam, or a "machine-gun" output where pulses of light appear periodically at different spatial positions on the laser output mirror ("transverse mode-locking")[1,2]. More often, the laser resonator can be apertured in such a way as to discriminate against all transverse modes except the lowest order (the fundamental TEM_{oo}) mode which has a simple Gaussian profile. For such a single-transverse-mode* laser, it is possible to fix the amplitudes and phases of the oscillating longitudinal modes ("longitudinal mode-locking") to obtain, on the one hand, a frequency modulated (FM) laser oscillation with output intensity being constant in time, or on the other a strongly amplitude modulated output consisting of a regularly spaced train of pulses, as shown schematically in Fig. 1-1. It has been demonstrated[9]

*In theory, a set of longitudinal modes having any transverse mode distribution may be mode-locked although the fundamental

Fig. 1-1(a) A Typical laser system. M_1, M_2: reflecting mirrors. Amplifier: gain medium. L: resonator length. Cavity round trip time $T_{RT} = 2L/c$.

(b) The resonator axial (longitudinal) modes with frequency spacing $c/2L$ between adjacent modes.

(c) and (d): Output of a free running laser.

(c): Intensity as a function of time. I_m = average intensity. (d): Oscillating modes. ν_o is the center frequency, $\Delta\nu$ is the oscillation bandwidth.

(e) and (f): Pulsing output of a mode-locked laser.

(e): A train of pulses separated by $T_{RT} = 2L/c$. $I_p \approx NI_m$, $\tau_p \approx T_{RT}/N$ where N is the number of oscillating modes. (f): Frequency spectrum.

(g) and (h): FM output of a mode-locked laser.

(g): Intensity is a constant in time. $I_{FM} \approx I_m$.

(h): Frequency spectrum: the oscillating modes have nearly Bessel function amplitudes.

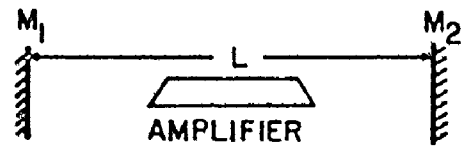
M1
M2
L
AMPLIFIER

(a)

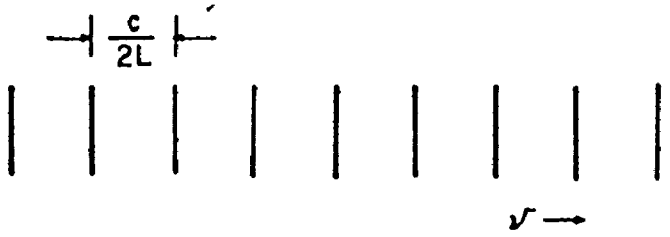
c
2L
ν

(b)

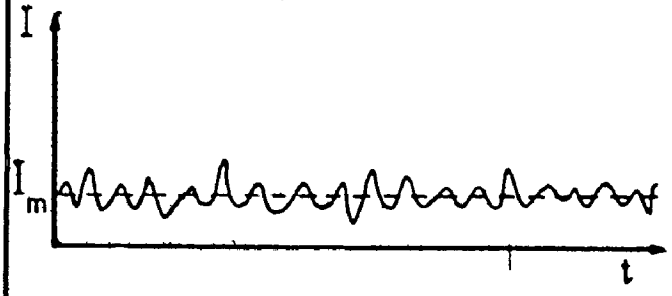
I
Im
t

(c)

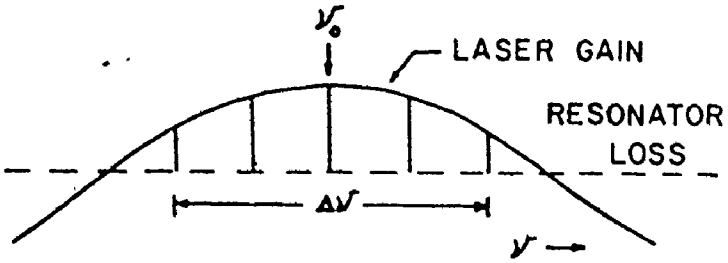
ν0
LASER GAIN
RESONATOR
LOSS
Δν
ν

(d)

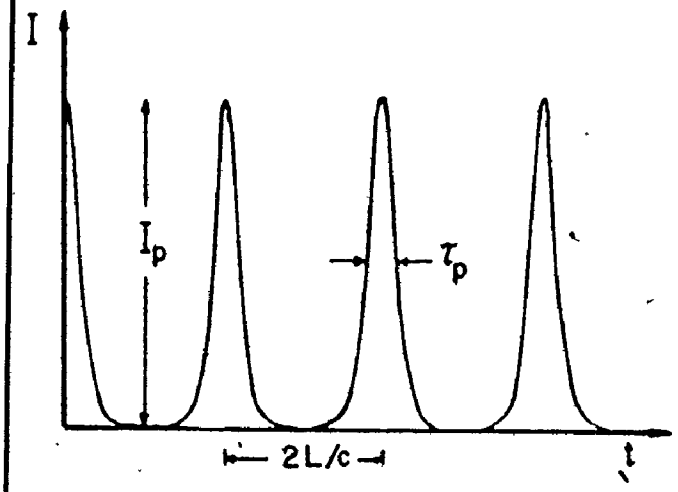
I
Ip
τp
2L/c
t

(e)


ν0
ν

(f)

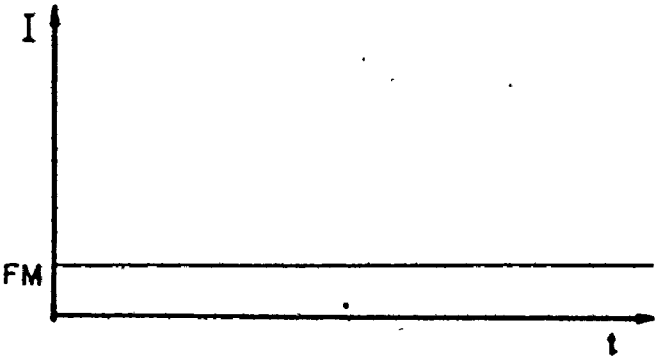
I
FM
t

(g)

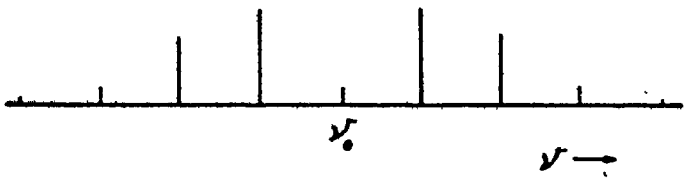
ν0
ν

(h)

that with an internal phase modulator, both types of mode-locked output can be produced depending on the relative magnitudes of the strength of the phase perturbation, the frequency difference between the driving frequency of the modulator and the axial mode interval (known as "detuning")[9], and the atomic gains, cavity losses and reactive mode pulling effects. For large perturbation strength and certain range of detuning, FM laser oscillation may be obtained. Alternatively, very small detuning and lower perturbation strengths may yield a time domain pulsing behaviour which is very similar to that obtained by means of internal loss perturbation, except the presence of a uniform shift of all modes from their free-running frequencies in the case of phase modulation. In what follows, the term "mode-locking" will always mean longitudinal mode-locking and in particular that type of mode-locking with pulsed output since longitudinal mode-locking is of much practical importance and we are dealing with saturable absorber mode-locking which can only produce pulsed output.

1.1.2 Experimental Techniques of Mode-Locking

We now discuss briefly the ways by which laser mode-locking can be achieved experimentally.

A. Self-locking:

Under certain conditions, the nonlinearity of the interaction between the laser medium and the laser radiation within the resonator may be such that a fixed relationship is produced between the oscillating modes. When this phenomenon occurs in the absence of any other mode-locking element, the laser is said

to be self-locked*. It has been shown that many laser systems can be made to self-lock[1,2]. However, some researchers believe that only partial self-locking occurs for many solid-state lasers[10-12]. On the other hand, there is no doubt that reliable self-locking can be obtained with gas lasers, notably the 6328 Å He-Ne laser where both single- and multiple-pulse operations of up to six output pulses in one round-trip period have been reported[13-17]. It is found that to achieve self-locking, the laser must be operated close to threshold; laser oscillation should be confined to a single transverse mode and the recovery time of the gain medium must be less than or of the order of the cavity round-trip time.

Apparently, self-locking is the simplest way in achieving mode-locking since no additional element other than the laser resonator and the gain medium is needed. However, in general, it is not possible to predict the exact conditions for self-locking, and very often the output of a self-locked laser is unstable. Because of the somewhat uncertain nature of self-locking, it is often necessary to introduce an external driving force or an additional nonlinear element to achieve good mode-locking. Some of the important techniques are described below.

*Note that this term has also been used by some authors to mean mode-locking with a saturable absorber. In this thesis, we will take it to describe mode-locking solely due to the laser medium itself.

B. Active Mode-locking:

Proper mode coupling can be achieved by inserting into the laser resonator a device for periodic modulation of either the loss (amplitude or loss modulation) or the refractive index (phase modulation) of the cavity. The method is called active mode-locking because the modulator is driven by a source independent of the laser. It is also known as internal modulation mode-locking since the modulator is placed inside the laser resonator. Usually, the modulator is driven at a frequency which is equal to, or integrally related with, the longitudinal mode-spacing frequency (c/2L) of the laser resonator.

Since the first demonstration on the active mode-locking of a 6328 Å He-Ne laser was reported in 1964[18], numerous experiments have been performed with different laser systems using either acoustic or electro-optic loss modulators to produce output pulses and using electro-optic phase modulators to produce FM or pulsing operation[1,19]. It has also been observed that there is a dramatic reduction of the low-frequency noise in the laser output when the laser is mode-locked[20,21].

A chief disadvantage of the internal modulation technique is that extreme stability of the driving frequency with respect to the resonator length is required. It has been pointed out[6] that due to this stability requirement, active mode-locking is not a promising approach to the generation of picosecond pulses in any type of laser, including the CW dye laser which has an

oscillating bandwidth of $\Delta\nu \sim 10^{13}$ Hz. In fact, the width of the output pulses from an actively mode-locked CW dye laser has never been shorter than 50 psec, although the limiting pulse width calculated from the Fourier uncertainty formula ($\Delta t \sim \Delta\nu^{-1}$) indicates that it is potentially possible to obtain subpicosecond pulses. Furthermore, active mode-locking of this laser was found to be incomplete and unstable[22,23].

C. Saturable Absorber Mode-locking

The most widely employed technique for inducing short-pulse mode-locking involves the use of a saturable absorber inside a laser cavity. A saturable absorber is a material whose absorption decreases as the incident light intensity is increased because the lower level of the absorber is partially depleted if the power density of the incident light is sufficiently high. Thus, a short, high-peak-power pulse will experience less loss in passing through the absorber than a long, less intense pulse of the same energy. In this context, a saturable absorber may be viewed as a loss modulation element although the actual mechanisms are much more complicated. In fact, when a saturable absorber is employed in the mode-locking process, the resulting modulation will be a function of both the pulse shape and the pulse energy. Furthermore, the way in which the absorber and the gain medium saturate, relative to each other, is also very important. In a system where the gain saturates too easily, high powers are discriminated against and the saturable absorber is less operative. As another requirement for achieving mode-

locking, it is found that the recovery time of the absorber should be shorter than the cavity round-trip time, otherwise the induced depth of modulation will be greatly reduced.

The technique of mode-locking with a saturable absorber has been applied to different laser systems, ranging from the solid-state and gas lasers to flashlamp-pumped and CW dye lasers. With the CW dye lasers,a continuous train of mode-locked pulses as short as 1.5 psec has been observed[24,25]. Up to date, this is the only technique with which a stable and continuous train of picosecond pulses can be produced from mode-locked lasers. In addition, this technique has proved to be the most useful and reliable one since it has a number of advantages over other methods. The more important ones are given below.

First, compared with self-locking where, besides the laser cavity, only the property of the gain medium can be varied whereas the present technique allows a variety of combinations between the gain medium and the saturable absorber. A suitable absorber can usually be found for any laser gain medium, given time and effort. It is by this method that many mode-locked lasers have been invented[1-3,5,7]. Second, for saturable absorber mode-locking, no external driving force is required so that the stability problem, which occurs in active mode-locking with the driving frequency, does not arise. As a very important consequence, stable and continuous train of picosecond pulses can be generated from a mode-locked CW dye laser over a long period of time[24].

D. Other Mode-locking Techniques

There are several other methods for producing mode-locking[1,2]. An important one is the technique of gain modulation, i.e. by pumping the laser which is to be mode-locked by the output of another mode-locked laser. Although this method is not of much use for most laser systems, it can be particularly suited for dye lasers which are usually optically pumped and have very broad absorption bands. To attain mode-locking, it is necessary to adjust the length of the dye laser resonator to be integrally related to that of the pumping laser which is often a mode-locked solid-state laser. The resulting pulses from such a dye laser can be as short as, or even shorter than, the pumping pulses.

1.1.3 Theoretical Approaches to Mode-locking:

In parallel with the development of experimental techniques, a great deal of work has also been done on the theory of laser mode-locking. Typically, either the "frequency domain" or the "time domain" approach is used. These two types of analysis are actually equivalent, although apparently different in the ways of interpreting the mode-locking phenomenon. Basically, this is a natural consequence arising from the two different points of view that can be taken in describing the oscillating fields inside the laser cavity. From the frequency viewpoint, the laser fields consist of a number of discrete longitudinal (axial) mode frequencies spaced approximately by the axial mode interval c/2L, each mode oscillating more or less

independently of the others in the absence of a modulating element. On the other hand, from a time domain viewpoint, the fields consist of some internal energy distribution which circulates around inside the cavity with a repetition period equal to the round-trip transit time $\sim 2L/c$. The fields lose energy due to output coupling and gain energy due to laser amplification on each round trip. According to these two approaches, a qualitative picture of how mode-locking is brought about can be given in the following ways.

In the frequency domain, modulation internal to the laser at the frequency c/2L (or a harmonic), either by an external field or by the nonlinear response of the gain and/or loss media to the beat between two modes, creates frequency sidebands on either side of each oscillating mode. These sidebands coincide approximately in frequency with the adjacent axial modes and hence can couple these modes together ("injection locking effects")[6] in a well-defined phase and frequency relationship. The phenomenon of mode-locking is thus accomplished if the coupling between the axial modes is sufficiently strong to overcome the mode pulling effects among the original oscillating modes. Alternatively, in the time domain, an intracavity modulating element, with its modulation period equal to the round-trip time 2L/c, can reshape the internal circulating field distribution repeatedly on each successive round trip inside the cavity. The resulting modulation effects can thus be accumulated over many passes so as to be much stronger than

the single-pass modulation strength of the intracavity modulator and mode-locking can therefore be achieved.

In principle, both the frequency and time domain approaches can be applied to the analysis of the mode-locking phenomenon. However, it has been found that, in practice, the frequency domain analysis can only be carried through for those laser systems which oscillate at a few axial modes. For example, in the theory of self-locking, only the case of three-mode oscillation at low power levels has been analysed in detail[26,27], using the formulation of combination tones (i.e. the radiation produced by the nonlinear interaction of two or more laser modes with the laser medium). It is not easy to extend such an analysis to the case of many oscillating modes since the equations involved will be very complicated and very difficult to solve. Similarly, in the frequency domain analysis of active mode-locking, although formal results can be obtained, in general, the resulting formulas must be solved by computer for the particular case of interest, and only the problem of a few oscillating modes can be handled[9,28].

Due to the complexity of the frequency domain analysis, the time domain approach has been attempted with some fruitful results. It has also been found that it is easier to work in the time domain. In self-locking, a first attempt at this type of analysis was made by Fox and Smith[29] by investigating the response of the gain medium to a train of pulses of stimulating radiation. Assuming a two-level system, they showed that under

certain rather restrictive conditions one would expect the pulses to invert the initial population difference between the laser levels completely - from the situation that all the atoms are in the upper level to the other extreme case that they are all in the lower level. It is evident that such a pulse (called a π or 180° pulse*) interacts most efficiently with the atomic gain system, in a sense that maximum power is given to the incident field. Experimentally, it has been shown that certain lasers indeed behave such that the self-locking pulses in the laser resonator approximate π pulses for the laser medium[13,29].

Other theoretical models for self-pulsing lasers have been established by a number of authors[31,32], employing a ring cavity configuration and assuming a homogeneously broadened

---

*The area of a propagating pulse through an active medium is defined as[30]

$$\theta = \int_{\text{pulse}} \frac{\mu E}{\hbar} \, dt$$

where μ is the electric dipole moment of the individual active atoms, E is the electric field amplitude of the pulse at local time t and $\hbar = h/2\pi$ is the reduced Planck's constant. Accordingly, the value of θ is a measure for the strength of interactions between the radiation field and the active atoms. In particular, a pulse is called a "$n\pi$ pulse" if $\theta = n\pi$, where $n = 0,1,2,\ldots\ldots$.

gain line. The gain medium and cavity losses are treated as uniformly distributed throughout the cavity in one model[31], while discrete components are accounted for in the other[32]. In both models, equations for the determination of self-locking conditions are derived from a perturbation analysis of the CW operation. Unfortunately, an expression for the pulse width cannot be obtained since the steady-state pulses can only be generated by numerical method and for specific cases. The computed pulse velocity turns out to be greater than the velocity of light c, a result which is contrary to that observed in He-Ne lasers[33,34]. However, it might be expected that these models may generate results in accord with experiments on other types of lasers, since the assumption of a homogeneously broadened gain medium is not strictly applicable to a He-Ne laser.

For active mode-locking, Kuizenga and Siegman[6,35,36] have recently developed a theory of internal phase and loss modulated lasers, assuming that the laser medium is homogeneously broadened. In both cases, it is assumed that a single mode-locked laser pulse has a Gaussian envelope (and hence a Gaussian frequency spectrum). By investigating the response of the gain medium and the modulator to this propagating pulse, and imposing the condition that in the steady-state the pulse shape should be unchanged after a complete round trip around the cavity, expressions for the pulse width are obtained in a closed form. It is shown that the pulse width is wider than that ex-

pected from the bandwidth of the gain medium, and for modulation frequencies much less than the gain bandwidth, as typical for solid-state lasers or dye lasers, the width of the mode-locked pulses will be considerably greater than the Fourier-transform limited pulse width. In addition, the different mechanisms involved in AM and FM mode-locking are also pointed out. For example, although AM and FM modulators produce the same mode-locked pulsewidth in the steady-state, the FM case arrives at this limit only by an indirect process which requires a finite laser linewidth to cause the generation of any pulse at all. This difference will become very important in the transient mode-locking of repetitively Q-switched Nd:YAG lasers and pulsed TEA CO_2 lasers, and also in the mode-locking process of extremely wide linewidth lasers such as the CW dye lasers. Predictions concerning the mode-locked pulsewidth and the differences in FM and AM mode-locking techniques have been extensively verified by experiments on mode-locked Nd:YAG lasers[37,38], on high-pressure CO_2 lasers[39] and on a number of other laser systems. For CW dye lasers[22], however, the observed pulsewidth (~100 psec) appears to be longer than that predicted by theory. The reason for this discrepancy is still not clear. Therefore, a better understanding for the dynamical behaviour of the dye laser gain is required.

Having reviewed the theoretical approaches of self-locking and active mode-locking, let us now turn to the case of saturable absorber mode-locking.

Discussions of the mode-locking of lasers produced by suitable saturable absorbers have been directed, in the main, towards two basically distinct situations. On the one hand, there is the mode-locking (subsequently referred to as Type II mode-locking) of Nd:glass, ruby or other similar giant-pulse laser systems. In this case, the saturable absorber acts in such a way as to select an intensity peak from the initial noise distributions during the growth of the giant pulse. In general, the mode-locked pulse length is limited to times no shorter than the recovery time of the absorber, and the dynamics of laser gain do not play a major role in the pulse development process. On the other hand, there is the mode-locking of CW (or quasi-CW) laser systems employing saturable absorbers. For this situation, both the gain and the absorber dynamics play an important role in the production of mode-locked pulses and the output pulses can be much shorter than the recovery times of either. A typical example is the recently developed CW dye laser[24,25]. This mode-locking situation (type I mode-locking) represents a true steady-state operation, as evidenced by the very high stability of the output pulse train[24]. In contrast, the type II mode-locking is a transient phenomenon which never attains a steady state. The type II laser output is such that the pulses generally broaden during the latter part of the output train and lasing is cut off by gain depletion. In addition, random satellite pulses and background radiation

are usually present due to the imperfect discrimination against the weaker fluctuations in the initial field distribution. Typically, the gain recovery time is much longer than the cavity round trip time, and the laser must be operated close to the threshold to ensure reliable pulse selection.

A number of analyses of pulse formation in Type II mode-locking systems such as Nd:glass and ruby lasers of varying degrees of complexity have appeared in the literature[40-45]. The basic processes involved are reasonably well-understood in principle, although the details of pulse production in experimental systems is not always so well comprehended or analysed.

For Type I mode-locking systems, an analysis has recently been presented by New[46,47]. In this model, he applied a rate equation theory to the determination of the laser operating regime in which a circulating pulse experiences loss on both the leading and trailing edges. This situation is determined subject to the explicit assumption that the pulse energy (suitably normalised) is a constant for each pass through a given point in the laser cavity. The conjunction of these two conditions implies that the pulse is shortened on each round trip in the laser cavity. Accordingly, such an operating regime is called the "pulse compression region". This model has been employed to explain the rapid pulse compression which has been observed[5,48] in the build-up of the output pulses obtained from a high gain, flashlamp-pumped dye laser. However, it is

important to observe that operation in the above pulse compression regime precludes the occurrence of steady-state pulses (SSP) since the laser pulses simply continue to narrow indefinitely. This circumstance renders the applicability of the analysis to CW lasers, for example, CW dye lasers, somewhat indeterminate, in that the output pulses are SSP. Furthermore, the postulation that the system reaches a constant energy state rapidly prior to the stage of pulse narrowing is questionable, since one might expect an actual system to behave in such a way that both the total pulse energy and the pulse shape tends towards their respective equilibrium values as the steady-state is approached. Therefore, although the analysis due to New may help to provide a simple and intuitive picture for the pulse formation in Type I mode-locked systems, a more general approach is necessary for generating a better understanding of the detailed mechanisms involved in the process.

1.2 OUTLINE OF THE CONTENTS OF THE THESIS:

The major purpose of the work described in this thesis is the development of a theoretical model for the mode-locked CW and quasi-CW lasers using a suitable saturable absorber, and the direct testing of the applicability of this model to some important systems.

In essence, the development of the theoretical model as described in Chapter 2 consists of three parts. First, the dynamical equations governing the laser operation are derived

employing a semiclassical approach, where both the gain and loss media are treated in the density matrix formalism and propagation of the electromagnetic radiation is governed by the Maxwell's equations. Second, the possibility of achieving mode-locking is investigated by examining the stability of the time-invariant (CW) solutions of the dynamical equations against small perturbations. The resulting characteristic equations can be used for the determination of mode-locking regimes for a given set of laser parameters. Finally, a finite difference approximation is employed as a means of solving the laser dynamical equations. The finite difference equations so developed can be used to generate the steady-state pulses (SSP) if the laser is operated in the mode-locking regime.

Before applying our theoretical model to any specific laser, a systematic study on the general behaviour of CW mode-locked lasers is undertaken in Chapter 3, employing appropriate model systems. There are a number of reasons for carrying out this investigation. Pedagogically, it will become clear that such a systematic study helps to provide an overall understanding of the physical mechanisms controlling the mode-locking process. In particular, it will be shown explicitly that the atomic coherence effects of the interactions between the radiation field and the active media are important for some laser systems and can be studied within the density matrix formalism. Furthermore, the general procedure and techniques employed for the numerical analysis will form the basic mathematical tool for handling more specific systems, such as those treated in the subsequent

chapters.

As one of the important laser systems to which our model is applicable, the behaviour of the mode-locked CW dye lasers is investigated in Chapter 4. It will be verified directly that the output pulses from such a mode-locked laser (Type I mode-locking) can indeed be much shorter than the recovery times of either the absorber or the gain, even if the system is operated very close to threshold. In addition, through a comparison of our model with that due to New[46,47], it is shown that our analysis represents a more gereral approach to the problem in that SSP can be generated within the mode-locking regime and the actual pulsewidth is obtainable for a given set of laser parameters.

Apparently, passive mode-locking in the CW lasers is very similar to that in some long-pulse flashlamp-pumped systems, it is naturally to be anticipated that our model will also be applicable to those systems under certain circumstances. Accordingly, as a representative case, the situation of flashlamp-pumped dye lasers is analysed in Chapter 5. It is to be expected that the steady-state solutions of laser dynamical equations will apply to a pulsed gain system provided that the laser operating time is longer than the time taken for the establishment of the steady-state solution. When this circumstance holds, the laser operating regime may be described as quasi-steady-state, and the laser system can be classified as quasi-continuous. Recall that the two distinct situations of Type I and Type II systems analysed, respectively, by using

our model and by other authors[40-45] represent two opposite extremes in a sense that for Type I systems only the (long-time) steady-state solutions are obtained, whereas for Type II systems the short-time transient solutions are obtained. In this context, the quasi-steady-state operating regime occurring in pulsed gain systems can be viewed as a transition region of laser operation between the two extreme cases.

As an integral part of our work, the interrelation between mode-locking and relaxation oscillations (passive Q-switching) is discussed in Chapter 6. Roughly speaking, the difference between these two basically distinct types of spontaneous pulsing is characterized by the observation that, for mode-locking, the length of the output pulses is considerably less than the cavity round-trip time whereas the inverse of the relaxation oscillation period is longer than the cavity round-trip time for passive Q-switching. In the work to be described, it will be shown that the passive Q-switching solutions follow as a special case of the analysis employed for mode-locking using saturable absorbers. A method of differentiating between these two instability regimes is given, and it is shown how the regions of mode-locking should be corrected, where necessary, by the subtraction of the relaxation oscillation regime. It will also be shown that our model for the analysis of relaxation oscillations constitutes a generalization of previously published work. Furthermore, the formalism is employed to study the transition from mode-locking regions of

operation to relaxation oscillation regimes for several continuous or quasi-continuous laser systems.

Finally, all the work described in this thesis is summarized in the concluding chapter. The implications of the results obtained are discussed, and motivation and suggestions for the generalization of the present model as well as for further theoretical research on the problem of saturable absorber mode-locking are pointed out.

CHAPTER 2

A THEORETICAL MODEL

2.1 INTRODUCTION:

In this chapter, a theoretical model for saturable absorber laser mode-locking is developed. An unidirectional ring laser cavity is employed and the propagation of the radiation is treated as one-dimensional so that travelling wave interactions and diffraction effects can be ignored.

In section 2.2, the laser coupled equations for both the gain and loss media are derived, employing semiclassical electrodynamics. In fact, such a semiclassical treatment has been widely used and well-justified in the development of laser theory [26,49-53]. In the present model, we assume that both the gain and loss media are composed of a collection of two-level atoms with homogeneously broadened lines and in exact resonance with the electromagnetic radiation in the cavity. For simplicity, the effects of medium dispersion are also ignored.

According to the prescription of semiclassical theory, both the gain and loss media are treated in the density matrix formalism and propagation of the electromagnetic radiation is governed by the Maxwell's equations. The rotating wave and the slowly varying envelope approximations are then used to simplify the coupled differential equations. Furthermore, the relaxation

mechanisms of the gain (loss) medium are taken into account phenomenologically by the recovery time $T_1(T_1')$ and the phase memory time $T_2(T_2')$ in analogy to the Bloch equations of magnetic resonance[54]. Finally, all the cavity (linear) losses are supposed to occur at an equivalent mirror with reflectivity R. It follows that the field amplitudes in the laser cavity must satisfy appropriate boundary conditions. For convenience, we adopt a normalization scheme to put the dynamical equations into a concise form more suitable for analysis[51,55].

Having established the laser dynamical equations, the problem of mode-locking is then pursued by investigating the stability of the time invariant (CW) solutions. First, in section 2.3, the CW solutions are derived exactly. A perturbation method is then employed in section 2.4 to investigate the stability of those solutions. Consequently, the characteristic equations are derived which can be used to determine the instability regions for specific laser parameters. However, the perturbation analysis just provides us a preliminary test of whether mode-locking is possible for a given system. Therefore, it remains to show whether an instability in the CW solutions actually implies pulsing, and if so, can steady-state pulses (SSP) be generated within the mode-locking regime. To verify this, one has to solve the original coupled non-linear partial differential equations numerically, as no analytical solutions can be found. Accordingly, in section 2.5, a finite difference approximation appropriate for the present problem is described.

Finally, for future reference, all the parameters needed for numerical calculations are summarized in the last section.

2.2 LASER DYNAMICAL EQUATIONS:

2.2.1 Ring Laser Cavity and the Equivalent Periodic Optical System

Consider a ring laser cavity as shown schematically in Fig. 2-1(a). Here, L_a, L_b and L are the optical lengths of the gain tube (amplifier), the loss cell (absorber) and the cavity perimeter respectively; M_1, M_2 and M_3 are the partially transmitting mirrors.

Generally, electromagnetic waves can propagate in both the clockwise and counterclockwise directions. However, practically, a ring laser can be operated in the unidirectional mode[56]. This situation is assumed here since it eliminates the need to consider the complicated travelling wave interactions. In addition, the propagation of the radiation is treated as one dimensional so that diffraction effects are ignored and only a single space coordinate (x) is employed in the theoretical analysis. For convenience, all the cavity losses, including the linear losses that may arise in both the gain and loss media, are supposed to occur at one mirror with an appropriate effective reflectivity. Consequently, the ring laser system can be represented by an equivalent periodic optical system as shown in Fig. 2-1(b) where M stands for the equivalent mirror with an effective reflectivity R.

Fig. 2-1(a) Schematic representation of a ring laser system with a gain cell (amplifier) and a loss cell (absorber) with optical lengths L_a and L_b respectively. L is the ring perimeter and M_1, M_2 and M_3 are the partially transmitting mirrors. Only one direction of propagation for the electromagnetic field is shown corresponding to the uni-directional operation.

(b) An equivalent periodic optical system of the uni-directional ring laser shown in (a), with M representing the equivalent mirror of effective intensity reflectivity R. The radiation propagates in the direction OABCDE . . . with the point E equivalent to O so that the path O → E corresponds to one round-trip in the laser cavity. Space coordinates to these points are o, x_1, x_2, x_3, x_4 and x_L respectively. The optical lengths of the three free regions are L_1 = OA, L_2 = BC and L_3 = DE.

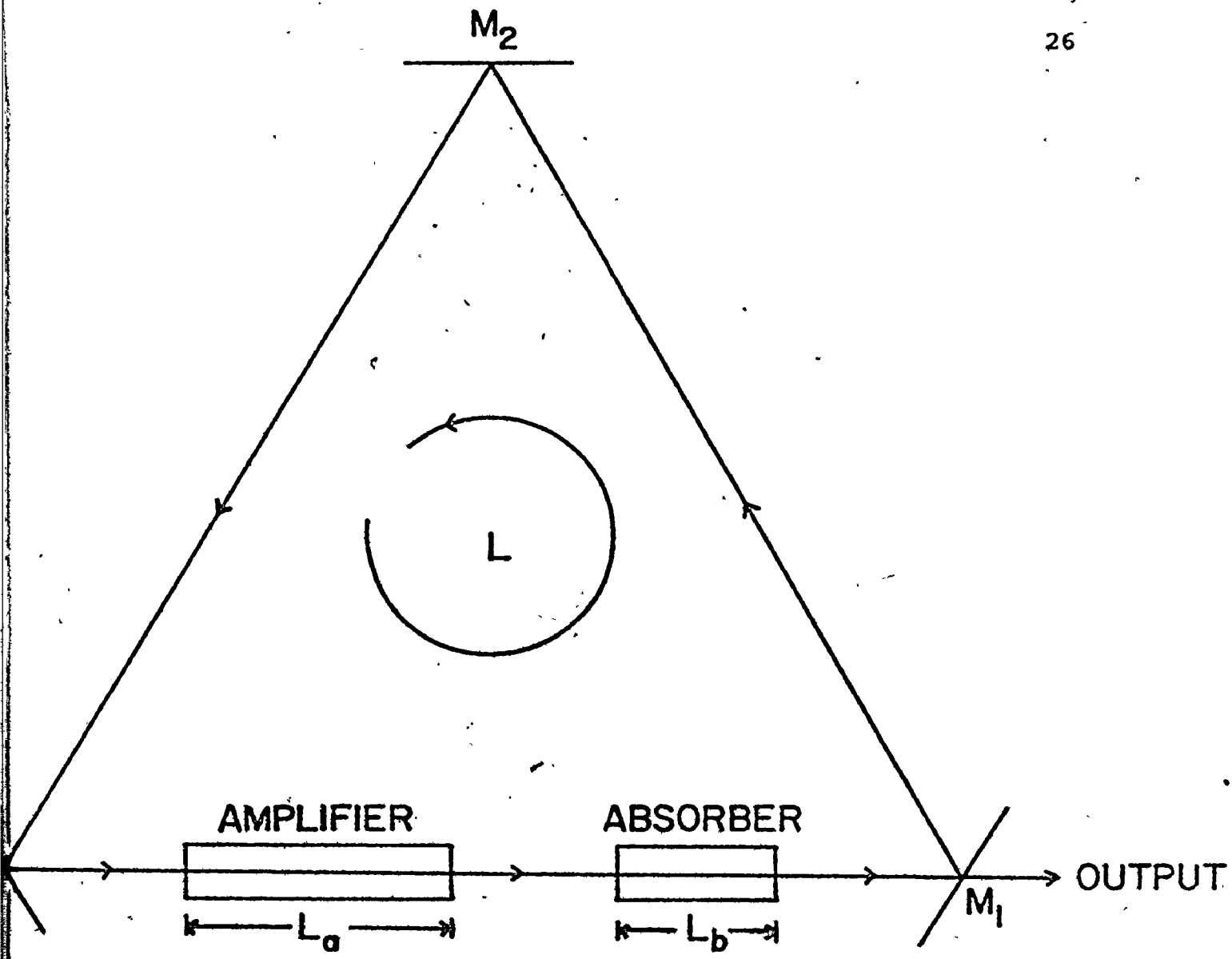
M2
L
AMPLIFIER
ABSORBER
OUTPUT
M1
La
Lb

(a)

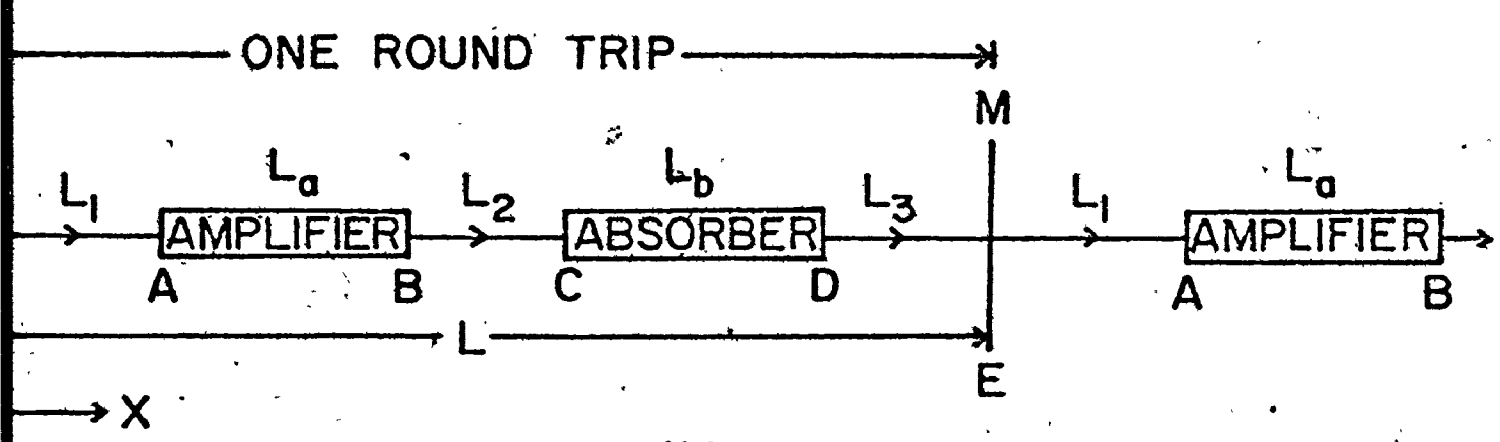
ONE ROUND TRIP
M
L1
La
AMPLIFIER
A
B
L2
Lb
ABSORBER
C
D
L3
L1
La
AMPLIFIER
A
B
L
E
X

(b)

Fig. 2-1

It will be shown in the latter part of this section that the reflectivity is accounted for by the boundary conditions which relate the field amplitudes in different parts of the cavity.

At this moment, it is appropriate to point out that a simple equivalence may be made between an unidirectional ring laser and a normal laser cavity when both the lengths of the gain and absorber cells and the spatial extent of the laser pulse are much less than the cavity lengths. Under these circumstances, the overlapping effect of the pulse(s) in the cavity can be ignored and the model described here is expected to work equally well for both types of laser cavity. Of course, to model a normal laser by an equivalent ring laser, some modifications are needed. First, the cavity perimeter (L) should be equal to twice the resonator length, i.e. the round-trip length of the normal cavity. Second, the effective reflectivity (R) should include the effects due to the reflectivities of both resonator mirrors. Finally, for a normal laser, a pulse circulating around inside the cavity passes through the gain and loss cells twice in each round-trip period whereas for a ring laser, the pulse will travel through the cells only once for each round-trip. Accordingly, the dependence of the response of the laser gain and absorber loss on the relative positions of the cells in the cavity can be very different for these two types of cavity, depending on the saturation and recovery behavior of the active media. Therefore, a careful analysis is

necessary to establish an equivalent laser gain and absorber loss per round-trip when a normal laser is described by a ring laser.

2.2.2 The Semiclassical Theory

In the semiclassical formulation of laser theory, the active medium is treated quantum mechanically whereas the propagation of the electromagnetic radiation is described by the Maxwell's equation of classical electrodynamics. In the present problem, both the gain and loss media should basically obey the same laws of motion. Accordingly, in what follows, a general account of the semiclassical theory is given first. The analysis is then applied to the gain and loss media separately and two different sets of laser coupled equations are established.

First of all, we assume:

(a) The active medium is composed of a collection of two-level non-interacting atoms which are coupled only through the interactions with the electromagnetic field.

(b) The resonance frequencies of all the atoms are the same, i.e. the resonance line of the medium is homogeneously broadened, so that an ensemble average is not needed.

(c) The electric field amplitude E is a scalar, linearly polarized in the y-direction and propagating in the x-direction.

(d) The dipole approximation holds for the interaction of the atoms and the radiation field.

(i) Equation of Motion for the Medium

Generally, for a two-level atom, the time-dependent wavefunction can be written as

$$\psi(t) = a_1(t)\psi_1 + a_2(t)\psi_2 \tag{2-1}$$

where ψ_1 and ψ_2 are respectively the eigenstates for the lower (1) and upper (2) levels in the unperturbed state and $a_1(t)$ and $a_2(t)$ are known as the probability amplitudes. In the language of quantum statistical mechanics, one defines a 2×2 density matrix

$$\tilde{\rho} = \begin{pmatrix} \rho_{11} & \rho_{12} \\ \rho_{21} & \rho_{22} \end{pmatrix} = \begin{pmatrix} a_1 a_1^* & a_1 a_2^* \\ a_1^* a_2 & a_2 a_2^* \end{pmatrix} \tag{2-2}$$

The motion of the two-level system can then be described by the time-dependent Schrödinger equation

$$i\hbar \frac{\partial \tilde{\rho}}{\partial t} = [H_o + V, \tilde{\rho}] \tag{2-3}$$

where H_o is the Hamiltonian of the unperturbed atom and

$$V = -E\mathcal{P} \tag{2-4}$$

is the electric field perturbation in the dipole approximation with $\mathcal{P}$ being the dipole moment operator of the atom. In the present representation, since ψ_1 and ψ_2 are the eigenstates of H_o, we have

$$H_o = \begin{pmatrix} E_1 & 0 \\ 0 & E_2 \end{pmatrix} = \hbar \begin{pmatrix} \omega_1 & 0 \\ 0 & \omega_2 \end{pmatrix} \tag{2-5}$$

and

$$V = \begin{pmatrix} 0 & V_{12} \\ V_{21} & 0 \end{pmatrix} = \begin{pmatrix} 0 & -\mu E \\ -\mu E & 0 \end{pmatrix} \tag{2-6}$$

where E_1 and E_2 are respectively the unperturbed eigen energies of level 1 and 2, and

$$\mu = \langle 1|\mathcal{P}|2\rangle = \langle 2|\mathcal{P}|1\rangle \tag{2-7}$$

is taken to be real without loss of generality. Observe that the diagonal matrix elements of $\mathcal{P}$ vanish by parity conservation.

The equation of motion (2-3) can be reduced to a simpler form by a transformation to the interaction representation[50]. This is done by rewriting the density matrix $\tilde{\rho}$ as

$$\tilde{\rho} = \begin{pmatrix} \rho'_{11} & \rho'_{12}e^{i\omega_o t} \\ \rho'_{21}e^{-i\omega_o t} & \rho'_{22} \end{pmatrix} \tag{2-8}$$

with

$$\omega_0 = \omega_2 - \omega_1 \tag{2-9}$$

being the resonance frequency of the atom, and substituting this expression into (2.3). Thus, we obtain

$$i\hbar \frac{\partial \tilde{\rho}'}{\partial t} = [\tilde{V}', \tilde{\rho}'] \tag{2-10}$$

where

$$\tilde{V}' = \begin{pmatrix} 0 & V'_{12} \\ V'_{21} & 0 \end{pmatrix} = \begin{pmatrix} 0 & V_{12}e^{i\omega_o t} \\ V_{21}e^{-i\omega_o t} & 0 \end{pmatrix} \tag{2-11}$$

$$\tilde{\rho}' = \begin{pmatrix} \rho'_{11} & \rho'_{12} \\ \rho'_{21} & \rho'_{22} \end{pmatrix} = \begin{pmatrix} \rho_{11} & \rho_{12}e^{-i\omega_o t} \\ \rho_{21}e^{i\omega_o t} & \rho_{22} \end{pmatrix} \tag{2-12}$$

are, respectively, the perturbation and density matrices in the interaction representation. In this representation, the motion of the atom can be further described geometrically by the motion of a vector $\underset{\sim}{R}$ in a 3-dimensional space defined by a set of unit vectors $(\hat{e}_1, \hat{e}_2, \hat{e}_3)$ and rotating at an angular velocity ω_0 [50,55]. The components of $\underset{\sim}{R}$ are defined as

$$\begin{aligned} R_1 &= \rho'_{12} + \rho'_{21} \\ R_2 &= i(\rho'_{12} - \rho'_{21}) \\ R_3 &= \rho'_{11} - \rho'_{22} = \rho_{11} - \rho_{22}. \end{aligned} \tag{2-13}$$

It can be shown from (2-10), and with additional terms added, that the equation of motion for $\underset{\sim}{R}$ is described by

$$\frac{\partial \underset{\sim}{R}}{\partial t} = \underset{\sim}{A} - B\cdot\underset{\sim}{R} + \underset{\sim}{\Omega}\times\underset{\sim}{R} \tag{2-14}$$

where the vector $\underset{\sim}{\Omega}$ stands for the interaction components

$$\begin{aligned} \Omega_1 &= \frac{1}{\hbar}(V'_{12} + V'_{21}) \\ \Omega_2 &= \frac{i}{\hbar}(V'_{12} - V'_{21}) \\ \Omega_3 &= 0 \end{aligned} \tag{2-15}$$

and the terms $\underset{\sim}{A}$ and $B\cdot\underset{\sim}{R}$ have been added to account, respectively, for the effects of pumping and the atomic relaxation processes. Here

$$\underset{\sim}{A} \equiv \frac{1}{T_1}\left(\frac{D_e}{N}\right)\hat{e}_3 \tag{2-16}$$

$$B \equiv \begin{pmatrix} 1/T_2 & 0 & 0 \\ 0 & 1/T_2 & 0 \\ 0 & 0 & 1/T_1 \end{pmatrix} \qquad (2\text{-}17a)$$

so that

$$B\cdot\underset{\sim}{R} = \frac{1}{T_2}(R_1\hat{e}_1+R_2\hat{e}_2) + \frac{1}{T_1}R_3\hat{e}_3 \qquad (2\text{-}17b)$$

where D_e is the population difference at equilibrium with the pump, N the active atom density, and T_1 and T_2 are respectively the recovery and phase memory (dephasing) times of the atom*.

Equation (2-14) can be employed to give a geometrical realization for the motion of the two-level system. It will be further simplified and interpreted when the rotating wave and slowly varying envelope approximations are applied.

(ii) The Electromagnetic Field Equations

The Maxwell's equations for the present problem are (in MKS units)

$$\begin{aligned} \nabla\times\underset{\sim}{E} &= -\mu'\dot{\underset{\sim}{H}} \quad , \quad \nabla\cdot(\mu'\underset{\sim}{H}) = 0 \\ \nabla\times\underset{\sim}{H} &= \varepsilon'\dot{\underset{\sim}{E}}+\dot{\underset{\sim}{P}} \quad , \quad \nabla\cdot(\varepsilon'\underset{\sim}{E}+\underset{\sim}{P}) = 0 \end{aligned} \qquad (2\text{-}18)$$

where ε' and μ' are respectively the dielectric constant and magnetic permeability of the host medium. The term involving the electric conductivity σ has been omitted from the third equation since we have assumed (section 2.2.1) that all the linear losses within the laser cavity are accounted for by the effective reflectivity R.

*It can be shown[57] that T_1 is approximately related to the life-times of the lower (t_1) and upper (t_2) atomic levels by $T_1 = (t_1+t_2)/2$, and $T_2 = 2t_1t_2/(t_1+t_2)$ if the width of the homogeneously broadened line is mainly controlled by the two levels concerned. Otherwise, T_2 can be calculated from the linewidth ($\Delta\nu$) by $T_2 = 1/(\pi\Delta\nu)$, assuming a Lorentzian profile.

By assumption (c), the fields $\underset{\sim}{E}$ and $\underset{\sim}{H}$, and hence the polarization $\underset{\sim}{P}$ are all linearly polarized and given by

$$\underset{\sim}{E} = E(x,t)\hat{y} \ , \ \underset{\sim}{H} = H(x,t)\hat{z} \ , \ \underset{\sim}{P} = P(x,t)\hat{y} \ . \qquad (2\text{-}19)$$

Consequently, using (2-19), we have from (2-18), after eliminating $\underset{\sim}{H}$, the following one-dimensional scalar field equation

$$\frac{\partial^2 E}{\partial x^2} - \frac{1}{c^2}\frac{\partial^2 E}{\partial t^2} = \mu' \frac{\partial^2 P}{\partial t^2} \qquad (2\text{-}20)$$

where $c = 1/\sqrt{\varepsilon'\mu'}$ is the phase velocity of propagation of the electromagnetic wave in the host medium. Equations (2-20) and (2-14) are the fundamental coupled equations for the active medium and the radiation field.

(iii) Simplification of the Fundamental Equations

The coupled equations (2-14) and (2-20) can be simplified if we further assume, in addition to assumptions (a) to (d), that

(e) The optical frequency ω_o is much larger than the natural linewidth T_2^{-1}, that is*

$$\omega_o >> T_2^{-1}, \qquad (2\text{-}21)$$

so that the rotating wave approximation holds, that is, harmonics of the frequency ω_o can be neglected.

(f) The field can be represented as a running wave with slowly varying amplitude and phase*,

$$E(x,t) = \mathcal{E}(x,t)\cos(\omega t - kx + \phi(x,t)) \qquad (2\text{-}22)$$

*The validity of the rotating wave and slowly varying envelope approximations will be discussed in the next subsection.

where ω and $k = \omega/c$ are constants and the amplitude $\mathcal{E}$ and phase ϕ are slowly varying with respect to the optical changes, that is

$$\left|\frac{\partial \mathcal{E}}{\partial x}\right| << k\mathcal{E}, \quad \left|\frac{\partial \mathcal{E}}{\partial t}\right| << \omega\mathcal{E},$$
$$\left|\frac{\partial \phi}{\partial x}\right| << k, \quad \left|\frac{\partial \phi}{\partial t}\right| << \omega. \tag{2-23}$$

Under these assumptions, the response of the active medium to the radiation field is characterized by a macroscopic volume polarization of the form

$$P(x,t) = C(x,t)\cos(\omega t - kx + \phi(x,t)) + S(x,t)\sin(\omega t - kx + \phi(x,t)) \tag{2-24}$$

where C and S can be called respectively the "in-phase" and "in-quadrature" components, and are both slowly varying in space and time as $\mathcal{E}$ does. By substituting (2-22) and (2-24) into the field equation (2-20), carrying out the differentiation (neglecting all the second order derivatives), and finally equating the sine and cosine terms separately, we arrive at the following two equations

$$\left(c\frac{\partial \phi}{\partial x} + \frac{\partial \phi}{\partial t}\right) = -\frac{\omega}{2\varepsilon'} C$$
$$c\frac{\partial \mathcal{E}}{\partial x} + \frac{\partial \mathcal{E}}{\partial t} = -\frac{\omega}{2\varepsilon'} S. \tag{2-25}$$

In addition, the equation of motion (2-14) for the medium can be rewritten. Using (2-22) in (2-6), the components of the original perturbation matrix are given by

$$V_{12} = V_{21} = -\mu\mathcal{E}\cos(\omega t - kx + \phi(x,t)). \tag{2-26}$$

Accordingly, by the definitions of (2-11) and (2-15), the components of the vector $\underset{\sim}{\Omega}$ become

$$\begin{aligned} \Omega_1 &= -\Lambda \cos[(\omega-\omega_o)t-kx+\phi(x,t)] \\ \Omega_2 &= \Lambda \sin[(\omega-\omega_o)t-kx+\phi(x,t)] \\ \Omega_3 &= 0 \end{aligned} \qquad (2\text{-}27)$$

with

$$\Lambda = \frac{\mu\mathcal{E}}{\hbar} . \qquad (2\text{-}28)$$

It can be shown that in the reference frame $(\hat{e}_1,\hat{e}_2,\hat{e}_3)$ which defined the motion of the vector $\underset{\sim}{R}$ (Eq. (2-14)), the vector $\underset{\sim}{\Omega}$ as given by (2-27) lies on the 1-2 plane and rotates at a velocity

$$\delta = (\omega-\omega_o) + \frac{\partial\phi}{\partial t} \qquad (2\text{-}29)$$

that is, its unit vector $\hat{n}$ rotates as

$$\frac{\partial\hat{n}}{\partial t} = -\delta\hat{e}_3\times\hat{n}. \qquad (2\text{-}30a)$$

Equation (2-14) can be rewritten in a new rotating frame $(\hat{e}_1',\hat{e}_2',\hat{e}_3')$ defined by

$$(\hat{e}_1',\hat{e}_2',\hat{e}_3') = (\hat{n}\times\hat{e}_3,\hat{n},\hat{e}_3). \qquad (2\text{-}30b)$$

In this rotating frame, the vector $\underset{\sim}{\Omega}$ transforms to $\underset{\sim}{\Omega}'$ with components

$$\Omega_1' = 0$$

$$\Omega_2' = -\Lambda$$

$$\Omega_3' = \delta$$

and Eq. (2-14) becomes, in component form

$$\frac{\partial R_1'}{\partial t} = -\delta R_2' - \Lambda R_3' - \frac{R_1'}{T_2}$$

$$\frac{\partial R_2'}{\partial t} = \delta R_1' - \frac{R_2'}{T_2} \qquad (2\text{-}32)$$

$$\frac{\partial R_3'}{\partial t} = \Lambda R_1' - \frac{1}{T_1}\left(R_3' - \frac{D_e}{N}\right) .$$

We can now interpret the physical meaning of the three components R_1', R_2' and R_3': R_3' is proportional to the population difference $D = n_1 - n_2$; R_2' and R_1' are, respectively, proportional to the "in-phase" and "in-quadrature" components of the polarization $P(x,t)$, that is

$$S = -\mu N R_1'$$

$$C = \mu N R_2' \qquad (2\text{-}33)$$

$$D = N R_3'$$

where the first and second equations can be shown by using the relation $P(x,t) = \mu N(\tilde{\rho}_{12} + \rho_{21})$, carrying out the appropriate transformation for $\tilde{\rho}$ (Eqs. (2-8) and (2-12)) and $\underset{\sim}{R}$, and comparing the coefficients with (2-24)[55].

Using (2-33), Eqs. (2-32) become

$$\frac{\partial S}{\partial t} = \delta C + \mu \Lambda D - \frac{S}{T_2}$$

$$\frac{\partial C}{\partial t} = -\delta S - \frac{C}{T_2} \qquad (2\text{-}34)$$

$$\frac{\partial D}{\partial t} = -\frac{\Lambda}{\mu} S - \frac{D - D_e}{T_1} .$$

2.2.3 Laser Dynamical Equations

The coupled equations (2-25) and (2-34) just derived can be used to treat the present problem. For simplicity, we further assume that both the gain and loss media are in exact resonance with the radiation field, that is $\omega=\omega_o$. In addition, it is appropriate to discuss the validity of the rotating wave and slowly varying envelope approximations which have been used in the derivation of the coupled equations (2-25) and (2-34).

The rotating wave approximation requires that the optical frequency (ω_o) be much greater than the natural linewidth (T_2^{-1}) of the active medium. For most of the laser media and saturable absorbers, $T_2 \gtrsim 10^{-13}$ sec whereas $\omega_o \sim 10^{15}$ sec^{-1}. Therefore, the condition that $\omega_o >> T_2^{-1}$ should generally be valid, and the rotating wave approximation is expected to hold. On the other hand, the situation for the slowly varying envelope approximation (SVEA) is not so intuitively clear and has been investigated recently[58,59]. From Eqs. (2-23), one may immediately conclude that the SVEA will hold provided that the laser pulse is much longer than an optical cycle ($\sim \omega_o^{-1}$). However, it has been recently reported[59] that the SVEA may not be an appropriate approximation even for pulses as long as several hundred optical cycles if the pulses are shorter than a certain coherence or "cooperation" time which depends on the optical frequency of the electromagnetic radiation, the active atom density and the electric dipole moments. Under this circumstance, a second (or higher) order approximation is necessary and will lead to the phenomenon of frequency chirping even if the disper-

sion of the host medium is neglected*. For the present problem, such a frequency chirping effect is not taken into account because it is usually small compared with the optical frequency. Consequently, the SVEA is assumed to be valid as long as the laser pulse is much longer than an optical cycle, i.e. Eqs. (2-23) hold. In addition, we assume that the phase ϕ will be stabilized during pulse propagation (which is usually the case)[32] so that we can set ϕ = constant and $\partial\phi/\partial t = 0$. As a consequence, it follows from the second equation of (2-34) that the "in-phase" (dispersive) component C of the polarization can be neglected since $\delta = (\omega-\omega_o) + \partial\phi/\partial t = 0$. The first equation of (2-25) can also be omitted. Finally, this leaves us with only three coupled equations for the active medium and the field, namely

$$\begin{aligned} \frac{\partial S}{\partial t} &= \frac{\mu^2 \mathcal{E} D}{\hbar} - \frac{S}{T_2} \\ \frac{\partial D}{\partial t} &= -\frac{\mathcal{E}}{\hbar} S - \frac{D-D_e}{T_1} \\ c\,\frac{\partial \mathcal{E}}{\partial x} + \frac{\partial \mathcal{E}}{\partial t} &= -\frac{\omega}{2\varepsilon'} S \end{aligned} \qquad (2\text{-}35)$$

where we have put in $\Lambda = \mu\mathcal{E}/\hbar$ explicitly. Observe that $D = n_1 - n_2$ is the population difference between the lower and upper levels. Practically, it is more appropriate to use $D' = n_2 - n_1$ instead of D since we are interested in the population "inversion". Accor-

---

*We have neglected the dispersion of the host medium by assuming that the dielectric constant (ε') (and hence the phase velocity c) is a constant when we derived Eq. (2-20).

dingly, we rewrite (2-35) as

$$\frac{\partial S_a}{\partial t} = \frac{\mu_a^2 \mathcal{E}_a}{\hbar} N_a - \frac{S_a}{T_2}$$

$$\frac{\partial N_a}{\partial t} = -\left(\frac{\mu_a \mathcal{E}_a}{\hbar}\right) \frac{S_a}{\mu_a} - \frac{N_a - N_a^e}{T_1} \qquad (2\text{-}36)$$

$$c\frac{\partial \mathcal{E}_a}{\partial x} + \frac{\partial \mathcal{E}_a}{\partial t} = \frac{\omega}{2\varepsilon'} S_a$$

where $N_a = -D$, $N_a^e = -D_e$, $S_a = -S$ and the subscript a refers to the amplifier*. Similar expressions can be obtained for the absorber using T_1' (T_2') instead of T_1 (T_2) and subscript b rather than a.

For convenience, we define

$$t' = t/T_2 \ , \ x' = x/cT_2 \qquad (2\text{-}37)$$

and

$$P_{a,b} = S_{a,b}/\mu_a N_a^e \ , \ D_{a,b} = N_{a,b}/N_a^e \ , \ E_{a,b} = \mu_{a,b}\mathcal{E}_{a,b}T_2/\hbar. \qquad (2\text{-}38)$$

The dynamical equations (2-36) for the amplifier and those for the absorber thus reduce to the following dimensionless form

$$\frac{\partial P_a}{\partial t'} = -P_a + D_a E_a$$

$$\frac{\partial D_a}{\partial t'} = -E_a P_a - \gamma(D_a - 1) \qquad (2\text{-}39)$$

$$\frac{\partial E_a}{\partial x'} + \frac{\partial E_a}{\partial t'} = G_a P_a$$

---

*The negative sign in $N_a^e = -D_e$ indicates that the population of the amplifier is inverted in absence of the electromagnetic field since D_e is defined as the population difference of the lower and upper level in equilibrium with the pump. From now on, an inverted population is taken as positive in accordance with the usual convention in laser theory.

and

$$\frac{\partial P_b}{\partial t'} = -\gamma_2 P_b + D_b E_b$$

$$\frac{\partial D_b}{\partial t'} = -E_b P_b - \gamma'(D_b + a_o) \qquad (2\text{-}40)$$

$$\frac{\partial E_b}{\partial x'} + \frac{\partial E_b}{\partial t'} = G_b P_b$$

where

$$\gamma = T_2/T_1 \ , \ \gamma' = T_2/T_1' \ , \ \gamma_2 = T_2/T_2' \qquad (2\text{-}41)$$

and

$$G_a = \alpha_a c T_2/2 \ , \ G_b = \alpha_b \gamma_2 c T_2/2a_o$$

$$a_o = -N_b^e/N_a^e \ , \ \alpha_{a,b} = \frac{\omega \mu_{a,b}^2}{\epsilon_{a,b} c\hbar} N_a^e T_2 \ . \qquad (2\text{-}42)$$

Note that a_o is a positive quantity since N_b^e is negative while N_a^e is positive according to the sign convention adopted in our analysis.

2.2.4 The Generalized Boundary Conditions for the Ring Cavity

The description of the ring laser system (Fig. 2-1) is not completed by the two sets of coupled equations (2-39) and (2-40) since the fields E_a and E_b in the amplifier and absorber are still unrelated. In addition, we have the field equation for regions outside the media* (Fig. 2-1(b))

$$\frac{\partial \mathcal{E}_f}{\partial x'} - \frac{\partial \mathcal{E}_f}{\partial t'} = 0 \qquad (2\text{-}43)$$

*Note that we use $\mathcal{E}_f$ (the actual amplitude) instead of the normalized amplitude $E_f = \mu_f \mathcal{E}_f T_2/\hbar$ since such a normalisation is not appropriate for the free space where no dipole moment exists, i.e. $\mu_f = 0$.

where the subscript f refers to free space. Using this equation, which has the solution $\mathcal{E}_f(x',t') = \mathcal{E}_f(t'-x')$, it follows that the radiation fields in the two media must satisfy the following boundary conditions

$$\begin{aligned} mE_a(x_2',t'-\Delta_{23}) &= E_b(x_3',t') \\ mE_a(x_1'+L',t') &= rE_b(x_4',t'-\Delta_{41}). \end{aligned} \tag{2-44}$$

Here $m = \mu_b/\mu_a$ is the ratio of the electric dipole moments; $x_i' = x_i/cT_2$ $(i=1,2,3,4)$ are the reduced space coordinates of the ends of the amplifier and absorber; $L' = L/cT_2$, $\Delta_{23} = x_3'-x_2'$ $\Delta_{41} = L'-x_4'+x_1'$ and $r = \sqrt{R}$. Observe that the two quantities Δ_{23} and Δ_{41} correspond, respectively, to the times taken for the radiation to propagate from B to C and from D to A (see Fig.2-1(b)), and r is the effective amplitude reflectivity of the equivalent mirror. In addition, the inclusion of the parameter m is a consequence of the normalization scheme (Eq. (2-38)) for the amplitudes $E_{a,b}$. However, the following discussion will show that the definition of m can be generalized to account for variations in the intensity between the gain and loss media due to changes in laser mode size between different positions in the resonator.

It has been pointed out in Chapter 1 that the effectiveness of a saturable absorber depends, among other things, on the relative way in which the absorber and the gain medium saturate. In a system where the gain is saturated too easily, high powers are discriminated against and the saturable absorber

is less operative. Under these circumstances, it is desirable to have an optical resonator in which the radiation is tightly focussed onto the absorber, using appropriate intracavity optical components such as lenses. This is usually the case for the widely used saturable absorbers - the organic dye solutions. Therefore, it is practically important and useful to generalize our theoretical model to account for this situation. A careful examination of the boundary conditions (2-44) reveals that such a generalization can be made directly by an appropriate modification for the quantity m. In fact, both the effects of the dipole moment difference and the intensity changes (other than those due to the cavity loss) at the boundaries between the two media can be incorporated into the parameter m by redefining it as

$$m = m_d m_o \tag{2-45}$$

with $m_d = \mu_b/\mu_a$ and m_o^2 being the ratio of the intensities in the absorber and amplifier due to intracavity optical components. In subsequent analysis, the parameter m will always refer to that defined by (2-45), unless otherwise specified. The choice of a suitable value for m in actual numerical calculations will be discussed in the next section.

For simplicity, the subscripts a and b for the quantities D, P and E will be dropped whenever this produces no ambiguity.

2.3 The Time-Invariant (CW) Solutions

The coupled equations (2-39) and (2-40) are nonlinear partial differential equations which cannot be solved analytically in general. However, expressions for the time-invariant (CW) solutions can be derived exactly.

For the CW solutions, we have

$$\frac{\partial \bar{D}}{\partial t'} = 0 \ , \ \frac{\partial \bar{P}}{\partial t'} = 0 \text{ and } \frac{\partial \bar{E}}{\partial t'} = 0 \qquad (2\text{-}46)$$

for both the gain and loss media ($\partial \bar{\varepsilon}_f / \partial t' = 0$ for the free space). Here, the bar on the top of the variables D, P and E denotes that they are time-independent. However, since the gain and loss media are not distributed throughout the cavity, the spatial derivatives of these variables are not zero. In this case, the boundary conditions (Eqs. (2-44)) reduce to

$$\begin{aligned} m\bar{E}(x_2') &= \bar{E}(x_3') \\ m\bar{E}(x_1') &= r\bar{E}(x_4'). \end{aligned} \qquad (2\text{-}47)$$

It will be shown later that it is convenient to use the intensity $\bar{I} = \bar{E}^2$ rather than the amplitude $\bar{E}$ in the analytical work. Accordingly, we rewrite (2-47) as

$$m^2\bar{I}_2 = \bar{I}_3 \ , \ m^2\bar{I}_1 = R\bar{I}_4 \qquad (2\text{-}48)$$

where we have abbreviated $\bar{I}(x_i')$ by $\bar{I}_i$ (i=1,2,3,4).

Applying the equalities (2-46) in (2-39), we obtain

$$\bar{P} = \bar{D}\bar{E}$$

$$\bar{D} = \gamma / (\gamma+\bar{I}) \quad (x_1' \leq x' \leq x_2') \qquad (2\text{-}49)$$

$$\frac{d\bar{I}}{dx'} = \frac{2G_a\gamma\bar{I}}{\gamma+\bar{I}}$$

for the gain medium. Here, we have replaced $\partial\bar{I}/\partial x'$ by $d\bar{I}/dx'$ since there is no time-dependence in $\bar{I}$. For clarity, we also state explicitly the space region where the equations are applicable. Similarly, using (2-46) in (2-40), we have, for the absorber

$$\bar{P} = \bar{D}\bar{E}/\gamma_2$$

$$\bar{D} = \frac{\gamma' a_o}{\gamma'+\bar{I}/\gamma_2} \quad (x_3' \leq x' \leq x_4') \qquad (2\text{-}50)$$

$$\frac{d\bar{I}}{dx'} = -\frac{2G_b\gamma_b a_o\bar{I}}{\gamma'+\bar{I}/\gamma_2}$$

where $\gamma_b = T_2'/T_1'$. Consequently, the problem of finding the CW solutions has been reduced to solving for the CW intensities $\bar{I}$ as a function of x' since $\bar{D}$ and $\bar{P}$ have been related to $\bar{I}$. By the technique of separation of variables, it can be easily shown that the solutions of the third equations of (2-49) and (2-50) are, respectively, given by

$$\begin{aligned} &\ell n[\bar{I}(x')/\bar{I}_1] + [\bar{I}(x')-\bar{I}_1]/\gamma = \alpha_a cT_2(x'-x_1') \\ &\ell n[\bar{I}(x')/\bar{I}_3] + [\bar{I}(x')-\bar{I}_3]/\gamma'\gamma_2 = -\alpha_b cT_2(x'-x_3') \end{aligned} \qquad (2\text{-}51)$$

where we have used (2-42) to simplify the notation. After putting $x' = x_2'$ in the first equation of (2-51) and $x' = x_4'$ in the second, we obtain, using $L_a = cT_2(x_2'-x_1')$ and $L_b = cT_2(x_4'-x_3')$,

$$\ell n(\bar{I}_2/\bar{I}_1) + (\bar{I}_2-\bar{I}_1)/\gamma = \alpha_a L_a$$
$$\ell n(\bar{I}_4/\bar{I}_3) + (\bar{I}_4-\bar{I}_3)/\gamma'\gamma_2 = -\alpha_b L_b \qquad (2\text{-}52)$$

where $\alpha_a L_a$ and $\alpha_b L_b$ are respectively the low signal intensity gain and loss per round trip of the two media.

By solving (2-51), the spatial dependence of the CW intensities throughout the whole cavity can be found. To start with, one solves the simultaneous equations (2-52), using (2-48), for the intensities at the ends of the gain and loss cells. In particular, we have

$$\bar{I}_2 = [(\frac{m^2}{\gamma_2 R} - \gamma_1)\bar{I}_1 + \gamma'\lambda\ell n(R)]/(\frac{m^2}{\gamma_2} - \gamma_1) \qquad (2\text{-}53)$$

where $\gamma_1 = T_1/T_1'$ and λ is defined by

$$\lambda = (\alpha_a L_a - \alpha_b L_b)/\ell n(R^{-1}) - 1 \qquad (2\text{-}54)$$

which is a measure of the net low signal gain over the linear loss and will be subsequently referred to as the "overall pump parameter".

At this point, it is appropriate to introduce the concept of saturation intensity as related to the CW solutions. Although this concept is primarily derived from the rate equations, it may provide some physical insight if properly interpreted and carefully applied to the present model. Indeed, rate equations are consistent with the present formalism as the CW solutions are concerned.

For a homogeneously broadened medium, it can be shown[60] that the relative intensity gain (loss) is given by

$$g(I) = \frac{1}{I}\frac{dI}{d\xi} = \frac{g_o}{1+I/I_{sat}} \qquad (2.55)$$

where ξ is an appropriate generalized coordinate and I_{sat} is known as the "saturation intensity" for which the gain (loss) coefficient is reduced to half of its low signal value, i.e. $g(I_{sat}) = g_o/2$. Comparing the third equations of (2-49) and (2-50) with (2-55), it is easy to see that the saturation intensities are

$$(\bar{I}_{sat})_a = \gamma = T_2/T_1$$
$$(\bar{I}_{sat})_b = \gamma'\gamma_2 = T_2^2/T_1'T_2'. \qquad (2\text{-}56)$$

for the gain and loss media respectively. Observe that the apparent paradox that $(\bar{I}_{sat})_a \propto T_2/T_1$ while $(\bar{I}_{sat})_b \propto (T_1'T_2')^{-1}$ is a consequence of the inclusion of T_2 in the normalization of the field amplitudes (Eq. (2-38)). In fact, the actual (un-normalized) saturation intensity for a homogeneously broadened medium is inversely proportional to the product of the recovery and phase coherence times.

Equation (2-56) indicates that a knowledge of the relaxation times would be useful for the estimation of the saturated gain and loss. Furthermore, the concept of saturation intensity has another important implication as related to the generalized parameter m (Eq. (2-45)) which is related, in part, to the mode sizes of the laser beams in the two media. Dynamically, for a given amplifier and absorber, the ratio of the radiation intensities in the two media should be comparable to the ratio of their saturation intensities for good mode-locking to be attainable. Consequently, it follows from (2-56)

and the boundary conditions (2-44) that

$$m \sim (\gamma_1 \gamma_2)^{1/2}. \qquad (2\text{-}57)$$

This relation* gives us a reasonable estimate for the choice of an appropriate value for m in actual calculations. In fact, it has been verified[61] that the optimal value of m in mode-locked system is not too different from that given by Eq. (2-57).

2.4 Stability of the CW Solutions

For a given system, the CW solutions sought in the last section may or may not be stable depending on the various laser parameters. The idealized output intensity from such a continuously pumped (CW) laser will be constant in time if the CW solutions are stable. Obviously, this is not the situation for a mode-locked CW laser where the output consists of a continuous train of pulses. Therefore, for such a laser system, mode-locking can only be possible if the CW operation mode is not favored. Accordingly, a possible way for the determination of mode-locking conditions is through the investigation of the stability of the CW solutions. As a common practice in dealing with stability problems, a perturbation method is employed here. This method is more general than the pulse discrimination[41] or pulse compression[46,47] treatments since no assumption

*It is also interesting to note that when $m^2 = \gamma_1 \gamma_2$, Eq. (2-53) leads to the solution for I_1 in a closed form, namely,

$$I_1 = - \frac{\gamma \lambda \ell n(R)}{\frac{1}{R} - 1}. \qquad (2\text{-}53')$$

concerning the pulse length is required, and both the recovery process and the phase coherence effects are taken into account. A comparison of our model with the pulse compression analysis due to New[47] will be given in subsequent chapters when dealing with mode-locked dye lasers.

2.4.1 A Perturbation Analysis:

First of all, let us assume that the (normalized) field, polarization and inversion be the sum of their respective CW values and a small perturbation

$$E = \bar{E}+e \ , \ P = \bar{P}+p \ , \ D = \bar{D}+\delta. \qquad (2\text{-}58)$$

Substituting these expressions into the laser dynamical equations (2-39) and (2-40) and neglecting all terms in second order of the perturbations, we obtain the following two sets of linearlized equations:

$$\begin{aligned} \frac{\partial p}{\partial t'} &= -p+\bar{E}\delta+\bar{D}e \\ \frac{\partial \delta}{\partial t'} &= -(\bar{E}p+\bar{P}e)-\gamma\delta \quad (x_1' \le x' \le x_2') \\ \frac{\partial e}{\partial x'} &+ \frac{\partial e}{\partial t'} = G_a p \end{aligned} \qquad (2\text{-}59)$$

and

$$\begin{aligned} \frac{\partial p}{\partial t'} &= -\gamma_2 p+\bar{E}\delta+\bar{D}e \\ \frac{\partial \delta}{\partial t'} &= -(\bar{E}p+\bar{P}e)-\gamma'\delta \quad (x_3' \le x' \le x_4') \\ \frac{\partial e}{\partial x'} &+ \frac{\partial e}{\partial t'} = G_b p \ . \end{aligned} \qquad (2\text{-}60)$$

We further assume that the time and space dependences of the small variations can be separated and represented in

the form

$$f(x',t') = f_o(x')\exp(i\alpha x'+\beta t') \qquad (2\text{-}61)$$

where f stands for e, p and δ. Here, α can take on only the discrete values $\alpha_n = 2n\pi/L'$. ($L' = L/cT_2$) with n being an integer as required by the second boundary condition of (2-44) and $\beta = \beta_r + i\beta_i$ is a complex quantity to be determined. The physical meaning of α_n and β will be given later.

Using (2-61), Eqs. (2-59) and (2-60) reduce to

$$\begin{aligned}
(\beta+1)p_o &= \bar{E}\delta_o + \bar{D}e_o \\
(\beta+\gamma)\delta_o &= -\bar{E}p_o - \bar{P}e_o \qquad (x_1'\le x'\le x_2') \qquad (2\text{-}62)\\
(i\alpha+\beta)e_o + \frac{de_o}{dx'} &= G_a p_o
\end{aligned}$$

and

$$\begin{aligned}
(\beta+\gamma_2)p_o &= \bar{E}\delta_o + \bar{D}e_o \\
(\beta+\gamma')\delta_o &= -\bar{E}p_o - \bar{P}e_o \qquad (x_3'\le x'\le x_4') \qquad (2\text{-}63)\\
(i\alpha+\beta)e_o + \frac{de_o}{dx'} &= G_b p_o \,.
\end{aligned}$$

In addition, by substituting the first equation of (2-58) into (2-44), it can be shown, using (2-61), that the amplitudes $e_o(x')$ must satisfy the following boundary conditions

$$\begin{aligned}
m e_o(x_2') &= e_o(x_3')\exp[(i\alpha+\beta)\Delta_{23}] \\
m e_o(x_1') &= r e_o(x_4')\exp[(i\alpha+\beta)\Delta_{41}].
\end{aligned} \qquad (2\text{-}64)$$

Equations (2-62) and (2-63) can be solved exactly for $e_o(x')$ in the amplifier and absorber respectively. Finally, a dispersion relation is obtained when the boundary conditions (2-64) are used to match the two sets of solutions. It is shown in Appendix A that $\beta = \beta_r + i\beta_i$ must satisfy the characteristic

equations

$$\begin{aligned}
&\beta_r^3-3\beta_r^2\beta_i+q(\beta_r^2-\beta_i^2)-2\alpha\beta_i\beta_r+u\beta_r-\alpha v\beta_i \\
&\qquad +[(b_1A_1-b_2A_2)-\beta_i(s_1B_1-s_2B_2)]/2L' = 0 \\
&3\beta_i\beta_r^2-\beta_i^3+\alpha(\beta_r^2-\beta_i^2)+2q\beta_i\beta_r+\alpha v\beta_r+u\beta_i+\alpha\gamma_2 \\
&\qquad +[\beta_i(s_1A_1-s_2A_2)+(b_1B_1-b_2B_2)]/2L'=0
\end{aligned} \tag{2-65}$$

where the quantities q, u, v, b_1, b_2, A_1, A_2, s_1, s_2, B_1 and B_2 are functions of β, the CW intensities and the laser parameters (Appendix A).

2.4.2 Solutions of the Characteristic Equations

The characteristic equations (2-65) are so complicated that no simple analytic solutions can be found. Accordingly, for a given set of laser parameters, the behaviour of β is investigated by numerical analysis. In particular, a positive value of β_r implies that the CW solutions are unstable and may evolve to pulsing solutions.

Observe that the value of the integer n for the discrete parameter $\alpha=\alpha_n = 2n\pi/L'$ corresponds to the number of pulses circulating in the laser ring cavity. We will only deal with positive values of n since the algebraic sign of n merely indicates the direction of propagation of the radiation so that a negative value of n does not lead to an independent solution for β. Indeed, for a given set of parameters, changing the sign of n would simply reverse the sign of β_i while leaving the value of β_r unchanged. This is a consequence of employing

an unidirectional ring cavity in our analysis. This property indicates that the relative positions and the sequence of the gain and loss cells assumed (see Fig. 2-1) in the present model is somewhat arbitrary.

Furthermore, it is important to point out that the present analysis does not preclude the case n=0 which may be called the "no pulse" solution of the characteristic equations. We defer this special case to Chapter 6 since it is an important and interesting issue in its own right.

For convenience, we define another parameter, the ratio of low signal loss to gain, as $\gamma_g = \alpha_b L_b / \alpha_a L_a$. An examination of the characteristic equations reveals that the independent parameters actually needed in numerical calculations are R, $\alpha_a L_a$, γ_g, m, n, $L' = L/cT_2$, $\gamma = T_2/T_1$, $\gamma_1 = T_1/T_1'$ and $\gamma_2 = T_2/T_2'$. In general, regions of instability can be determined by setting $\beta_r = 0$ in (2-65) and solving for β_i and λ (or R) when all the other parameters are given. Usually, two pairs of independent solutions for (β_i, λ) will be found (provided that such solutions exist) which serve as the lower and upper limits for the instability region of the CW solutions. Practically, as one of the parameters, say γ_g, is varied and the solutions are plotted in the (λ, γ_g) plane, boundaries separating the stable and unstable regions will be formed. In actual calculations, it may be more useful and convenient to plot λ_o defined by

$$\lambda_o = \frac{\alpha_a L_a}{\ln(R^{-1})} - 1 \qquad (2\text{-}66)$$

instead of the overall pump parameter λ (Eq. (2-54)). Observe that λ_o is a measure of the low signal gain to the linear loss and is known as the "pump parameter" in the analysis of self-locking of lasers[32]. Note that from the definitions of λ and λ_o, we have

$$\frac{\lambda+1}{\lambda_o+1} = 1 - \gamma_g \qquad (2\text{-}67)$$

so that λ reduces to λ_o when $\gamma_g = 0$ which corresponds to the absence of the absorber[31,32]. Furthermore, it is evident that the "laser threshold" is given by

$$\lambda_{th} = 0 \quad \text{or,} \quad \lambda_{o,th} = (1-\gamma_g)^{-1} - 1. \qquad (2\text{-}68)$$

It can be shown, from the relation $\lambda_{th}=0=(\alpha_a L_a-\alpha_b L_b)/\ell n(R_{th}^{-1})-1$, that the threshold reflectivity is given by

$$R_{th} = \exp[-(\alpha_a L_a-\alpha_b L_b)] = \exp[-\alpha_a L_a(1-\gamma_g)]. \qquad (2\text{-}69)$$

These defintions for the laser threshold are very useful and will be frequently employed in subsequent analysis.

2.5 Generation of Steady-State Pulses (SSP)

The investigation of the stability of the CW solutions in the last section provides a preliminary test of whether mode-locking is possible for a given system. However, due to the limitation of the first order perturbation method which linearizes the original non-linear partial differential equations (PDE) it is not possible to ascertain, by an examination of the characteristic equations (2-65), whether an instability in the time-invariant solutions implies pulsing. To verify this, one

has to solve the coupled non-linear PDE's (2-39) and (2-40) to see if steady-state pulse (SSP) solutions exist. As a common practice, this can be done by a finite difference technique[62] since analytical solutions cannot be found.

For the present problem, the space-time coordinate plane is divided into a grid network of appropriate spacings and the original PDE's (2-39) and (2-40) are approximated by finite difference equations (FDE). Using these FDE's, pulse propagation can be carried out by a step-by-step iteration once the initial conditions are specified. Details of the derivation of the FDE's are given in Appendix B. Observe that four sets of FDE's, two for each medium, are obtained. This is a consequence of the discontinuity of matter in the laser cavity, where the gain and loss media are not distributed uniformly throughout the cavity, so that in the propagation simulation, the input section of each cell has to be treated differently from the bulk medium.

In actual calculations, a forward iteration in the time domain is used and we assume that the SSP solutions have been generated when the maximum and minimum field amplitudes and the population inversion have approached certain constant values within the accuracy of the numerical calculations. In essence, this is a numerical simulation for the buildup of the laser pulses from some appropriately chosen initial distribution of radiation in the cavity.

It should be pointed out that the accuracy of the finite difference approximation depends on the time increment size (Δt) used in the numerical iteration. To obtain reliable results, Δt cannot be, under any circumstances, greater than or equal to the recovery times (T_1 and T_1') or phase memory times (T_2 and T_2'). Accordingly, a fairly large amount of computer time is usually required if the buildup time for the SSP is long compared to the relaxation times of the gain and loss media and the cavity round trip time. Fortunately, it is found[61] that changing the lengths of the absorber and amplifier cells in the ring cavity does not give rise to any significant changes in the output pulses as long as the saturated gain and loss are sufficiently low. Consequently, a good deal of computer time can be saved by assuming short gain and loss cells. Practically, this is the actual situation of some laser systems, for example, the CW dye lasers where the lasing and the mode-locking dyes are usually confined to thin optical cells.

2.6 Summary

We have developed a theoretical model for saturable absorber laser mode-locking employing the semiclassical theory together with the rotating wave and slowly varying envelope approximations. Laser dynamical coupled equations have been established and solved exactly for the time-invariant solutions, and a perturbation method is used to investigate the stability of such solutions. The characteristic equations thus derived can be employed to determine whether mode-locking is possible

for a given system. Finally, a finite difference approximation is adopted to facilitate the generation of steady-state pulse solutions by numerical simulation.

For future reference, a summary of all the independent laser parameters needed in actual numerical calculations is given in Table 2-1, where some of the important derived parameters are also listed.

In the following chapters, the theoretical model developed here will be applied to different laser systems.

TABLE 2-1

A summary of the laser parameters employed

(A) Independent Parameters:

Definition	Physical Meaning
R	Equivalent intensity reflectivity of the laser cavity, accounts for all the linear losses.
$\gamma = \frac{T_2}{T_1}$	Ratio of phase coherence time (T_2) to recovery time (T_1) of the amplifier.
$\gamma_1 = \frac{T_1}{T_1'}$	Ratio of recovery times of amplifier (T_1) and absorber (T_1').
$\gamma_2 = \frac{T_2}{T_2'}$	Ratio of phase coherence times of amplifier (T_2) and absorber (T_2')
$m = m_d m_o$	$m_d = \mu_b/\mu_a$ is the ratio of electric dipole moments of absorber (μ_b) and and amplifier (μ_a), m_o^2 is the ratio of laser beam sizes in amplifier and absorber.
$\alpha_a L_a$	Low signal gain per round trip of amplifier.
$\gamma_g = \frac{\alpha_b L_b}{\alpha_a L_a}$	Ratio of low signal loss of absorber ($\alpha_b L_b$) to low signal gain of amplifier
$L' = \frac{L}{cT_2}$	Normalized ring cavity perimeter, c is the phase velocity of radiation propagation
n	An integer associated with the discrete parameter $\alpha_n = 2n\pi/L'$ and corresponds to the number of pulses circulating in the ring cavity.

(continued)

Table 2-1 (continued)

(B) Derived Parameters:

Definition	Physical Meaning
$r = \sqrt{R}$	Equivalent amplitude reflectivity
$\gamma' = \frac{T_2}{T_1'}$	Ratio of phase coherence time of amplifier to recovery time of absorber
$\gamma_b = \frac{T_2'}{T_1'}$	Ratio of phase coherence and recovery times of absorber
$\lambda = \frac{\alpha_a L_a - \alpha_b L_b}{\ell n(R^{-1})} - 1$	Overall pump parameter $= \frac{\text{"net" low signal gain}}{\text{cavity linear loss}} - 1$
$\lambda_o = \frac{\alpha_a L_a}{\ell n(R^{-1})} - 1$	Pump parameter $= \frac{\text{low signal gain}}{\text{cavity linear loss}} - 1$
$\lambda_{th} = 0$ $\lambda_{o,th} = \frac{1}{1-\gamma_g} - 1$ $R_{th} = \exp[+(\alpha_a L_a - \alpha_b L_b)]$	Laser threshold

CHAPTER 3

A SYSTEMATIC STUDY OF MODE-LOCKED CW LASERS

3.1 Introduction:

The theoretical model developed in Chapter 2 can be applied to some mode-locked laser systems provided that all the assumptions made therein hold for those systems. A typical example is the tunable mode-locked CW dye lasers where both the gain and loss media can be approximated by a homogeneously broadened line and can be described fairly well as two-level systems. Besides this, the assumption of homogeneously broadened line also apply for high pressure CO_2 and the CW Nd:YAG lasers. However, before applying our model to any specific system, it seems appropriate to undertake a systematic study on the general behaviour of mode-locked CW lasers, particularly for those circumstances under which atomic coherence effects are important. Accordingly, in this chapter, some model systems are employed for this purpose. It will be shown that such a systematic investigation helps to provide an overall understanding of the physical mechanisms controlling the mode-locking process. In addition, the general procedure and techniques employed for the numerical analysis will form the basic mathematical tool for handling more specific

systems, such as those studied in subsequent chapters.

For the model systems employed, it is assumed that the recovery and the phase coherence times* of both the gain and loss media are comparable to the cavity round-trip time. There are a number of reasons in doing so. First, by using such values for the phase coherence times (T_2 and T_2'), atomic coherence effects will be manifested since the length of the mode-locked pulses will be comparable to T_2 and T_2'. Such coherent phenomena cannot be investigated for parameter ranges typical of mode-locked CW dye lasers since the length of the output pulses is usually much longer than the phase coherence times. Second, in a systematic investigation of the various mode-locked lasers, besides the determination of mode-locking conditions, it is necessary to carry out a good deal of numerical simulation so that SSP from different systems can be compared. This is only possible when all the atomic relaxation times are not too short compared to the cavity round-trip time (L/c) since the time increment (Δt) size used in the finite difference equations (Appendix B) is dictated by these relaxation times. In this context, the use of dye laser media is prohibited as T_2 and T_2' are of the order of 10^{-12} - 10^{-13} sec, while the cavity round trip time is typically $\sim 10^{-9}$ sec.

---

*For conciseness, the term "relaxation times" will be used hereafter, when both the recovery and phase coherence times are referred to.

Finally, the laser parameters used in this chapter are quite close to a 6328 Å He-Ne laser mode-locked by a Ne absorber[63-66], except that the inhomogeneous broadening effect is not accounted for. As this kind of mode-locked system has been well investigated experimentally, some useful information may be obtainable from the results of the theoretical calculations.

In section 3.2, instability regions of the CW solutions are determined for different sets of laser parameters. Variations of mode-locking regions* with the cavity round-trip time and the properties of the gain and loss media are investigated.

In section 3.3, steady-state pulses (SSP) are generated for a range of laser parameters within the mode-locking regime. First of all, the evolution of the SSP from the perturbed CW solutions is shown for some specific cases. In particular, the effects of the positions and lengths of the gain and loss cells on the shape of the SSP and the variation of the build-up time of the SSP for different systems are discussed. Furthermore, the characteristic properties, such as pulse length and peak intensities, of the SSP from different systems are compared. The phenomena of pulse delay and atomic coherence effects are also related to experimental observations.

---

*Although instability in the CW solutions does not necessarily imply mode-locking, the two terms will be used interchangeably since it has been verified by generating the steady-state pulses that instability does imply mode-locking in all the cases investigated.

Finally, some general remarks and comments are presented in the last section. In addition, as an important addendum, the effect of the variation of the parameter $m = m_d m_o$ (Eq. (2-45)) on the mode-locking condition is investigated. Observe that such analysis is not useful for the model systems employed in sections 3.2 and 3.3 since the product $\gamma_1\gamma_2 = T_1T_2/T_1'T_2'$ is of the order of unity for those systems.

3.2 Determination of Mode-Locking Regions:

In this section, a systematic investigation concerning the conditions of mode-locking is described. Attention is focussed on the variation of mode-locking regions with the cavity length, the ratio of the low signal loss to gain and the ratio of the recovery and phase coherence times of the gain and absorption media. The problem of single- and multiple-pulse operation is also discussed.

3.2.1 Numerical Method:

As described in section 2.4.2, regions of instability of the CW solutions can be determined by setting $\beta_r = 0$ in the characteristic equations (2-65) and solving for β_i and R numerically when all other parameters are specified. However, in practice, it is necessary to know first whether such solutions exist (i.e. whether there is an instability region) for a given set of laser parameters, and if so, what are the approximate solutions that can be used as initial values in the numerical iteration process. For the present problem, the

3.2.3 Effects of Varying the Characteristics of the Absorber:

We now investigate the variation of mode-locking regions with the nature of the absorber for a given amplifier and cavity configuration. The values of parameters used for the amplifier and the cavity length are such that self-locking is not attainable for the given value of n. On the other hand, the characteristics of the absorber are treated parametrically, regarding the low signal loss ($\alpha_b L_b$), the recovery (T_1') and phase coherence (T_2') times as independent parameters.

In Fig. 3-2, the relaxation times of the absorber are changed while keeping the low-signal loss constant, whereas in Fig. 3-3, the variable parameter is the low-signal loss. The family of curves presented in Fig. 3-2 shows an interesting tendency; it is more and more difficult to achieve mode-locking as γ_1 decreases, i.e., as T_1' increases (since T_1 is being held constant). This is manifested in two correlated ways. On the one hand, as γ_1 decreases, the mode-locking domain shifts, as a whole, towards higher values of λ_o and γ_2, i.e. towards the regions of lower cavity loss (higher R) and broader absorption line (smaller T_2'). On the other hand, the mode-locking domain shrinks as γ_1 is decreased which indicates that the conditions for mode-locking are more difficult to attain for those absorbers which recover more slowly. Indeed, for $\gamma_1 \lesssim 1.19$ which corresponds to $T_1' \gtrsim L/c$, no mode-locking regions can be found within the parameter range investigated.

Fig. 3-1 Comparison of the regions of instability with and without the saturable absorber by varying the reduced cavity perimeter $L' = L/cT_2$. Parameters: $\alpha_a L_a = 0.30$, $\gamma = 0.182$, $\gamma_1 = 2.500$, $\gamma_2 = 0.900$, $m = 1$ and $\gamma_g = 0.25$ when the absorber is present. The values of n shown are the lowest ones allowed within those regions of L'. Observe the changes in n with the incorporation of the absorber. Note that the value of m=1 is used throughout this chapter except in Fig. 3-10.

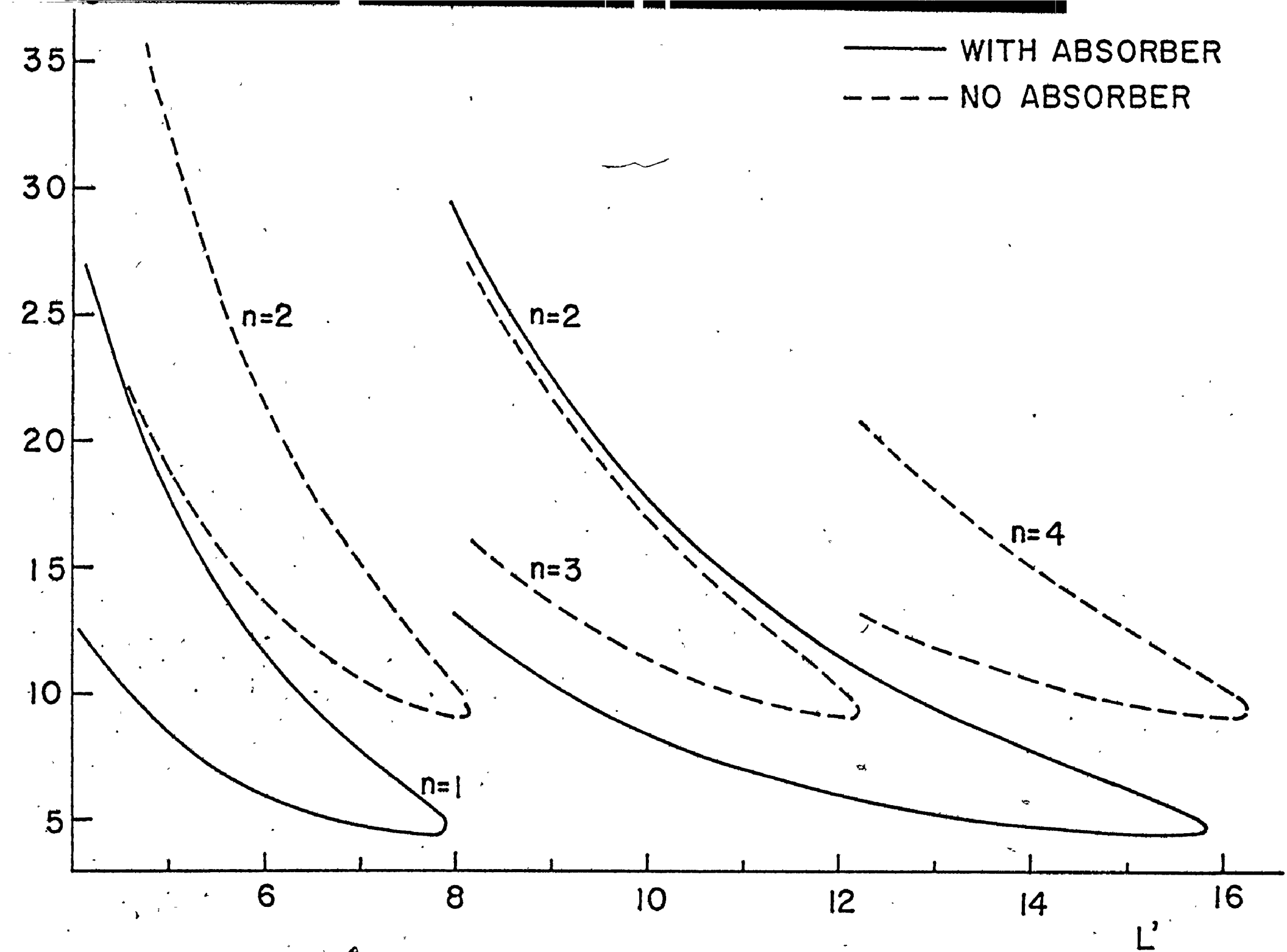
WITH ABSORBER
NO ABSORBER
35
30
25
20
15
10
5
n=2
n=2
n=3
n=4
n=1
6
8
10
12
14
16
L'

Fig. 3-1

mode-locking and CW operation regimes. In this figure, it can be seen that for a given cavity perimeter, mode-locking can be achieved more easily with the insertion of the absorber since the minimum value of λ_o required is lower. In other words, for a given amplifier and cavity length, the minimum value of the reflectivity R required for attaining mode-locking is lower, since λ_o is defined as $\alpha_a L_a / \ell n(R^{-1}) - 1$. Clearly, a linear loss will not give the same results. Note particularly the changes in n to lower values with the incorporation of the absorber. This indicates that for a given cavity and amplifier, it may be possible to suppress the multiple-pulse mode-locked operation and convert to single-pulse operation by using an appropriate absorber so that more intense pulse can be obtained.

In addition, for a given pump parameter and active media, the preference for higher n as the cavity length increases can also be seen from Fig. 3-1, for both self and induced mode-locking. In fact, if one draws a line of constant λ_o, it will cut, respectively, the lower and upper mode-locking boundaries belonging to different n's at those points where the ratios of L/n are approximately equal. This is not unexpected since it merely shows that the number of pulses per round-trip period will increase in proportion with the increase in the cavity length. Indeed, the phenomenon of multiple-pulse operation for sufficiently long laser cavities has been observed experimentally[13,14].

3.2.3 Effects of Varying the Characteristics of the Absorber:

We now investigate the variation of mode-locking regions with the nature of the absorber for a given amplifier and cavity configuration. The values of parameters used for the amplifier and the cavity length are such that self-locking is not attainable for the given value of n. On the other hand, the characteristics of the absorber are treated parametrically, regarding the low signal loss ($\alpha_b L_b$), the recovery (T_1') and phase coherence (T_2') times as independent parameters.

In Fig. 3-2, the relaxation times of the absorber are changed while keeping the low-signal loss constant, whereas in Fig. 3-3, the variable parameter is the low-signal loss. The family of curves presented in Fig. 3-2 shows an interesting tendency; it is more and more difficult to achieve mode-locking as γ_1 decreases, i.e., as T_1' increases (since T_1 is being held constant). This is manifested in two correlated ways. On the one hand, as γ_1 decreases, the mode-locking domain shifts, as a whole, towards higher values of λ_o and γ_2, i.e. towards the regions of lower cavity loss (higher R) and broader absorption line (smaller T_2'). On the other hand, the mode-locking domain shrinks as γ_1 is decreased which indicates that the conditions for mode-locking are more difficult to attain for those absorbers which recover more slowly. Indeed, for $\gamma_1 \lesssim 1.19$ which corresponds to $T_1' \gtrsim L/c$, no mode-locking regions can be found within the parameter range investigated.

Fig. 3-2 Regions of instability with the incorporation of the absorber. Parameters: $L' = 4.615$, $n = 1$, $\gamma = 0.182$, $\alpha_a L_a = 0.30$ and $\gamma_g = 0.25$. The pump parameter λ_o is plotted as a function of γ_2 with γ_1 as a variable parameter. No regions of instability can be found (as if the absorber is absent) for $\gamma_1 \lesssim 1.19$ which corresponds to $T_1' \gtrsim L/c$.

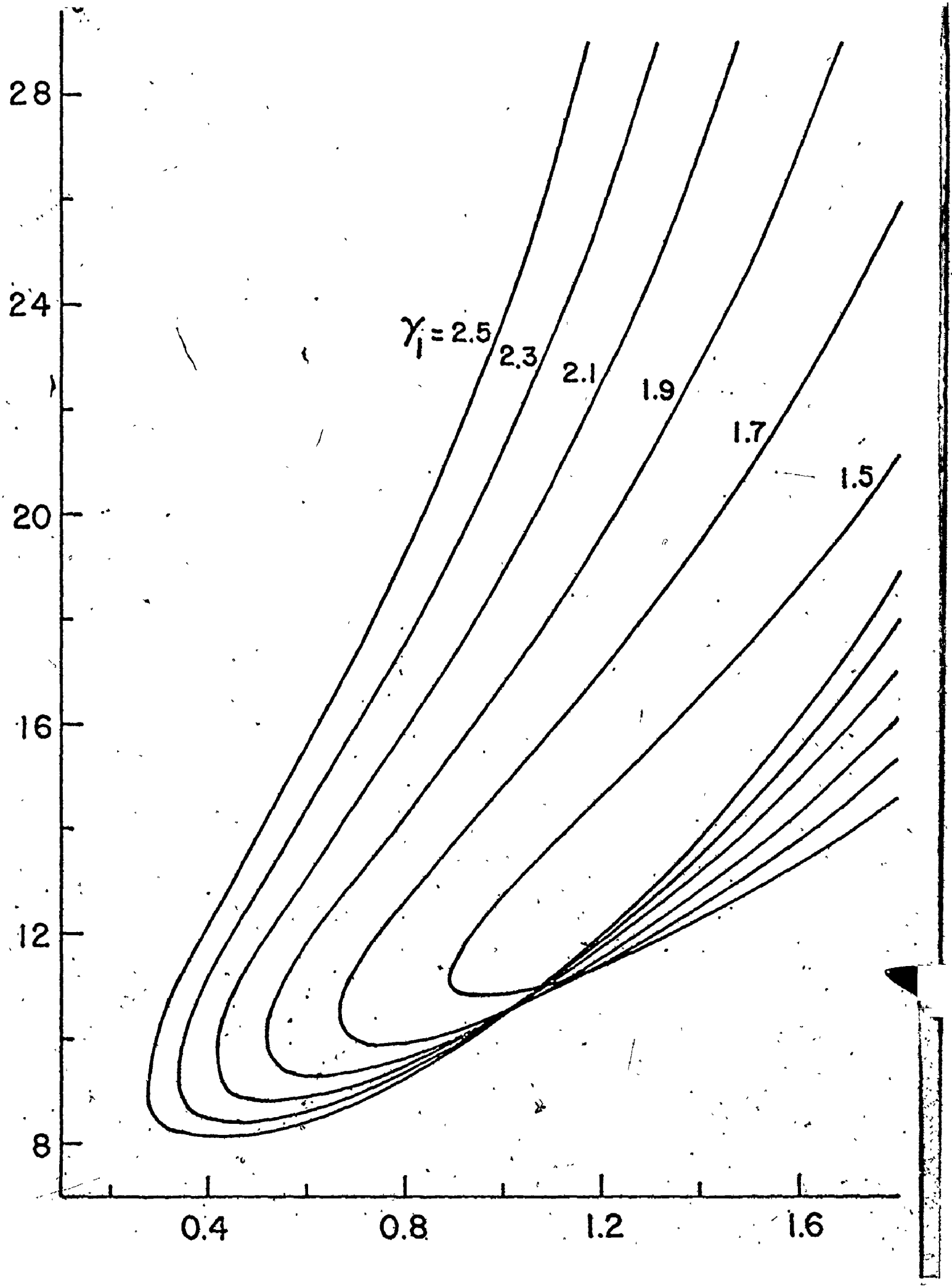
28
24
20
16
12
8
0.4
0.8
1.2
1.6
$\gamma_1 = 2.5$
2.3
2.1
1.9
1.7
1.5

Fig. 3-3 Variation of instability regions with γ_g for $L' = 4.231$, n = 1 mode. Other parameters: $\alpha_a L_a = 3.000$, $\gamma = 0.182$, $\gamma_1 = 2.500$, $\gamma_2 = 0.900$. Mode-locking cannot be attained for $\gamma_g \lesssim 0.037$ and for γ_g approaches unity.

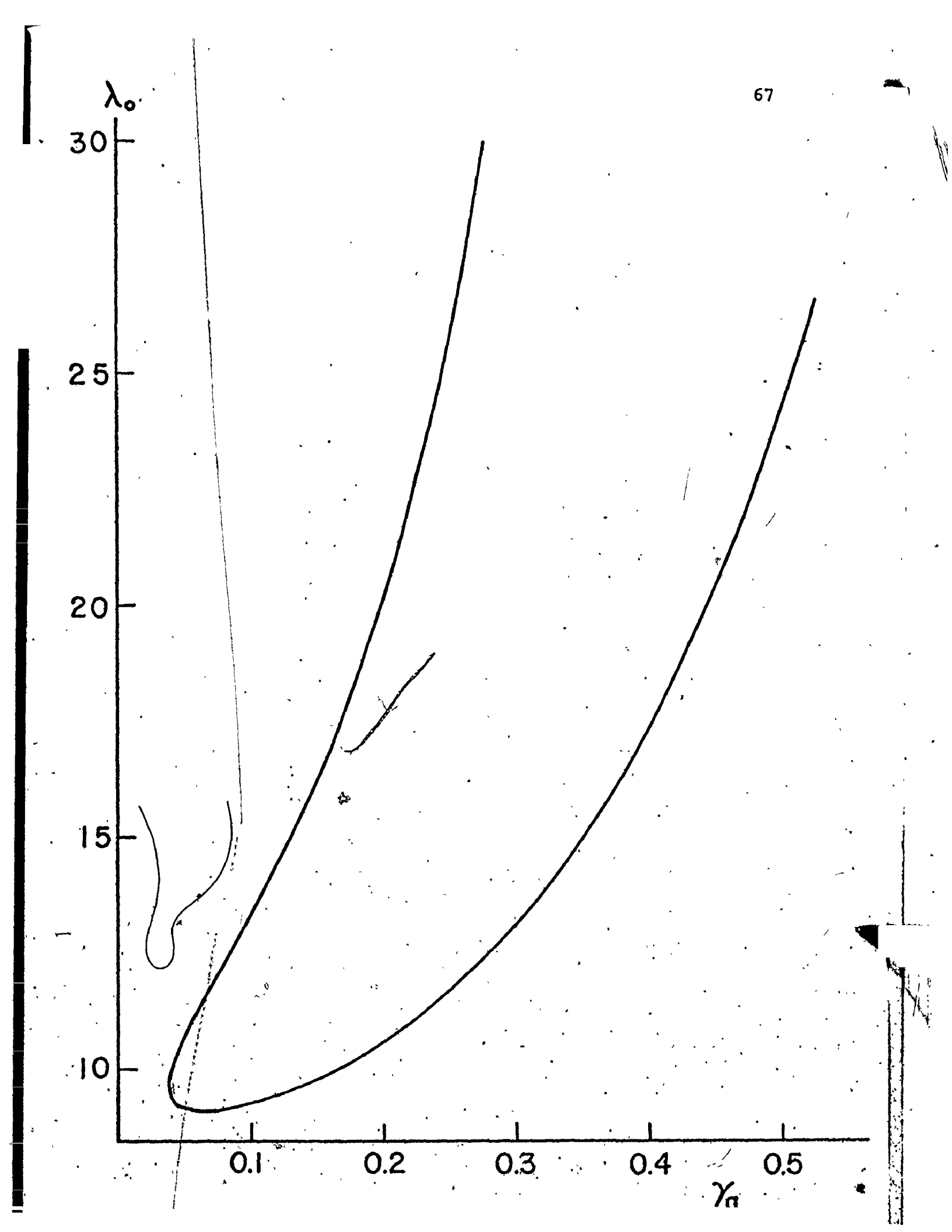
λo
30
25
20
15
10
0.1
0.2
0.3
0.4
0.5
γn

Note that this lower limit of γ_1 depends on the parameter values used for the amplifier and the resonator. However, the restraint upon the absorber that the recovery time should be shorter than, or of the order of the cavity round-trip time is generally true for all cases investigated.

In Fig. 3-3, the variation of mode-locking regions with the low signal loss of the absorber is shown. It indicates that the ratio γ_g of the low-signal loss of the absorber to the low-signal gain of the amplifier should be appropriately chosen in order to attain mode-locking. In general, for a given amplifier and cavity length, there is a minimum value for γ_g below which mode-locking is not possible. Furthermore, the value of $\lambda_{o,min}$ for the lower boundary of mode-locking regime increases very rapidly as γ_g goes towards unity, which shows that it is very difficult to achieve mode-locking as the low-signal loss of the absorber approaches the low-signal gain of of the amplifier. On the other hand, further investigation shows that mode-locking regions do not change significantly over a fairly wide range of either the low-signal gain ($\alpha_a L_a$) or the low-signal loss ($\alpha_b L_b$), provided that they are varied in proportion so that γ_g is a constant. This property is also shown up in the steady-state pulse solutions which will be discussed in the next section.

3.3 Steady-State Pulse (SSP) Solutions:

The analysis presented in the last section provides a preliminary test of whether mode-locking is possible for a given system. In this section, we employ the finite difference equations (Appendix B) to generate the SSP solutions for some specific cases. The aims of such analysis are two fold. First, it verifies directly whether an instability in the time-invariant (CW) solutions implies pulsing for a given system since, as mentioned in Chapter 2, it is not possible to ascertain this point by an examination of the characteristic equations. Second, by comparing the output pulses from different mode-locked systems, it may be possible to predict how to obtain shorter and more intense pulses by a proper choice of the laser parameters.

To carry out a systematic study, we will first show the evolution of the SSP from the perturbed CW solutions. The relationship between the build up time of the SSP and the numerical value of β_r in the exponent of the perturbation $\sim \exp(\beta_r t')$ will also be discussed. After this, the characteristics of the output pulses, in particular, the pulse length and the peak intensity, from different laser systems are compared.

3.3.1 Evolution of the SSP from the Perturbed CW Solutions:

(a) Effects of the Lengths and Positions of the Gain and Loss Cells

The mathematical form of the dispersion equation for β_r and β_i indicates that the conditions of mode-locking will not be affected by varying the lengths and/or position of the

gain and loss cells in the laser cavity, provided that the low-signal gain and loss per round trip are both held constant. This has been discussed in Chapter 2. It has also been pointed out that the SSP solutions will not be changed significantly by such variations. To illustrate this, typical results are presented in Fig. 3-4 where the evolution of the field amplitudes are plotted as a function of the number of round trips N for both long and short gain and loss cells. It can be seen that there is just a little difference in the build-up rates for both cases, while the final maximum and minimum amplitudes are essentially the same. In addition, it has been found that the relative positions of the cells in the cavity are also immaterial. As a consequence, in subsequent presentation of the numerical results, both the lengths and positions of the amplifier and absorber cells will not be stated explicitly.

It should be noted that the phenomenon that the shape of the output pulses does not depend on the lengths and positions of the gain and absorption cell is a consequence of employing a uni-directional ring cavity in our model. In a normal laser resonator, it has been observed[63] that the positions of the cells are very important in the determination of the number of pulses in the laser cavity. This difference indicates that certain modifications are required when a normal laser is described by an equivalent ring laser, as already pointed out in Chapter 2 (section 2.2.1).

Fig. 3-4: The maximum and minimum (normalised to the CW value) electric field amplitudes at the output mirror as a function of N, the number of round trips. Parameters: $L' = 4.231$, $\alpha_a L_a = 3.00$, $\gamma_g = 0.25$, $\gamma_1 = 2.50$, $\gamma_2 = 0.90$ and $\lambda_o = 18.74$. Note that the difference in growing rates for long (solid lines) and short (dotted lines) cells is small and the values of E_{max} and E_{min} of the SSP are essentially the same.

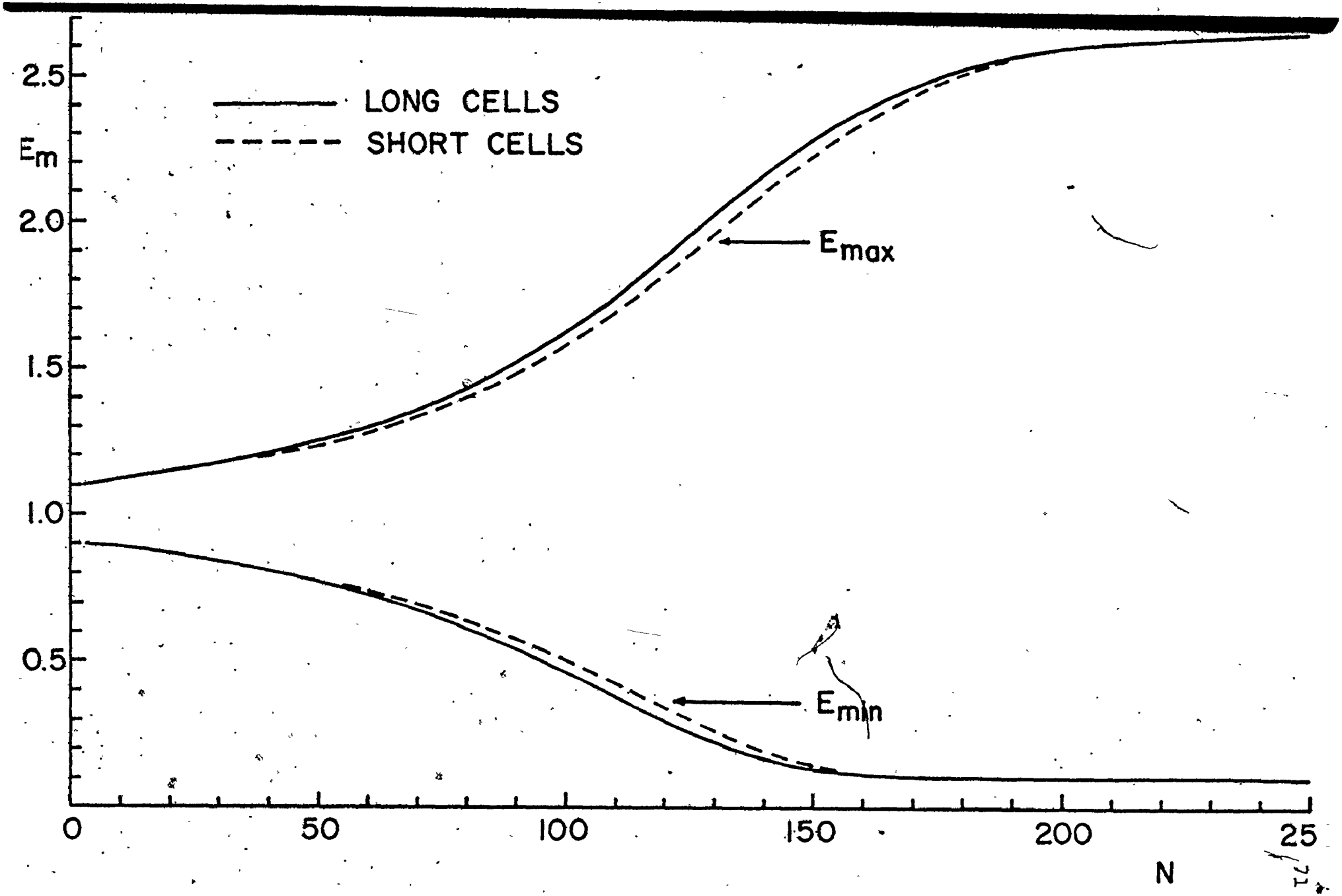
LONG CELLS
SHORT CELLS
E_m
E_{max}
E_{min}
2.5
2.0
1.5
1.0
0.5
0
50
100
150
200
25
N

Fig. 3-4

(b) Relationship Between the Value of β_r and the Establishment Time of the SSP:

Recall that in the perturbation analysis (section 2.4), we have assumed the functional form $f(x',t') = f_o(x')\exp(i\alpha x'+\beta t')$ with $\beta=\beta_r+i\beta_i$ for the small perturbations about the CW solutions. Accordingly, if the CW solutions are unstable ($\beta_r>o$), the small variations will grow in time as $\sim \exp(\beta_r t')$. Therefore, the numerical value of β_r as solved from the characteristic equations may give us an estimate of the establishment time of the SSP from the perturbed CW state. However, observe that the evolution of the SSP solutions will follow the envelope defined by the functional form $\exp(\beta_r t')$ only during the initial stage. This is a consequence of the first order perturbation adopted in our analysis. Accordingly, for different systems, the actual buildup time of the SSP is not always proportional to the value of β_r. This is illustrated in Fig. 3-5. As a matter of fact, it is fair to say that the eigenvalue β_r may give us a rough estimate for the establishment time of the SSP.

(c) Justification of the Steady-State Pulse Solutions:

As the generation of the SSP employing the finite difference equations is a kind of numerical simulation, it is important to determine when the iteration process can be terminated. In practice, one can judge this by observing that the maximum and minimum field amplitudes and population inversions have approached certain constant values (within the precision of the numerical calculations) and maintain these values over a

Fig. 3-5: Plot of the maximum and minimum (normalized to the CW value) electric field amplitudes as a function of N showing the relationship between the growing rate of the field and the value of the real part of β:

(a) $L' = 4.615$, $n = 1$, $\gamma_g = 0.25$, $\alpha_a L_a = 3.00$, $\lambda_o = 15.00$ and $\gamma_1\gamma_2 = 2.40$. The values of $\beta_r = 3.43$, 2.15 and 0.89×10^{-3} for $\gamma_1 = 2.40$, 2.00 and 1.60 respectively.

(b) $L' = 4.231$, $n = 1$, $\gamma_1 = 2.50$, $\gamma_2 = 0.90$, $\lambda_o = 18.74$ and $\gamma_g = 0.25$. The values of $\beta_\gamma = 4.11$, 6.05, 7.08 and 7.12×10^{-3} for $\alpha_a L_a = 3.00$, 5.00, 7.00 and 9.00 respectively. The growing rate as shown in (a) is proportional to β_r. However, this is not always true as can be seen from (b).

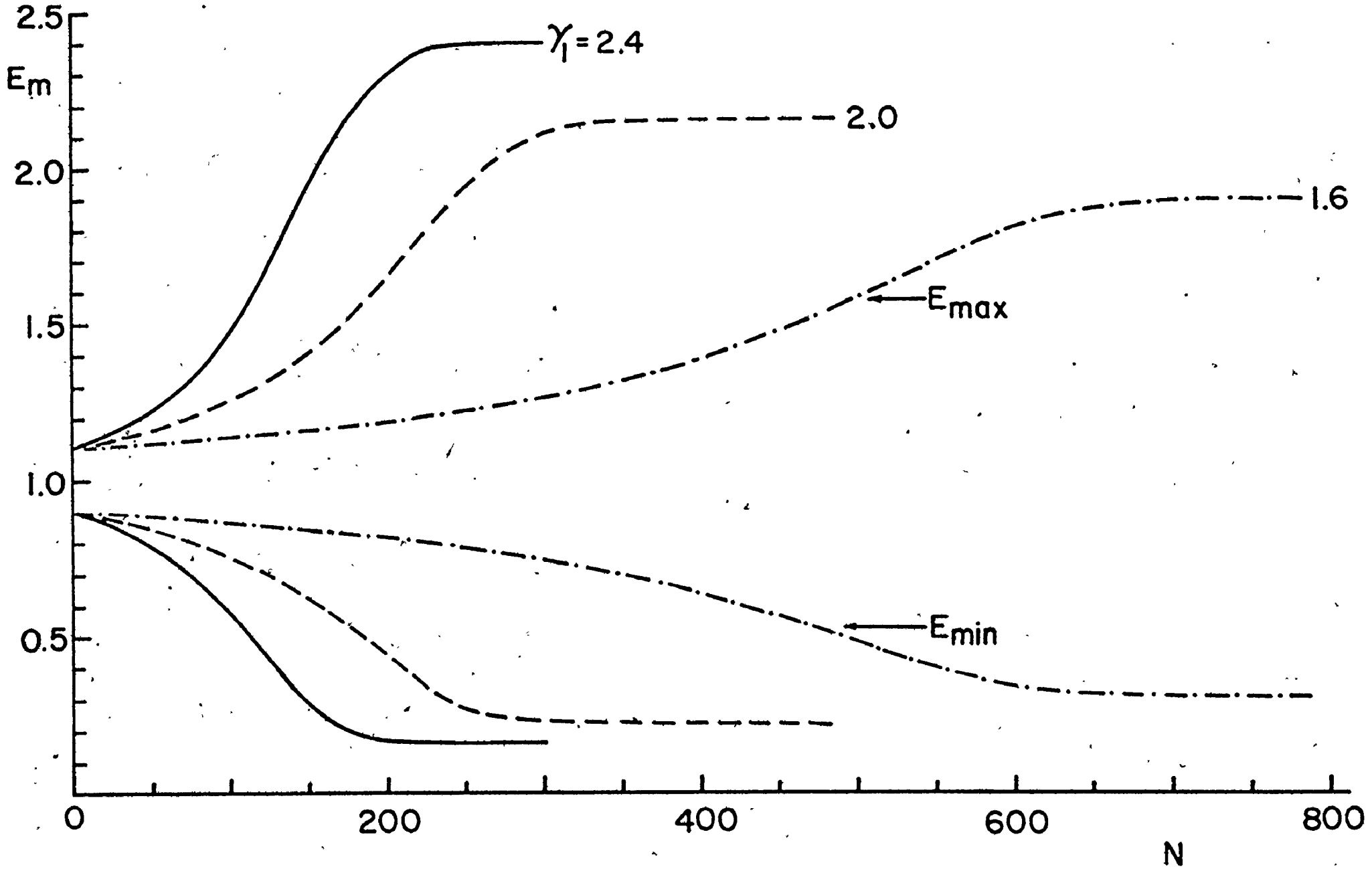

Fig. 3-5(a)

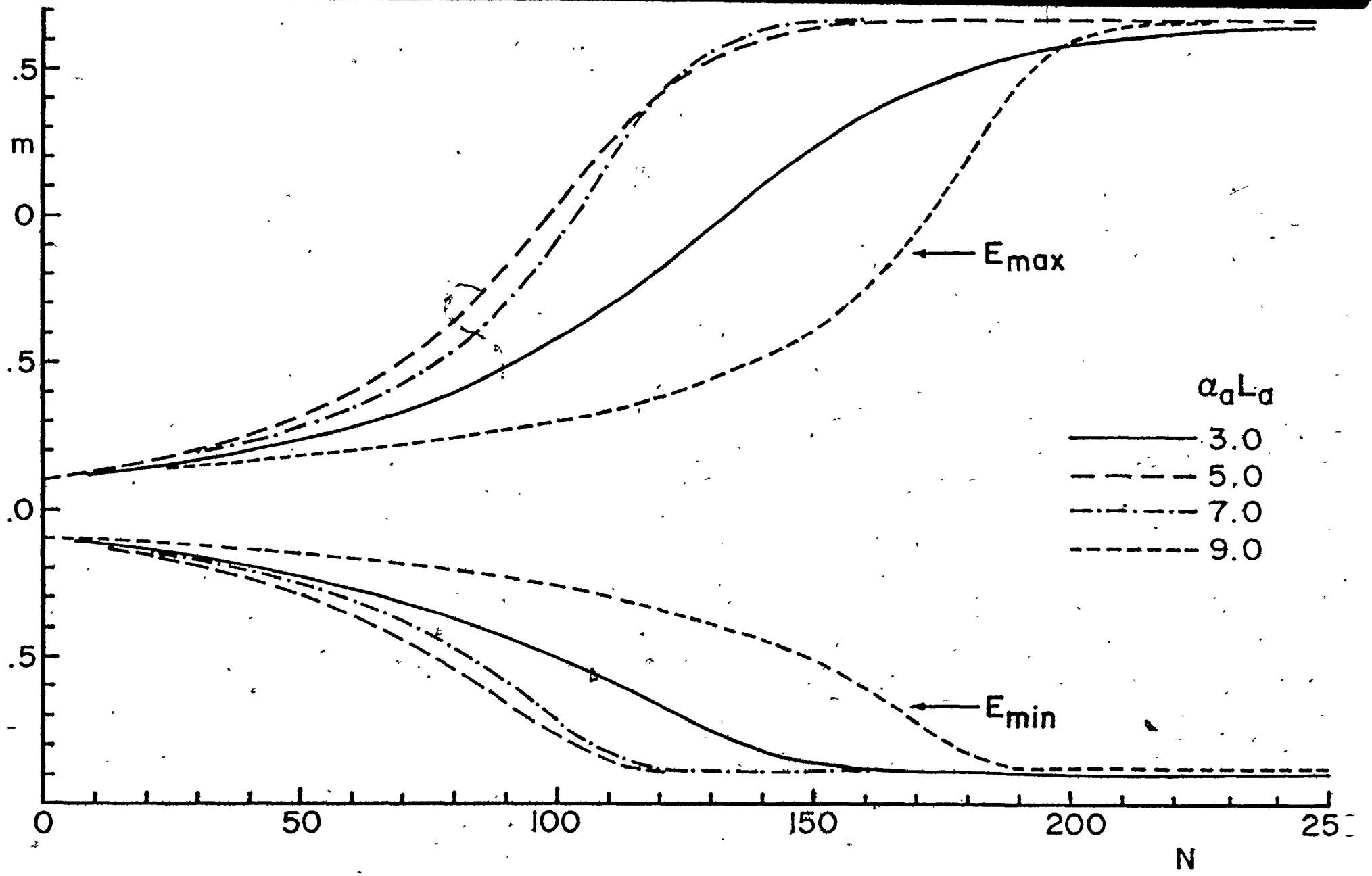

Fig. 3-5 (b)

reasonable period of time. A typical example is shown in Fig. 3-6, where the pulse velocity is also plotted as a function of the number of round-trips. It can be seen that the pulse velocity (v) also tends towards a constant value as the steady-state is approached. This indicates that the repetition rate of the mode-locked pulses has a well defined value since it is proportional to v/L.

3.3.2 Characteristic Properties of SSP:

To further our physical insight into the mechanisms of the production of the mode-locked pulses, it is useful to compare the variation of the SSP properties as the laser parameters are changed. Extensive calcualtions have been done for this purpose and some representative results are tabulated in Table 3-1 with the corresponding SSP plotted in Figs. 3-7 and 3-8.

As an arbitrary standard, all the numerical data for the SSP are taken from the output section of the absorber which corresponds to the point D (reduced space coordinate x_4') in Fig. 2-1(b). In Table 3-1, I_{max} and I_{min}' are, respectively, the maximum and minimum intensities of the SSP normalized to the CW intensity (I_{CW}). The pulse widths ($\Delta\tau_I$) are the full-width at half maximum (FWHM) obtained by using an appropriate interpolation technique. The quantity <I> is the average intensity (normalized to I_{CW}) over one pulse period and θ is the pulse area defined by*

---

*See footnote on page 13 (Chapter 1) for the definition and physical significance of θ.

Figure 3-6: Maximum and minimum inversion and the electric field amplitudes (normalized to the CW values) at the output section of the absorber and the relative excess velocity (v-c)/c of the pulse as a function of the number of round trips. Parameters: the same as in Fig. 3-4.

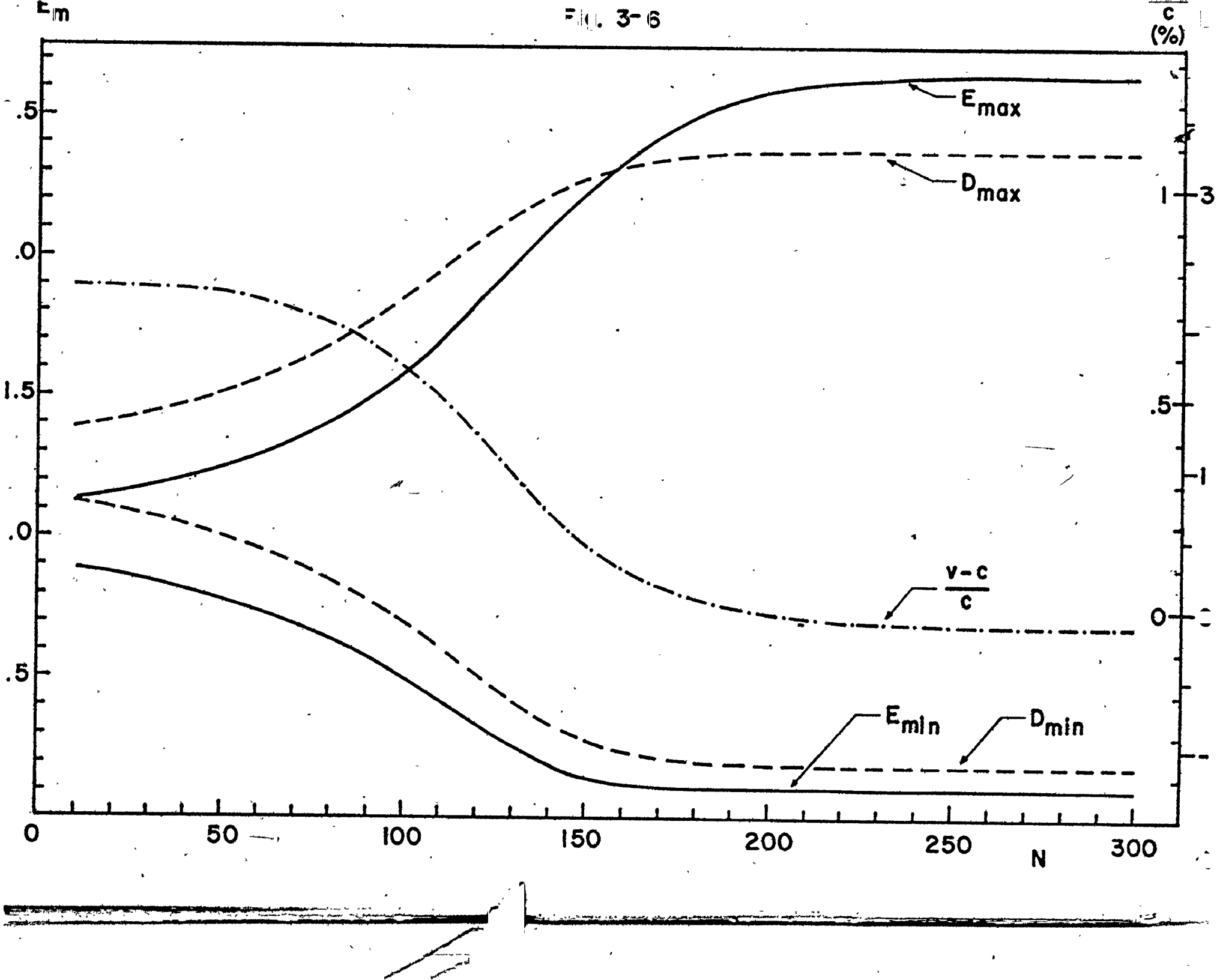
Em
c (%)
.5
.0
1.5
.0
.5
1
.5
0
1
3
Emax
Dmax
V-C / C
Emin
Dmin
0
50
100
150
200
250
N
300

$$\theta = \int \frac{\mu_b \mathcal{E}_b}{\hbar} dt = \int E_b dt'$$

as $E_b = \mu_b \mathcal{E}_b T_2/\hbar$ and $t' = t/T_2$. Note that r is the amplitude reflectivity so the $\theta \times r$ is the pulse area at the input section of the amplifier (point A in Fig. 2-1(b)). Furthermore, the pulse shape is described by the asymmetricity A defined as

$$A = (T_r - T_f)/T$$

where T_r and T_f are respectively the rise time of the leading front and the falling time of the trailing edge, and T is the pulse duration so that $T = T_r + T_f$. By this definition, a negative (positive) asymmetricity implies that the pulse is steeper in the leading (trailing) edge. Finally, the excess velocity $(v-c)/c$ indicates the difference between the pulse velocity v (the velocity of the pulse peak) and the phase velocity c. Therefore, v is greater than c if the excess velocity is positive.

The SSP plotted in Figs. 3-7 and 3-8 correspond to the output pulses over two round trip periods. All pulses are normalized to their respective CW intensities and the pulse minima are adjusted to fall at the time origin so that deviation of the intensities from the CW values and the difference in rise times can be easily compared.

In Table 3-1(a) and Fig. 3-7, the variation of the pulse characteristics with the ratio (γ_g) of the low-signal loss of the absorber to the low-signal gain of the amplifier is shown. The cavity loss is kept constant, since λ_o is fixed. It can

Table 3-1

Characteristic Properties of the SSP

(a) Parameters: $L' = 4.231$, $\gamma = 0.182$, $\gamma_1 = 2.5$, $\gamma_2 = 0.9$, $\lambda_o = 18.74$, $\alpha_a L_a = 3.0$

Pulse Properties

γ_g	I_{CW}	I_{max}	I_{min}	$\Delta\tau_I^*$	$\langle I \rangle$	θ	θxr	A	$(v-c)/c$ (%)
0.20	2.084	8.264	0.005	0.464	1.061	3.872	3.588	0.028	0.024
0.25	1.717	7.035	0.012	0.549	1.082	3.869	3.586	-0.043	-0.043
0.30	1.371	5.584	0.027	0.707	1.096	3.821	3.541	-0.093	-0.130
0.35	1.054	4.065	0.069	0.961	1.092	3.729	3.546	-0.121	-0.239
0.40	0.778	2.456	0.255	1.421	1.049	3.553	3.293	-0.079	-0.396

(b) Parameters: $L' = 4.615$, $\gamma = 0.182$, $\lambda_o = 15.0$, $\alpha_a L_a = 3.0$, $\gamma_g = 0.25$, $\gamma_1\gamma_2 = 2.40$

Pulse Properties

γ_1	I_{CW}	I_{max}	I_{min}	$\Delta\tau_I^*$	$\langle I \rangle$	θ	θxr	A	$(v-c)/c$ (%)
3.00	1.334	7.460	0.006	0.612	1.139	3.686	3.356	-0.136	-0.149
2.60	1.334	6.382	0.018	0.668	1.092	3.918	3.567	-0.036	-0.065
2.20	1.334	5.220	0.038	0.772	1.051	4.142	3.771	0.033	0.042
1.80	1.334	4.126	0.070	0.937	1.019	4.374	3.982	0.081	0.191

*The values of pulse length $\Delta\tau_I$ are in units of T_2 since we have defined $t' = t/T_2$.

Fig. 3-7 Steady-state output pulses of mode-locked lasers with saturable absorber. All pulses are normalized to their respective CW values and pulse minima are adjusted to fall exactly at the time origin. Parameters: $L' = 4.231$, $\gamma = 0.182$, $\gamma_1 = 2.500$, $\gamma_2 = 0.900$, $\lambda_o = 18.74$, $\alpha_a L_a = 3.00$. For $\gamma_g = 0.20$, 0.25, 0.30, 0.35 and 0.40, pulse widths = 0.464, 0.549, 0.707, 0.961 and 1.421 (in units of T_2) respectively.

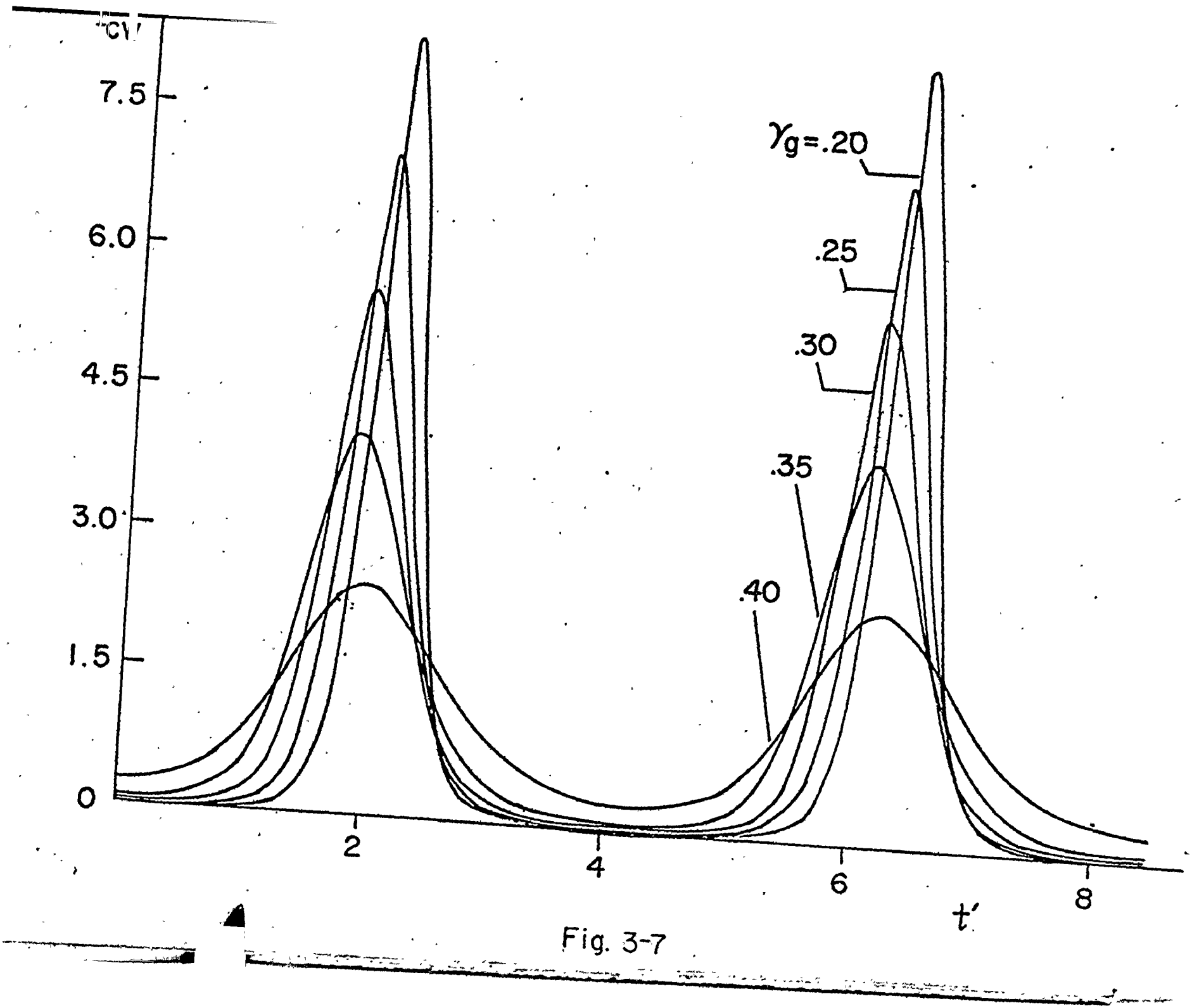

Fig. 3-7

Fig. 3-8 Steady-state output pulses of mode-locked lasers with saturable absorber. All pulses are normalized and adjusted as done in Fig. (3-7). Parameters: $L' = 4.615$, $\gamma = 0.182$, $\lambda_o = 15.00$, $\alpha_a L_a = 3.00$, $\gamma_g = 0.25$ and $\gamma_1\gamma_2 = 2.40$. For $\gamma_1 = 3.00$, 2.60, 2.20 and 1.80, pulse widths = 0.612, 0.668, 0.772 and 0.937 (in units of T_2) respectively.

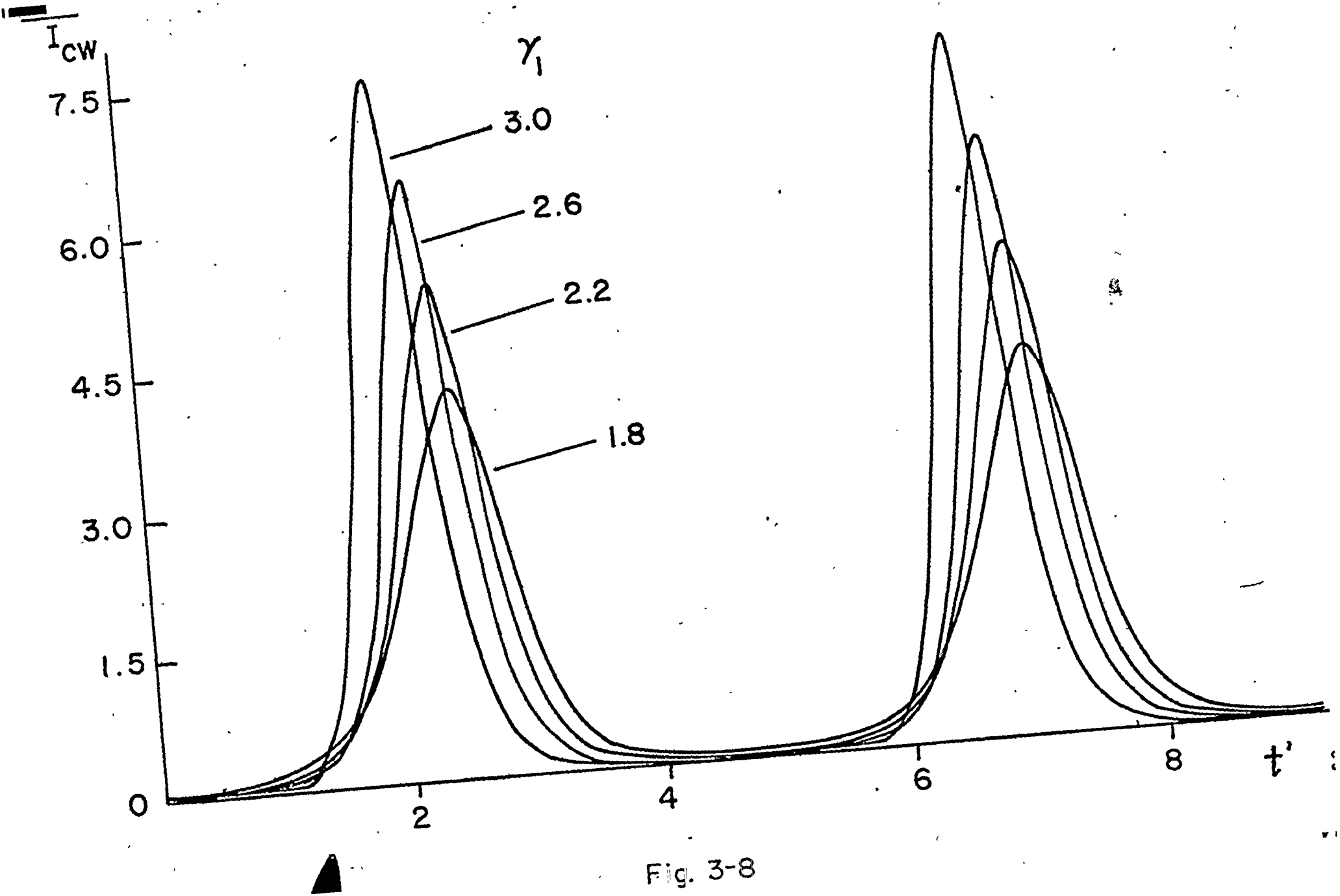

Fig. 3-8

be seen that, all pulses are asymmetrical but the leading front is not always steeper than the trailing edge. Furthermore, the pulse becomes narrower and more intense as the value of γ_g is decreased. However, note that there exists a limit for this process since for a given λ_o', mode-locking will not be possible if γ_g is smaller than some minimum value (see Fig. 3-3). This implies that, for the production of short pulses, the absorption of the loss medium should be kept as low as possible. It is also evident that the pulse delay caused by the absorber increases with increasing γ_g. Similar results are presented in Table 3-1(b) and Fig. 3-8 except that here γ_g is fixed and the relative magnitudes of γ_1 and γ_2 are varied while keeping their product $\gamma_1\gamma_2$ constant, i.e., the saturation intensities of both the gain and absorbing media are not altered. Physically, it turns out that although the saturation intensity of the absorber is kept constant, output pulses will be narrower, more intense and travel more slowly if the absorbing two-level systems recover more rapidly and dephase more slowly compared to the round-trip time (L/c), within the mode-locking regime. This indicates that the concept of saturation intensity is not strictly applicable for the pulsing solutions.

In addition, observe that for all the SSP's shown, the pulse length is comparable to the phase coherence times of the active media and the pulse area θ is of the order of π . As a consequence, coherence effects are important for these systems. To examine this more closely, a representative case is shown

in Fig. 3-9 where the (normalized) field amplitude, the polarization and the inversion are plotted as a function of the local time for two round-trip period. The coherent pulsation of the population inversion as the radiation passes by can be seen clearly. Observe that the pulse is so intense that the inversion drops very fast and changes sign after the passage of the pulse peak. This phenomenon is very similar to the π-pulses observed in self-locked lasers[13,29] and in laser amplifiers[58]. It should be pointed out that the rate equation approach will certainly not give rise to this kind of steady-state solution.

From a practical point of view, the coherence-pulse phenomenon is very important for the generation of ultrashort pulses from high gain and/or narrow line lasers, although such effects may not be of major significance for low-gain mode-locked systems. In fact, the values of the relaxation times used in the model systems are close to the actual values of the 6328 Å He-Ne laser mode-locked by a Ne absorber and the results presented here are in qualitative agreement with the experimental observations[63,64].

3-4 Concluding Remarks:

A systematic investigation concerning the general behaviour of mode-locked CW lasers has been presented in this chapter. It is shown that passive mode-locking of a laser system can be attained by employing a suitable absorber and relatively short and intense pulses can be generated if the relaxation

Fig. 3-9 The steady-state electric field amplitude, polarization and inversion (normalized to the CW values) at the output section of the absorber as a function of time for the parameters given in Fig. 3-6. Observe that the inversion changes sign after the passage of the pulse.

Fig. 3-9

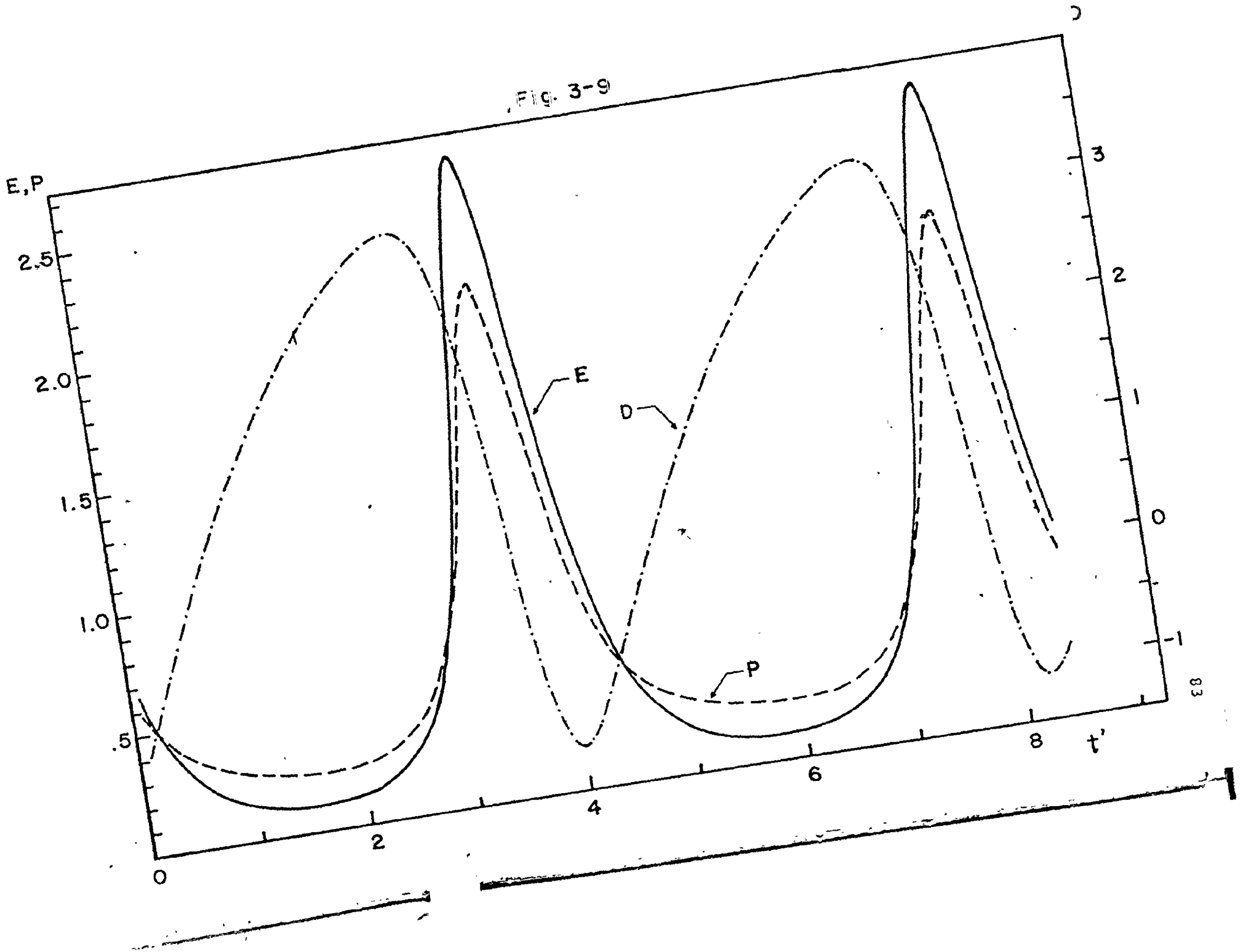

times and the low signal loss of the absorber are appropriately chosen. Furthermore, it is demonstrated that atomic coherence effects are important for some laser systems. In subsequent chapters, the general procedure employed for the analysis in this chapter will be used when the theoretical model is applied to particular laser systems, including the CW dye and other CW or quasi-CW lasers.

Before we proceed to the next chapter, it is important to make a final remark. Observe that for the model systems used throughout this chapter, we have assumed the value of unity for the parameter $m = m_d m_o$ since the product of $\gamma_1\gamma_2 = T_1T_2/T_1'T_2'$ is not too different from one and $m \sim (\gamma_1\gamma_2)^{1/2}$ according to the criterion given by Eq. (2-57). In practice, however, the product of $\gamma_1\gamma_2$, which is proportional to the ratio of the saturation intensities of the absorber and the gain media (section 2.3), is not always close to unity and the behaviour of an actual system may be strongly dependent on the value of m chosen for the numerical analysis. Accordingly, it is very important to investigate how well the criterion that $m \sim (\gamma_1\gamma_2)^{1/2}$ works for a given system. An illustrative example is presented in Fig. 3-10, where the variation of mode-locking regions with m for a given amplifier and absorber is shown. Note that the relaxation times are so chosen that a very wide range of the values of m can be investigated. In fact, the laser parameters used are typical of a practical system consisting of a low-pressure gaseous amplifier and a dye solution absorber[67] in which the radiation is tightly

Fig. 3-10 Variation of mode-locking regions with the parameter m for given amplifier and absorber with $(\bar{I}_{sat})_a << (\bar{I}_{sat})_b$. Parameters: L = 1.80 m, n = 1, $\alpha_a L_a = 0.30$, $\gamma_g = 0.25$, $c = 3.0 \times 10^8$ m-sec^{-1}, $T_1 = 7.15$ nsec., $T_2 = 1.30$ nsec., $T_1' = T_1/\gamma_1$ and $T_2' = T_2/\gamma_2$ with $\gamma_1 = 1.5$, $\gamma_2 = 300.0$. As defined previously, R and λ_o are related by $\lambda_o = \alpha_a L_a / \log(R^{-1}) - 1$. For illustrative purposes, the parameters L, c, T_1 and T_2 rather than the normalised parameters L' and γ are given explicitly.

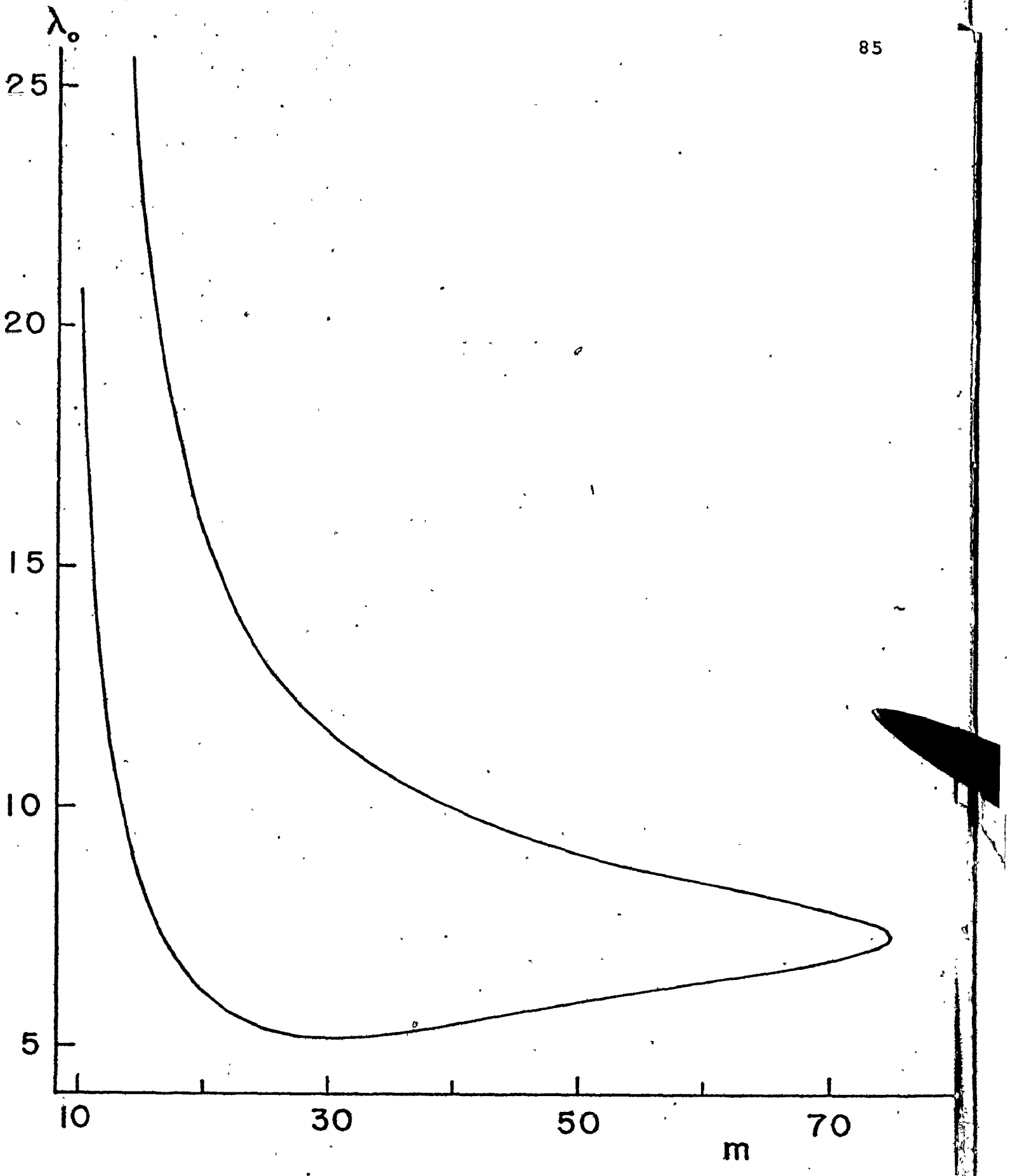

F

focussed onto the absorber so that the value of m_o is quite large. For this figure, it can be seen that there is a broad minimum at $m \approx 30$ which is fairly close to the value of $(\gamma_1\gamma_2)^{1/2}$. Away from this minimum, the curves rise very rapidly for small values of m indicating that mode-locking is more and more difficult to attain as m decreases. Furthermore, there is an upper limit for m beyond which mode-locking is not possible. Therefore, these calculations support the proposition that in order to achieve mode-locking effectively, the value of m should be chosen to be comparable to the square root of the product $\gamma_1\gamma_2$. This rule is very useful and will be frequently employed in subsequent analyses.

CHAPTER 4

THE MODE-LOCKED CW DYE LASERS

4.1 Introduction:

It is well known that the broadband emission of a single dye solution can provide a laser output which is continuously tunable over a wide range of frequencies or wavelengths. In addition, the absorption band of a single dye is broad enough to allow efficient pumping with any one of a variety of lasers as well as with flashlamps[68]. In particular, the development of the laser-pumped CW dye laser and the subsequent mode-locking of this laser are recent achievements of very great interest and importance[7,22-25,69-74]. A typical example is the argon-laser pumped Rhodamine 6G laser[24,25] which has an extremely wide effective atomic linewidth ($\Delta\nu \sim 10^{13}$ Hz) and yet is also capable of stable continuous laser operation at low pumping and oscillation power levels, in the 100 mW to 1 W range. As the limiting pulsewidth capability of any mode-locked laser is given, to first order, by the Fourier uncertainty formula $\tau_p \sim \Delta\nu^{-1}$, the mode-locking of a CW dye laser could produce a continuous train of subpicosecond pulses. More importantly, such a mode-locked laser can

be a source of wavelength-tunable picosecond pulses since the oscillating bandwidth required for a picosecond pulse is considerably less than the effective linewidth of the laser medium.

Mode-locking of the CW dye laser was first accomplished by active modulation within the laser cavity by using an internal acoustic loss modulator or phase modulator[22,23]. In addition, experiments with mode-locked-pump excitation of CW dye lasers have also been performed[72-74]. However, neither of these techniques has led to the production of picosecond pulses.

Most recently, passive mode-locking of the CW Rhodamine 6G dye lasers has been reported[24,25]. Continuous train of pulses as short as 1.5 psec were observed. Several interesting and important questions have been raised concerning this type of mode-locked laser. In the first place, it has been noted that the observed pulse length is much shorter than the recovery time of the saturable absorber (DODCI*) or its photoisomer, which is believed to play a dominant role in the mode-locking process[75-77]. Furthermore, the recovery time of the laser dye (Rhodamine 6G)[78] is comparable to the cavity round trip time. As a consequence, both the gain and absorber dynamics should play an important role in the formation of the mode-locked pulses. These aspects are all very different from the situation of the mode-locked solid-state lasers for which only the absorber is responsible for the "mode-locking"

*An abbreviated name for the cyanine dye 3,3'-diethyloxadicarbocyanine iodide.

process and the overall pulse length is limited by the recovery time of the absorber. Accordingly, the analysis of pulse formation in solid-state lasers[40-45] is not applicable to dye lasers.

Recently, an analysis of passive mode-locking in quasi-continuous lasers has been presented by New[46,47]. This model has been applied to the investigation of mode-locking regimes of operation for both pulsed and CW dye lasers. Certain criteria for pulse-compression operation have been established arising from the requirement that there be a net loss on both the leading and trailing edges of the circulating pulse whose energy is a constant. It is proposed that the combined actions of the gain and loss dynamics may lead to the formation of ultrashort pulses. However, the analysis cannot be employed to generate a stable temporal solution for the laser pulse since the pulse simply continues to narrow indefinitely for operation in the pulse compression regime. Therefore, the actual pulse width for a given set of operating conditions cannot be determined.

In this chapter, the theoretical model developed in Chapter 2 is adapted to the analysis of mode-locked CW dye lasers. The experimental situations will be briefly described to indicate that our model is a good approximation to such a system. Mode-locking regions will be determined for parameter range appropriate to the practical systems. Furthermore, steady-state pulses will be generated for some representative cases

to show that the pulse length of the mode-locked pulses is not limited by the recovery time of the absorber and that ultrashort pulses can be obtained under the experimental conditions. In this context, it is evident that our analysis represents a more general approach to the problem. On the other hand, New's analysis has the advantage of simplicity and directness. Accordingly, it is useful to investigate the degree of equivalence between the two analyses. Such investigations constitute the second half of this chapter.

There are, as will become apparent, several differences in principle between the two theoretical approaches. New applied his rate equation theory to the determination of the laser operation regime in which a circulating pulse experiences loss on both the leading and trailing edges. This situation is determined subject to the explicit assumptions that the pulse energy (suitably normalized) is a constant for each pass through a given point in the laser cavity. The conjunction of these two conditions implies that the pulse is shortened on each round trip in this laser cavity. It is this situation, the pulse compression or stable region, which New has subjected to detailed investigation. It is important to observe that operation in the above pulse compression regime precludes the occurrence of steady-state pulses (SSP) and the laser pulses narrow indefinitely, subject to the limitations of the rate equation approach. This circumstance renders the applicability of the analysis to the CW dye lasers somewhat indeter-

minate, in that the observed output pulses are evidently SSP. This raises several interesting questions concerning the relation between the pulse compression and the mode-locking region of operation. In particular, are there mode-locked solutions in parameter ranges outside the pulse compression regime, where either the leading or trailing edge of the pulse "sees" gain, and if so can SSP be generated under these circumstances within the rate equation approximation? Further, assuming the CW mode-locking and pulse compression regions overlap, can SSP be generated wtihin this regime in the rate equation approximation, and if so, how? The investigations presented in the later part of this chapter are addressed to these and related questions.

4.2 Production of Ultrashort Pulses (USP) from Mode-Locked CW Dye Lasers:

4.2.1 Theoretical Consideration:

Typically, the thickness of the dye cells employed is of the order of a millimeter while the cavity is one to two meters long[24,25]. As pointed out in section 2.2, a normal laser with long cavity and short gain and loss cells can be approximated by an unidirectional ring cavity with the ring perimeter being equal to the round trip cavity length, i.e. twice the actual cavity length. This approximation is especially suitable if the cells are in optical contact with the cavity mirrors provided that the overlapping effects of the pulses in the media can be ignored. In addition, a dye molecule responsible for the laser action can be regarded as a two-level system and the

spectral profile of such molecule can be approximated by a homogeneously broadened line, if the effects of intersystem crossing between the singlet and triplet electronic states and the thermal inhomogeneous broadening can be ignored[79,80]. For Rhodamine 6G and DODCI, both of these conditions are satisfied reasonably well[75,79-81].

All the properties of the dye laser system described in the last paragraph are in accord with the assumptions made in our theoretical model. Furthermore, the slowly varying envelope and rotating wave approximations (section 2.2) require* that the optical frequency greatly exceed T_2^{-1} and $(T_2')^{-1}$, which is expected to hold since the values of T_2 and T_2' are estimated to be $\sim 10^{-13}$ sec[82] from the corresponding linewidths of the fluorescence and absorption spectra respectively, whereas the optical frequency (ω) is $\sim 10^{15}$ Hz. In addition, in our model, the radiation field is assumed to be in resonance with both the gain and loss media, and the dispersion effects are ignored. These approximations are not strictly valid, but the errors introduced are not expected to be serious provided that either the system is operated close to laser threshold, or the SSP are reasonably long compared to T_2 or T_2'.

The foregoing discussion shows that the theoretical model developed in Chapter 2 can be applied to a dye laser system.

---

*Originally, the slowly varying envelope approximation (SVEA) requires that the temporal width (τ_p) of the laser pulse be much longer than ω^{-1}. For a mode-locked laser, the limiting pulsewidth is given by $\tau_p \sim \Delta\nu^{-1}$ or $\tau_p \sim T_2$ since $T_2 \sim \Delta\nu^{-1}$. Therefore, in this case, the SVEA holds provided that $\omega >> T_2^{-1}$.

Accordingly, the model is employed for the analysis of the mode-locked CW dye lasers in this chapter. Furthermore, the situation of the flashlamp-pumped dye lasers will be investigated in the next chapter.

4.2.2 Numerical Calculations:

In Figs. 4-1 and 4-2, typical results of the numerical calculations are presented concerning the mode-locking regions and the SSP for certain range of laser parameters. The parameter values are chosen to represent, as closely as possible, the practical CW dye laser systems[24,25]. In these figures, the lifetimes measured experimentally for Rhodamine 6G[78] and the photoisomer of DODCI[75,76] are used for T_1 and T_1' respectively, while the values of T_2 and T_2' are estimated from the widths of the corresponding fluorescence and absorption spectra[75,79]. Furthermore, the values of L = 3.60 m and 2.40 m for n = 1 are used, corresponding to the round trip times of $\sim$ 12 nsec and $\sim$ 8 nsec respectively as found in refs. (24) and (25). For other parameters, representative values have been used since the exact numerical values are not available. The values we have chosen for these parameters are reasonable for an actual CW dye laser. As an example, consider the parameter $m = m_d m_o$ (Eq. (2-45)). The experimental arrangements used in refs. (24) and (25) show that m_o (the ratio of the actual electric field amplitudes in the absorber and amplifier) is of the order of unity. Furthermore, it can be shown[13,83] that the dipole moment (μ) associated with a two-level transition

is inversely proportional to the square root of the spontaneous lifetime (t_{spont}) of the upper level. This lifetime can be approximated by the recovery time for a fluorescence dye solution whose quantum efficiency is relatively high. Accordingly, we have

$$m_d = \mu_b/\mu_a \simeq (T_1/T_1')^{1/2} \simeq 4.3$$

for the recovery times used in our calculations. In addition, it has been shown (Chapter 3) that in order to achieve effective mode-locking, the value of m should be of the order of $(T_1T_2/T_1'T_2')^{1/2}$ (Eq. (2-57)) which is 3.76 for the relaxation times used. Consequently, the numerical values of m used in our calculations should be reasonable.

In Fig. 4-1, variation of mode-locking regions with γ_g are shown where the quantity m is treated as a variable parameter. In this figure, the upper and lower curves serve as boundaries between the mode-locking and CW operation regions for each value of m. Only one line (dotted and labelled $\lambda_{o,min}$) is shown for the lower boundary of the mode-locking regions since for all the cases investigated, it is found that $\lambda_{o,min}$ is very close to the laser threshold given by $\lambda_{o,th} = (1-\gamma_g)^{-1}-1$ (Eq. (2-68)). On the other hand, it can be seen that the variations of the upper limits of the mode-locking regions ($\lambda_{o,max}$) with L, m and γ_g are very large.

In addition, we have investigated the variations of the mode-locking regions with the low signal gain of the amplifier ($\alpha_a L_a$), keeping γ_g constant. It is found that the lower

Fig. 4-1 Variations of mode-locking regions with γ_g for L = 2.40m and 3.60m with n = 1 corresponding to a repetition rate of one pulse per round trip period in the output pulse train. Parameters: T_1 = 5.5 nsec, T_2 = 0.05 psec, T_1' = 0.3 nsec, T_2' = 0.065 psec and $\alpha_a L_a$ = 0.30. Only one line (dotted and labelled $\lambda_{o,min}$) for the lower bounds is drawn since the variations of $\lambda_{o,min}$ with L and m are relatively small.

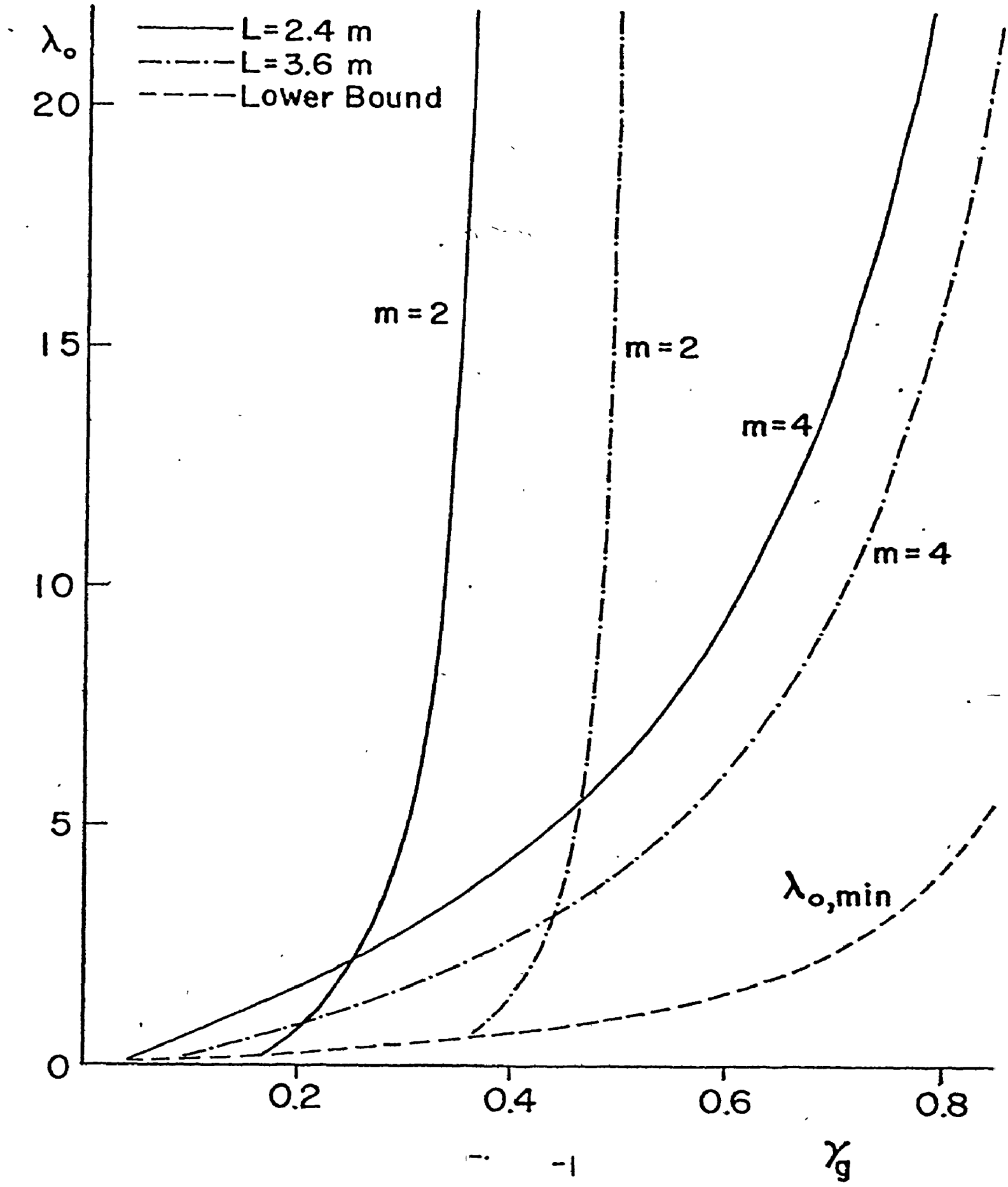
λo
L=2.4 m
L=3.6 m
Lower Bound
20
15
10
5
0
m=2
m=2
m=4
m=4
λo,min
0.2
0.4
0.6
0.8
γg

-limit of the mode-locking regions are also very close to laser threshold. However, the dependence of $\lambda_{o,max}$ on $\alpha_a L_a$ is less profound than the dependence on γ_g. This result is very similar to those presented in Chapter 3 for the model systems despite the very significant difference in the values of the phase coherence times for the two types of laser systems. Practically, this common feature implies that the low signal gain and loss of the amplifier and absorber may be simultaneously increased or decreased in proportion without strongly affecting the mode-locking operation. This suggests a potentially useful method of changing the intensity of the output pulses to any desired level, without greatly affecting the pulse length.

The prediction of instabilities in the CW solutions shows the possibility of achieving mode-locking for a given set of laser parameters. In particular, the results that mode-locking can be attained in the regime just above laser threshold are in accord with the experimental conditions[24]. It remains to show whether picosecond pulses can be produced and to study how the peak intensity and width of the mode-locked pulses vary with the laser parameters.

In Fig. 4-2, typical steady-state pulses generated by computer simulation using the finite difference method are shown. The intensities, normalized to their respective pulse peak values, are plotted as a function of time and the repetition rate of the output pulse train is one pulse per round trip period for all three cases. Observe that the values

Fig. 4-2 Steady-state mode-locked pulses for L = 2.40m [(a) and (b)] and L = 3.60m [(c)]. The normalized intensity is plotted as a function of time and the repetition rate is one pulse per round trip period for all three cases. The values of T_1, T_2, T_1' and T_2' are the same as in Fig. 4-1, $\alpha_a L_a = 0.30$ and $\gamma_g = 0.20$. Other parameters: L = 2.40m, m = 2, $\lambda_o = 0.30$ and 0.50 for (a) and (b) respectively; L = 3.60m, m = 3, $\lambda_o = 0.30$ for (c). The widths (FWHM) of the pulses (a), (b) and (c) are 1.32, 0.48 and 0.30 psec respectively, and the relative magnitudes of the peak intensities at the output section of the absorber are approximately 1:10:32.

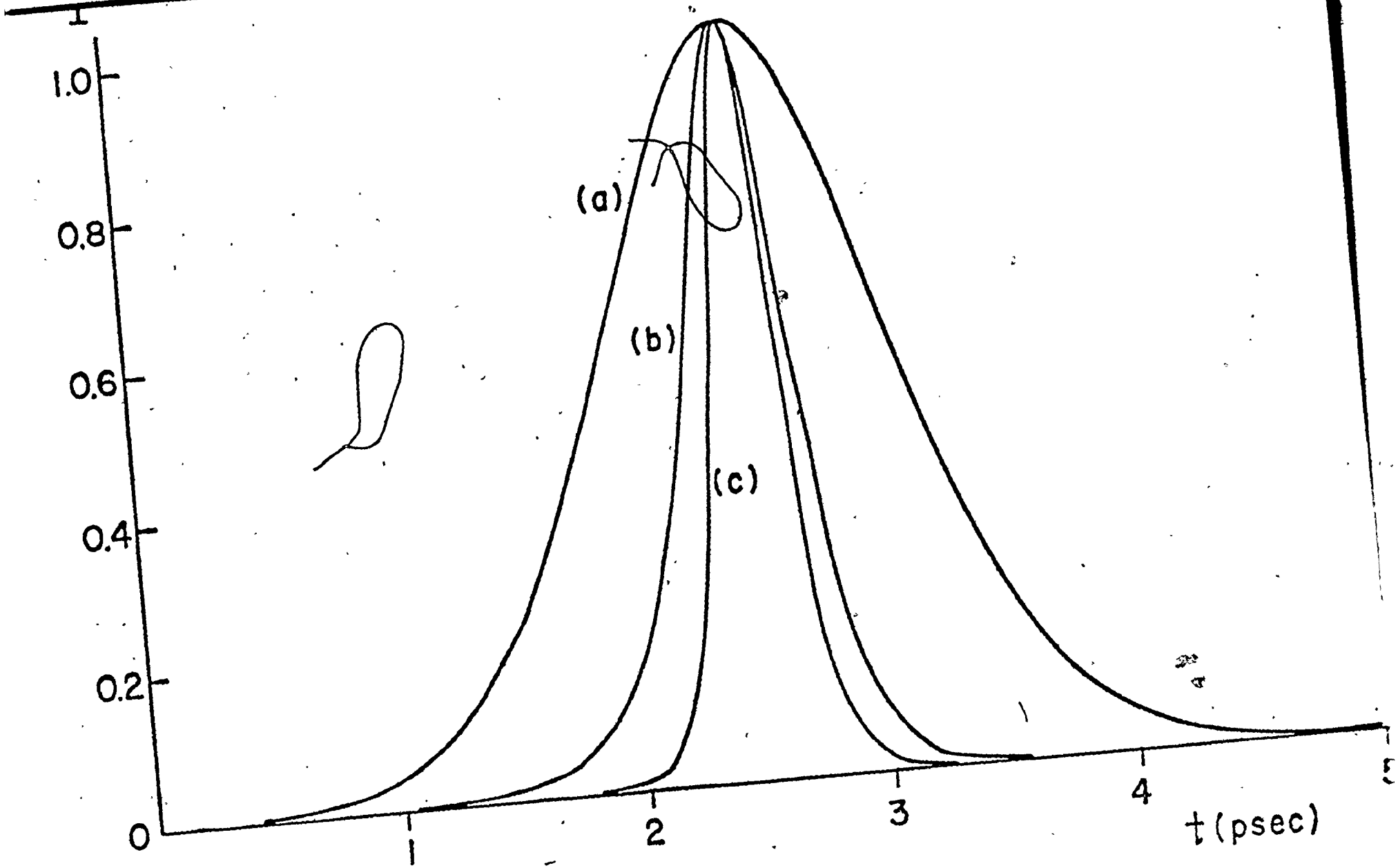

Fig. 4-2

of λ_o employed are quite close to the laser threshold as is the case for the reported experimental situations[24], and the pulse widths are two to three orders of magnitude shorter than the recovery time (T_1') of the absorber. The results for these pulses generated are of a length encouragingly close to those observed experimentally.

In addition, we have found that there is a general tendency that, within the mode-locking regions, the output pulses become narrower and more intense as the pump parameter λ_o is increased. This is exemplified by the two pulses shown in Fig. 4-2 for L = 2.40 m with λ_o = 0.30 and 0.50. Alternatively, for a given λ_o, i.e. for given amplifier gain and cavity loss, shorter pulses can be produced by reducing the low signal loss of the absorber, within the mode-locking range. Recall that similar results have been shown in Chapter 3 for the model laser systems. Accordingly, this phenomenon represents another common feature of the mode-locked CW lasers.

Finally, observe that the output pulses from the CW dye laser operated very close to laser threshold are substantially longer than the phase coherence times of the active media. The pulse areas are also small compared to that of a π-pulse. As a consequence, coherence effects are not of significant importance and rate equation approach may be a good approximation. Accordingly, a rate equation model is introduced and compared where possible with our theoretical model in the following sections.

4.3 The Pulse Compression Model:

4.3.1 General Treatment

In this model[46,47], New assumes that the laser pulse is short compared to the relaxation times of the gain ($T_{1a} \equiv T_1$) and absorption ($T_{1b} \equiv T_1'$) media. Furthermore, it is assumed that the cavity round trip time (T_{RT}) is much greater than the relaxation time of the absorber* and is comparable to the relaxation time of the gain medium. Under these circumstances, the propagation of a pulse through a gain or loss medium can be treated within the rate equation approximation, provided that the pulse length does not become comparable with the phase coherence times (T_2 and T_2') of the gain or loss media. The analysis is carried out in terms of the (normalized) integrated photon flux[46,47,84,85].

$$j(\tau) = \sigma_a \int_{-\infty}^{\tau} \rho(\tau')d\tau' \qquad (4\text{-}1)$$

where $\rho(\tau')$ is the photon flux at local time $\tau'(=t-x/c)$ and σ_a (σ_b) is the resonance gain (absorption) cross-section. It can then be shown that (Appendix D), for the propagation of a pulse through a slab of gain (loss) medium

$$j_f(\tau) = \ell n\{1+\alpha(-\infty)[\exp(j_i(\tau))-1]\} \qquad (4\text{-}2)$$

where i and f denote input and output values and $\alpha(-\infty)$ is the gain on the leading edge of the pulse. It is also straightforward to show that the gain as a function of local time is

---

*It will be shown in section 4.4 that this is not essential to the analysis and can be dropped without strongly affecting the main results.

given by

$$\alpha(\tau) = \alpha(-\infty)\exp[j_i(\tau)-j_f(\tau)]. \qquad (4\text{-}3)$$

Evidently, the same analysis will apply to the loss, except that the normalization factor for $j(\tau)$ will be different. This can be dealt with by using the variables $sj(\tau)$ in equations for the loss, where s is a constant depending, amongst other things, on the ratio σ_b/σ_a . The method of solution now proceeds as follows (Appendix D). A pulse is permitted to circulate within the laser cavity, and steady-state pulse energy solutions are sought. The final values (after the pulse passage) of gain and loss are required to recover to the relevant initial values in the time between passes of the pulse through the media. Furthermore, the (normalized) pulse energy $j(\infty)$ passing a given position in the cavity is required to be a constant. Observe that the treatment of pulse energy effectively removes information concerning the pulse length. Accordingly, to investigate actual pulse propagation, the equations governing the photon flux must be treated directly.

4.3.2 The Composite Medium Model:

The constraints described above on the gain, loss and pulse energy are sufficient to specify the problem once initial values are known for appropriate parameters. The particular case where the amplifying and absorbing media, together with the linear loss, are uniformly distributed in a single dye cell (the composite medium model) can be treated according to the above scheme with particularly simple results (Appendix D). New treated this problem[47] by assuming

values for B_o (loss/unit length)*, Γ (equivalent linear loss/unit length) and s, and then solving for $j(\infty)$. For each given value of $j(\infty)$ the value of g_o (the unsaturated net gain per round trip) and ξ ($= T_{RT}/T_{1a}$) can vary. The pulse compression region (where the gain on both the leading and trailing edges is less than unity) is bounded by the lines for which either the gain on the leading edge or the gain on the falling edge is just unity. The value of $j(\infty)$ can be found for each case, and thereby the pulse compression region can be displayed in the (g_o,ξ) plane. In order to make comparison with our theory, it is preferable to permit the linear cavity loss to vary at given values of the low signal gain in the absence of a field (A_o), B_o, E ($=\exp(-\frac{1}{2}\xi)$) and the parameter s. Accordingly, we have rewritten the analysis somewhat.

For the case of unity gain on the leading edge ($g_L=1$), it can be shown that the following equation must hold (Appendix D):

$$F_L(j_\infty)=[1-j_\infty-\exp(-j_\infty)]A_{ie}(j_\infty)-B_o s^{-1}[1-sj_\infty-\exp(-sj_\infty)]=0 \quad (4\text{-}4)$$

where

$$A_{ie}(j_\infty) = \frac{A_o(1-E)}{1-E\exp(-j_\infty)} \text{ and } j_\infty \equiv j(\infty). \quad (4\text{-}5)$$

This equation can then be solved iteratively for j_∞ when A_o, B_o, E and s are given. Similarly, it can be shown that, for unity gain on the trailing edge ($g_T=1$) of the pulse, the following equation must be satisfied:

---

*In the analysis, the composite medium cell is assumed to be a thin slab with thickness set to unity. Furthermore, a normal cavity is employed in New's model.

$$F_T(j_\infty) = [1-(1+j_\infty)\exp(-j_\infty)]A_{ie}(j_\infty)$$
$$- B_o s^{-1}[1-(1+sj_\infty)\exp(-sj_\infty)] = 0 \qquad (4\text{-}6)$$

which can also be solved iteratively for j_∞. In either of the above cases, once j_∞ has been found, the value of Γ (and hence g_o) can be calculated directly, and the pulse compression region is determined.

Observe that in the derivation of Eqs. (4-4) and (4-6), it has been assumed that the cavity round-trip time is much longer than the relaxation time of the absorber so that the loss of the absorber will resume its low signal value (B_o) in the time interval $\frac{1}{2} T_{RT}$ after the passage of the pulse. This assumption can be dropped to allow for the possibility that the cavity round trip time and the absorber recovery time are commensurate. It can be shown (Appendix D) that this modification can be made by simply using $B_{ie}(sj_\infty)$ instead of B_o in Eqs. (4-4) and (4-6) with

$$B_{ie}(sj_\infty) = \frac{B_o(1-E')}{1-E'\exp(-sj_\infty)} \qquad (4\text{-}7)$$

where

$$E' = \exp(-\tfrac{1}{2}\xi') \quad , \quad \xi' = \frac{T_{RT}}{T_{1b}} . \qquad (4\text{-}8)$$

This modification will be important if the cavity length is sufficiently short. Accordingly, in the determination of the pulse compression region, we generally use the modified theory.

4.4 Comparison of Mode-Locking and Pulse Compression Operations:

4.4.1 Relationship Between the Parameters Used in the Two Models:

Observe that a normal laser cavity with the composite medium located at the center has been employed in New's approach. Furthermore, the phase coherence times have been implicitly treated as scaling factors in the cross-sections in the rate equation formalism. As a consequence, it is necessary to establish certain equivalences between parameters we have employed and those used by New. The more important of these are given below.

(i) The parameter s (ratio of the generalized cross-sections of the absorber and the amplifier) is equivalent to our m^2/γ_2 with $m = m_d m_o$ and $\gamma_2 = T_2/T_2'$ as defined in Chapter 2. (see also Appendix D)

(ii) The parameter ξ is equivalent to $(2)L/cT_1$, where the factor 2 is employed for ring lasers, and L is the round-trip length. Similarly, $\xi' = (2)\ L/cT_1'$.

(iii) The parameter $g_o \equiv \exp[2(A_o - B_o - \Gamma)]$ is equivalent to $\exp(\alpha_a L_a - \alpha_b L_b)R$ and is related to the overall pump parameter $\lambda (= (\alpha_a L_a - \alpha_b L_b)/\ell n(R^{-1}) - 1)$ by

$$\lambda = \ell n(g_o)/\ell n(R^{-1}) = \ell n(g_o)/2\Gamma. \qquad (4\text{-}9)$$

Similarly, the pump parameter $\lambda_o (= \alpha_a L_a/\ell n(R^{-1}) - 1)$ is related to A_o and Γ by

$$\lambda_o = A_o/\Gamma - 1. \qquad (4\text{-}10)$$

4.4.2 Mode-Locking and Pulse Compression Regions:

The scheme described in the previous section can be used to determine the pulse compression regions by solving Eqs. (4-4) and (4-6). Figure 4-3 shows the results for parameters appropriate to CW dye lasers, where the region between the two lines corresponding to $g_L = 1$ and $g_T = 1$ is the pulse compression region. Also shown on the same figure are the lower and upper boundaries of the mode-locking regions employing our theoretical model. Note that the finite absorber recovery time has been allowed for (Eq. (4-7)) in the calculation of the pulse compression regions. It has been found[86] that this modification makes little change to the results for the parameters typical of CW and flashlamp-pumped dye lasers*. However, there are other laser configurations and systems for which the inclusion of this modification would be important.

Observe that, for the parameters chosen, there are mode-locking regions occurring on either side of the pulse compression regime. Propagating pulses occurring for parameters appropriate to the region on the right of $g_L = 1$ in the figure have gain on the leading edge and loss on the trailing edge. The inverse situation occurs to the left of the line $g_T = 1$. And so, one of the questions raised in the introduction (section 4.1) has been answered. It appears that CW mode-locking regions can occur outside the pulse compression region. The next issues to be considered relate to the existence (or otherwise) of SSP

*The case of flashlamp-pumped dye lasers will be treated in the next chapter.

Fig. 4-3 Comparison of mode-locking and pulse compression regions for parameters appropriate to CW dye lasers. Note that the pulse compression regions are calculated using the composite medium model with the effect of finite recovery time of the absorber taken into account. Parameters: $\alpha_a L_a$, T_1, T_2, T_1' and T_2' are the same as for Fig. 4-1, $\gamma_g = 0.20$, $m = 2$ ($s = 5.2$).

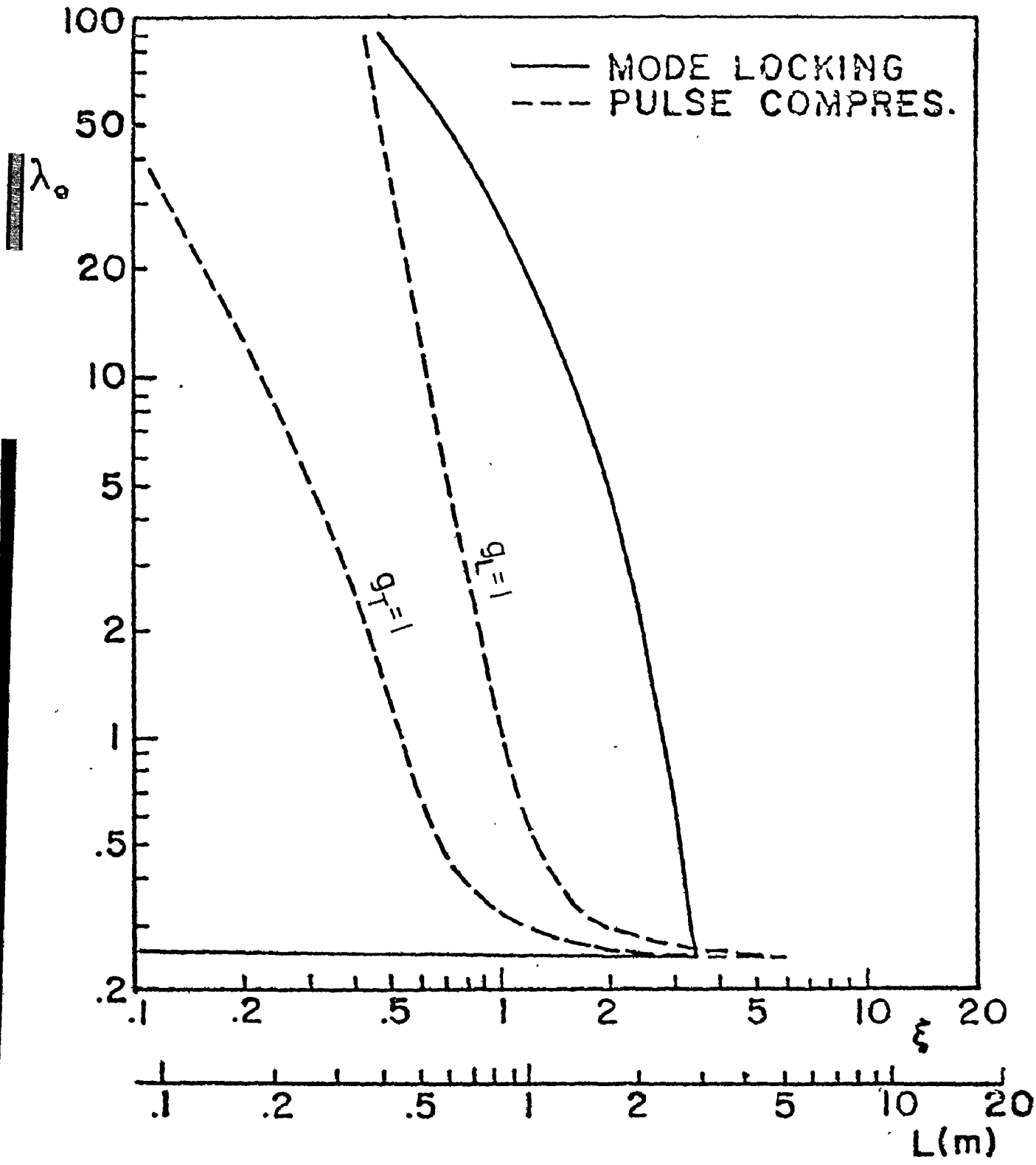
MODE LOCKING
PULSE COMPRES.
λ_o
100
50
20
10
5
2
1
.5
.2
$g_T L = 1$
$g_L L = 1$
.1
.2
.5
1
2
5
10
20
ξ
L(m)

Fig. 4-3

in the rate equation approximation both within and without the pulse compression region. This question cannot be answered within the framework of New's analysis, which can be used to obtain the pulse energy but not the pulse width or intensity separately (although pulse narrowing relative to a chosen initial state with the energy j_∞ can be obtained). Furthermore, according to New's approach, no SSP can be found under any circumstances since a propagating pulse (with a constant energy) will either narrow or lengthen indefinitely depending on whether the system is operated within or outside the pulse compression region. However, in reality, the response of the laser gain and loss to the pulse depends on both the pulse energy and pulse structure (shape). Therefore, results based on an analysis in which the effects of pulse shape are not taken into account will not generally be reliable. In other words, the possibility that there be net loss (or gain) in the leading or trailing edges will be very sensitive to the pulse structure, especially when the operating regime is very close to threshold. As a consequence, it should not be too surprising that no SSP can be generated by using New's propagation equations in which the spatial variations of the laser gain and loss is neglected which effectively removes the temporal (local) variations of the pulse shape inside the active media. Accordingly, to investigate whether SSP exists for a given set of conditions within the rate equation approximation, propagation equations similar to those for the density matrix formalism are developed

employing a finite difference approximation (Appendix C). The results of pulse propagation calculations for selected cases are presented in the next subsection.

4.4.3 Existence and the Associated Properties of the SSP

For parameters appropriate to CW dye lasers (Fig. 4-3), SSP have been sought both within and outside the pulse compression region of operation, employing the finite difference equations in the rate equation approximation (Appendix C). During this investigation, it becomes apparent that the behaviour of the system is sensitive to the way the gain and losses are distributed in the cavity, in contrast with the high gain and high loss situation[47]. To illustrate this, Fig. 4-4 shows the gain on the leading and trailing edges as a function of ξ calculated according to the composite medium model and that employing discrete gain and loss elements*. Clearly, the changes are considerable. However, since this does not affect our main conclusions, we have not attempted to correct the $g_T=1=g_L$ curves shown in Fig. 4-3. The major effect is to shift these curves to the right for low values of λ_o. It is found that SSP can be generated to the right, to the left and within the pulse compression regions as indicated in Fig. 4-3. Representative results are shown in Fig. 4-5 where SSP generated for three different cavity lengths are plotted. It is also found that the SSP generated within the rate equation formalism are in good

---

*Expressions for the gain on the leading and trailing edges employing discrete gain and loss elements can be found in Appendix D.

Fig. 4-4 Variation of gain on the leading (g_L) and trailing (g_T) edges as a function of ξ for both the discrete component and the composite medium models. Parameter: $\lambda_o = 0.30$, the rest are as for Fig. 4-3. Observe that for the discrete model the pulse compression region (both g_L and g_T are less than 1) shifts to higher values of ξ relative to that of the composite medium model.

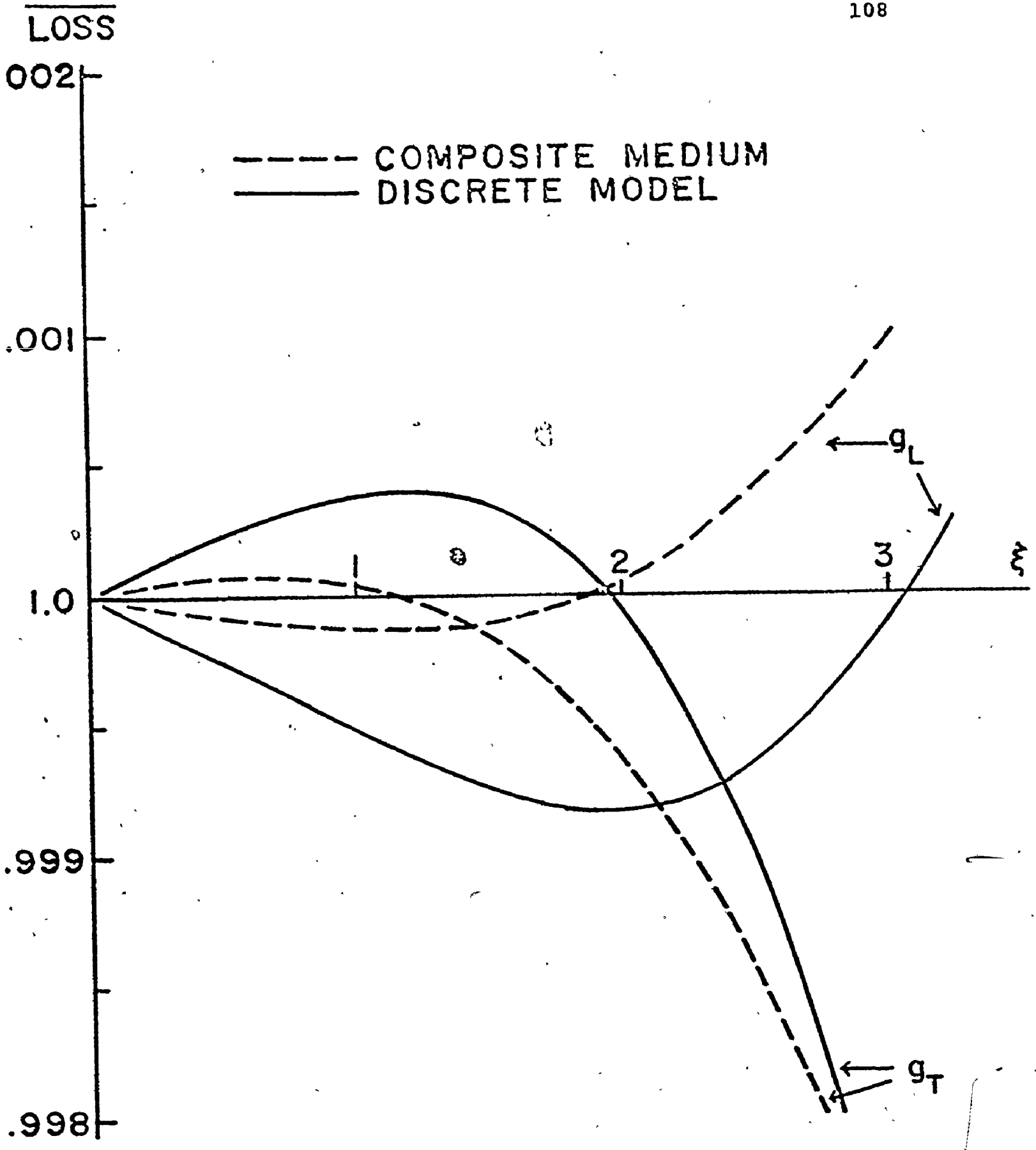
LOSS
.002
.001
1.0
.999
.998
COMPOSITE MEDIUM
DISCRETE MODEL
g_L
g_T
1
2
3
ξ

Fig. 4-5 Steady-state mode-locked pulses for L = 0.6, 1.20 and 2.40 m. Parameters: λ_o = 0.30, the rest are as for Fig. 4-3. Note that the three operating points are so chosen to represent the three operation regimes situated, respectively, to the left (L = 0.60 m), within (L = 1.20 m) and to the right (L = 2.40 m) of the pulse compression regions shown in Fig. 4-3. In this figure, the normalized intensity is plotted as a function of time. The widths (FWHM) of the pulses (a), (b) and (c) are 2.05, 1.90 and 1.25 psec respectively, and the relative magnitudes of the peak intensities at the output section of the absorber are approximately 1:2.7:11.7.

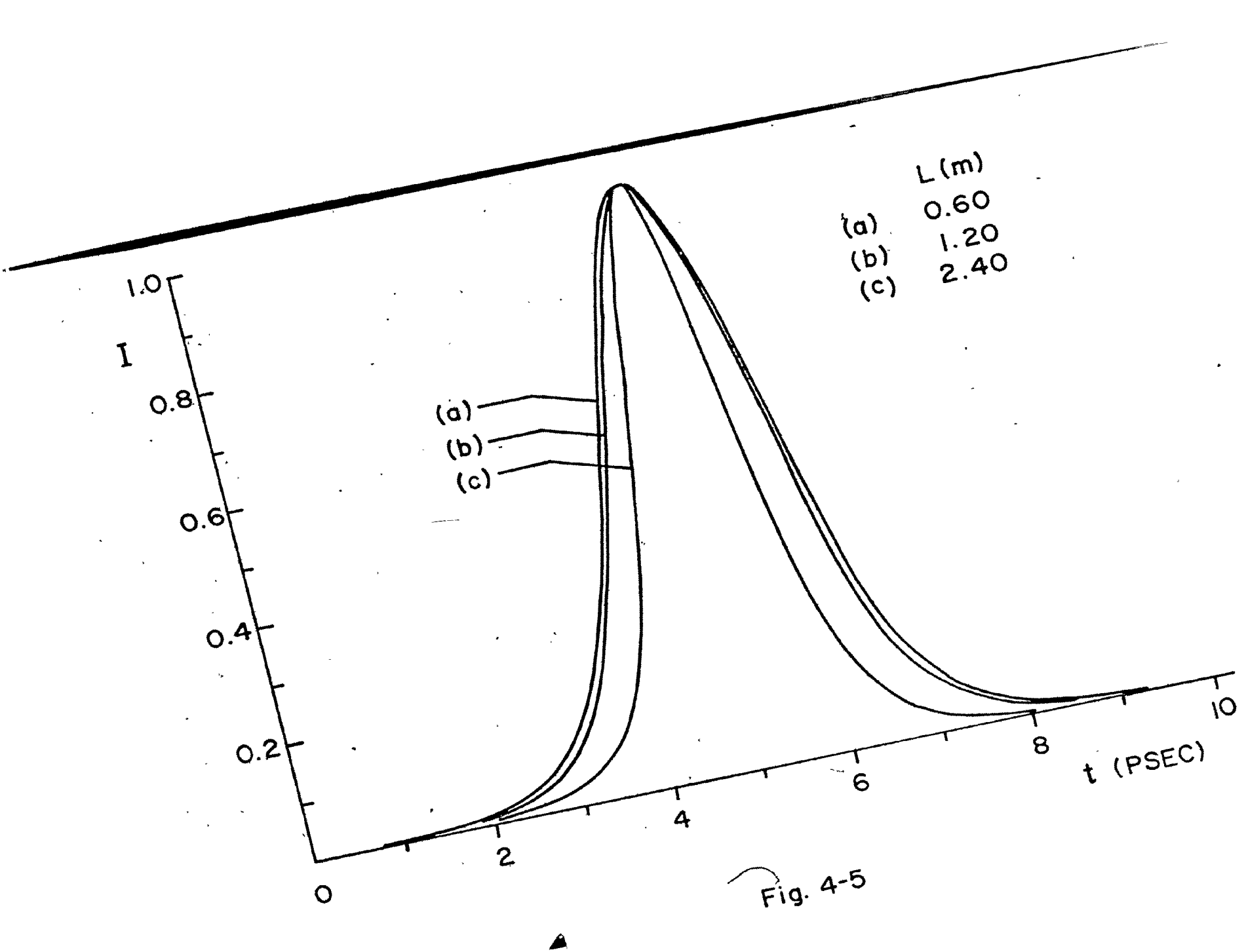

Fig. 4-5

Fig. 4-6 Comparison of the SSP generated within the rate equation approximation (REA) and using the full coupled equation formulation. Parameters: $L = 2.40$ m, $\lambda_o = 0.30$, the rest are the same as in Fig. 4-3. Observe that the results are in good agreement except that the pulse generated by the REA has longer tails. The differences of the actual pulse peak intensities and pulse widths are, respectively, within 3 and 5 per cent.

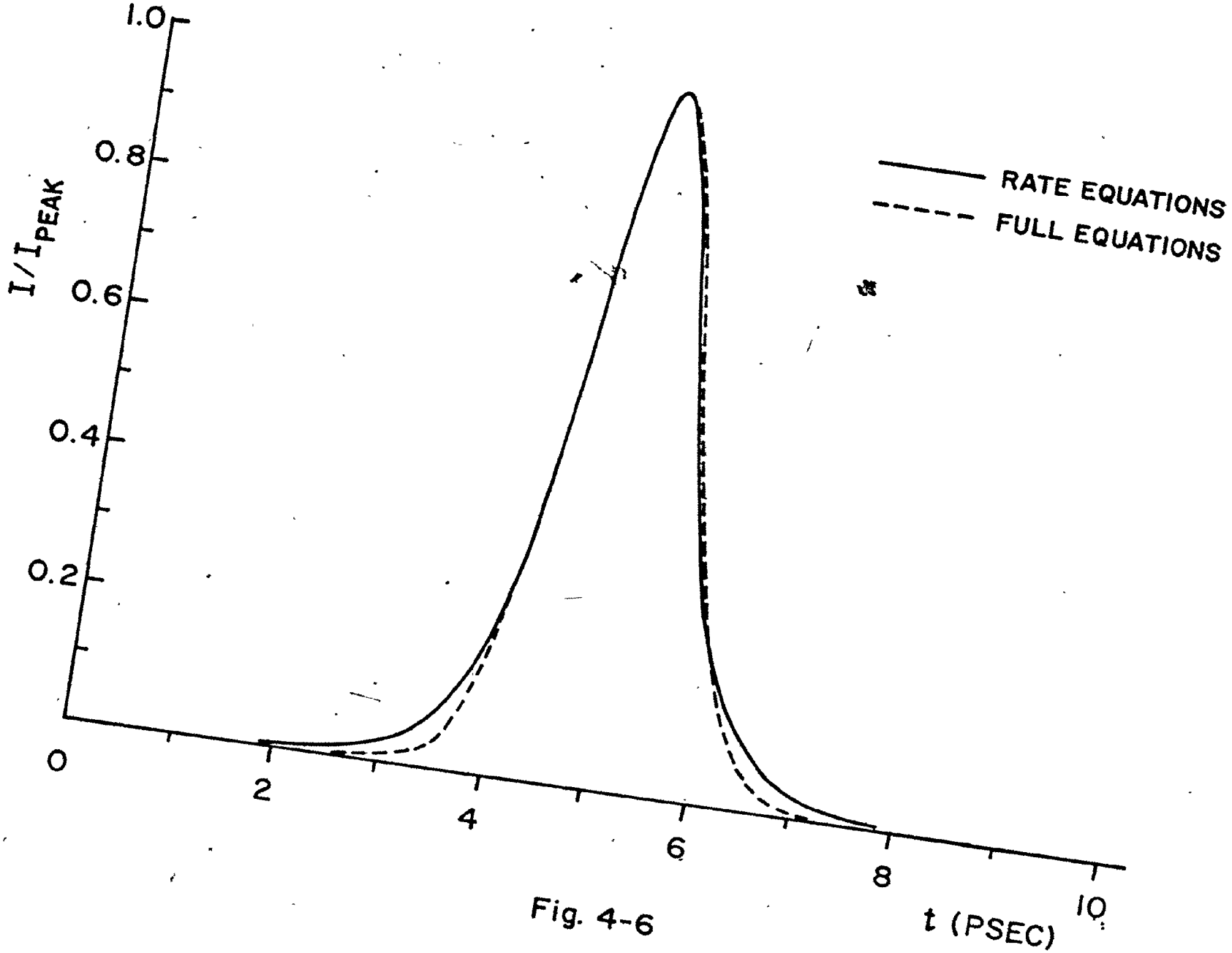
1.0
0.8
0.6
0.4
0.2
0
I/I_{PEAK}
2
4
6
8
10
t (PSEC)
RATE EQUATIONS
FULL EQUATIONS

Fig. 4-6

agreement with results obtained using the full coupled equation formulations, as can be seen from Fig. 4-6. This is expected to be so provided that the pulse length of the SSP is much longer than the phase coherence times of the gain and loss media and the pulse area is small compared with π, so that the phase coherence effects are not important.

Observe that for the steady-state pulses, there is nothing to be obtained from plotting the gain as a function of the normalized pulse energy. In fact, the gain so plotted has the value of unity. This can be seen from Fig. 4-7 where the intensity (normalized to I_{CW}) is plotted as a function of the normalized pulse energy for a propagating pulse as the steady-state is approached. The round-trip relative gain for a given normalized pulse energy J will be proportional to the ratio of I(K+N)/I(K) with K and N being the appropriate number of round trips. As can be seen from this figure, the values of I(K+N) and I(K) tend to be equal for any given J as the SSP is approached. This indicates that the gain as a function of J will have the value of unity for all J. In addition, it is clear that both the peak intensity and the total pulse energy (J(∞)) tend towards constant values as the steady-state is approached.

The discussion of the previous paragraph suggests that it may be more appropriate, for the SSP, to consider the gain as a function of local time τ. Figure 4-8 shows the round trip relative gain for a propagating pulse as it approaches equili-

Fig. 4-7 Plot of intensity $I(\tau)$ versus the integrated normalized pulse energy $J(\tau)=\int_{-\infty}^{\tau} I(t)dt/J_{CW}$ ($\tau = -\infty$ corresponds to the leading edge) with J_{CW} defined as the total CW output energy in one round trip period, i.e. $J_{CW} = T_{RT}\, I_{CW} = LI_{CW}/c$. Note that as the propagating pulse approaches steady-state, the curves for the K- and the (K+N)-th round-trips tends to be over-lapped. Parameters: $\lambda_o = 0.30$, $L = 2.40$ m and the rest are the same as in Fig. 4-3.

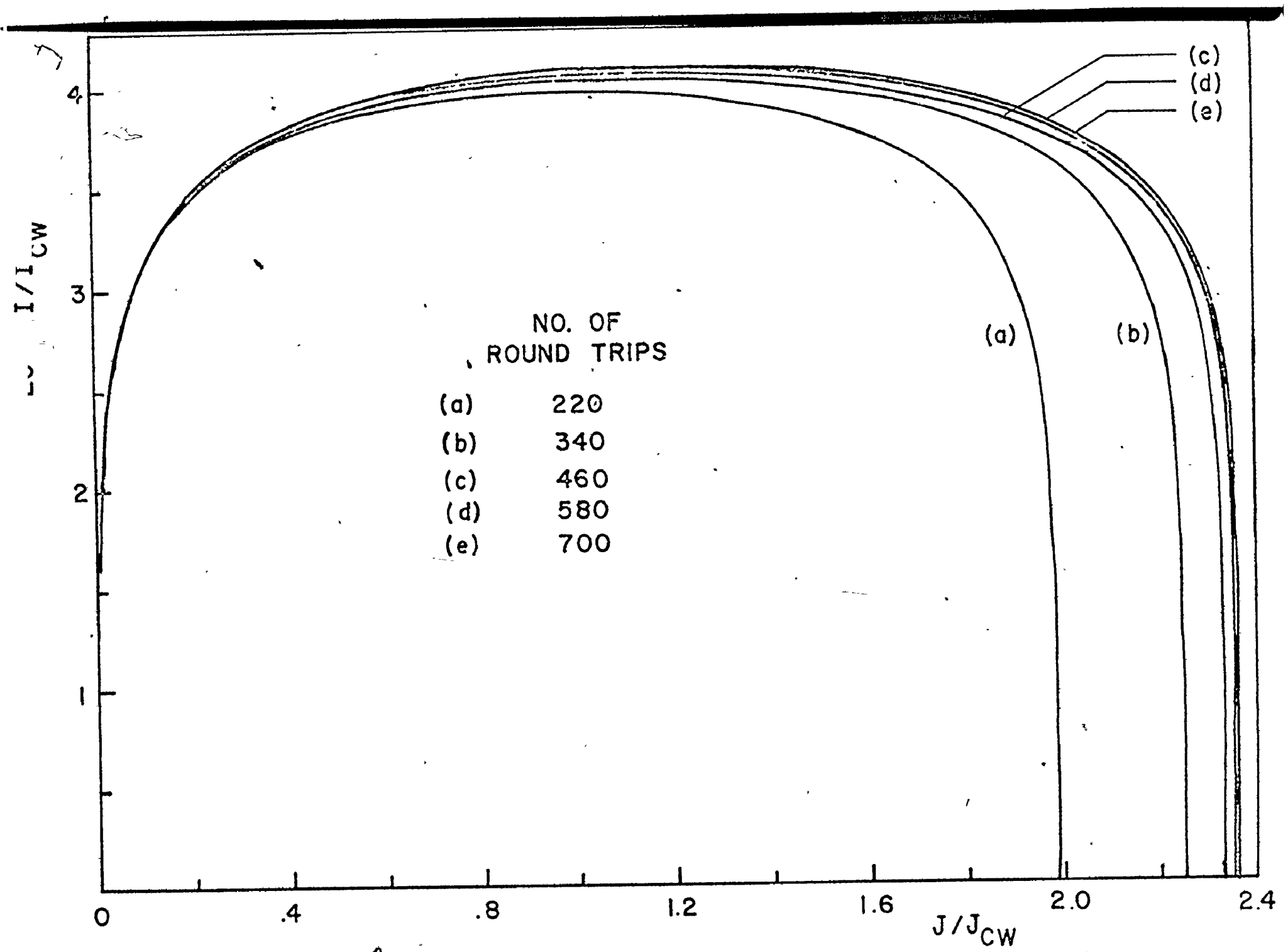
I/I_CW
4
3
2
1
0
.4
.8
1.2
1.6
2.0
2.4
J/J_CW
(a)
(b)
(c)
(d)
(e)
NO. OF
ROUND TRIPS
(a) 220
(b) 340
(c) 460
(d) 580
(e) 700

Fig. 4-7

Fig. 4-8 Plot of the relative gain as a function of local time when the propagating pulse approaches the steady-state. For a given τ, the value of $I(K + N)/I(K)$ is the ratio of the field intensities at the $(K + N)$-th and K-th round-trips. Since the relative gain per round trip is small, a large value of N (= 120) is chosen. Parameters: $\lambda_o = 0.30$, L = 1.2 m, the rest are as for Figure 4-3.

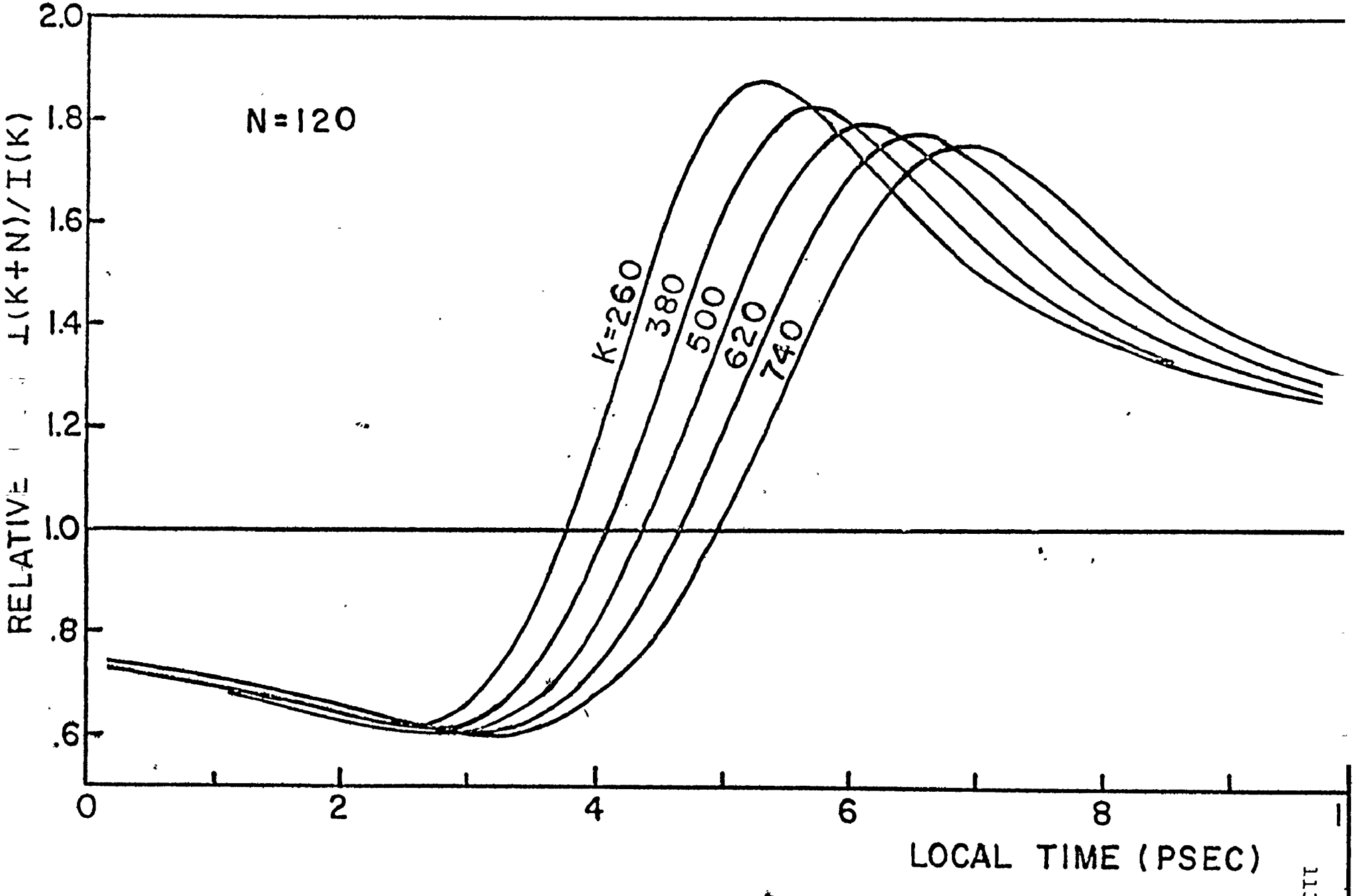
N=120
K=260
380
500
620
740
RELATIVE I(K+N)/I(K)
2.0
1.8
1.6
1.4
1.2
1.0
.8
.6
0
2
4
6
8
LOCAL TIME (PSEC)

Fig. 4-8

brium, plotted as a function of local time $\tau = t-x/c$. Note that the zero of local time is arbitrary and the relative shifts of the gain curves in local time corresponds to the shifts of the SSP maximum in local time during propagation. In this case, since the pulse experiences loss on the leading edge (small values of local time in Fig. 4-8) and gain on the falling edge, the pulse velocity is less than the velocity of light and so it shifts to higher values of local time during propagation. Conversely, a pulse with gain on the rising edge and loss on the falling edge will have a pulse velocity greater than the velocity of light. Within the pulse compression region (when corrected as indicated earlier), the SSP obtained have variations of the gain in local time much like that shown in Fig. 4-8. Whether or not loss occurs far out on the trailing edge is not entirely clear. It is important to point out that the pulse behaviour at large values of local time depends very sensitively on how rapidly the pulse intensity falls off in this region. Consequently, although the pulse solution has reached a steady-state everywhere else, it is still possible for small changes to occur far out on the trailing edge (which, it should be noted, is also far out on the leading edge).

4.5 Conclusion:

The calculations presented in this chapter indicate that the recovery time of the absorbing medium does not impose a restraint on the width of the mode-locked pulses. Generation of picosecond and subpicosecond pulses from a dye laser, mode-

locked by an absorber with a recovery time of several hundred picoseconds and operated close to laser threshold, shows good agreement between experimental observations and theoretical calculations. In addition, comparison of mode-locking and pulse compression regions of operation and the generation of SSP both within and outside the pulse compression regime as predicted by New's approach shows that our model represents a more general theoretical analysis towards the problem. These results suggest that our model should prove useful in the search for optimal mode-locked CW dye laser performance although the detailed mechanisms controlling and limiting the pulsewidth still remain to be explored. Moreover, as passive mode-locking in the CW lasers is apparently similar to that in long-pulse flashlamp-pumped systems which, as will be shown, can be regarded as operating in a quasi-continuous mode, it is anticipated that our model may also be applicable to those systems under certain circumstances. Accordingly, in the following chapter, the extent of the applicability of our theoretical model to the mode-locked pulsed lasers will be investigated.

CHAPTER 5

THE DYNAMICS OF MODE-LOCKING IN PULSED GAIN LASERS

5.1 Introduction:

It has been pointed out in Chapter 1 that there are two basically distinct types of mode-locked lasers produced by a suitable saturable absorber. On the one hand, there is the mode-locking (Type II) of Nd:glass, ruby or other similar giant-pulse laser systems. In this case, the saturable absorber acts in such a way as to select an intensity peak from the initial noise distribution during the growth of the giant pulse. In general, the mode-locked pulse length is limited to times no shorter than the absorber recovery time and the dynamics of the laser gain do not play a major role in the pulse development process. On the other hand, there is the mode-locking (Type I) of CW or quasi-CW laser systems employing saturable absorbers. For this situation, both the gain and the absorber dynamics play an important role in the production of mode-locked pulses and the output pulses can be much shorter than the recovery times of either. This mode-locking situation represents a true steady-state solution of the dynamical equations governing the laser operation. In contrast, the type II mode-locking is a transient dynamical solution which

never attains a steady-state. The type II laser output is such that the pulses generally broaden during the latter part of the output train and lasing is cut off by gain depletion. Typically, the recovery time of the gain is much longer than the cavity round trip time, and the laser must be operated close to threshold.

A number of analyses of pulse formation in type II mode-locking systems such as Nd:glass and ruby lasers of varying degrees of complexity have appeared in the literature[40-45]. The basic processes involved are reasonably well-understood in principle, although the details of pulse production in experimental systems is not always so well comprehended or analysed. On the other hand, the case of CW laser mode-locking employing saturable absorbers has been analysed in the foregoing chapters of this thesis. In a sense, the two situations analysed represent opposite extremes in that for type I systems only the (long-time) steady-state solutions are obtained, whereas for type II systems the short-time transient solutions are studied. Whether a time interval is to be regarded as long or short in the above can be approximately determined by comparison with the gain recovery time. The range of validity of these two analytical approaches has not been fully explored, nor have any studies been made of the transition region between these two extreme cases. Accordingly, in this chapter we address ourselves to these and related problems by investigating the dynamics of mode-locking in pulsed gain systems. The flashlamp-

pumped dye lasers[5,76] are taken as representative examples both because they are important sources of wavelength-tunable high-intensity picosecond pulses, and because the laser operating time of these systems is typically ∿ 1 μsec which is relatively long compared with the gain recovery and the cavity round-trip times both of which are a few nanoseconds. It is to be anticipated that the steady-state solutions of the dynamical laser equations will apply to a pulsed gain system provided that the laser operating time is longer than the time taken for the establishment of the steady-state solution. When this circumstance holds, the laser operating regime may be described as quasi-steady-state. The work to be described in this chapter is aimed at investigating whether and if so, where such an operating regime occurs for flashlamp-pumped dye lasers, and at comparing the solutions generated by numerical simulation with observed output pulses.

5.2 Analysis:

The plan of attack is to investigate the stability of the time-invariant solutions of a CW dye laser with parameters appropriate to flashlamp-pumped dye lasers. The regions of instability of these initially time-invariant solutions will then be tested directly by studying numerically the dynamics of the build-up of pulsing solutions from initial low intensity states. Interest is centered on the time taken to establish steady-state pulses (SSP) over a range of laser parameters typical of flashlamp-pumped dye lasers. For specific cases,

the observed laser output pulses and the numerical simulations are compared. It will be shown that, for a significant range of typical laser parameters, flashlamp-pumped dye lasers operate over a sufficiently long time to attain steady-state conditions. That is, in essence, the output pulses are SSP.

The theoretical model employed in the calculations presented here is just that developed in Chapter 2 and used in Chapters 3 and 4. The only modification is that, in some calculations, the effect of the photoisomer formation of the absorber (DODCI)[76] during the build-up of the mode-locked pulses is taken into account by assuming a simple form of time dependence to the low-signal loss of the absorber. As will be shown, with this simple simulation, it is possible to study and compare with experimental observations the variations in the establishment times of the SSP as the laser is being tuned to operate at different wavelengths.

The case of saturable absorber mode-locking in high gain dye lasers has been investigated by New employing his pulse compression model[46,47]. Accordingly, it is appropriate to discuss the connection between the approach due to New and the problem we are now dealing with. Details of the pulse compression model have been introduced in Chapter 4. In this model, constant energy solutions are sought within a rate-equation formalism, in which the propagating pulse is compressed during each round-trip within the laser. As we have already pointed out (Chapter 4), such a calculation cannot be employed to generate

a stable temporal solution for the laser pulse - the pulses simply continue to narrow indefinitely (subject to the applicability of the rate-equation model). In fact, New postulates that the system reaches a constant energy state rapidly, and then the pulse proceeds to narrow each round-trip for operation in the pulse compression regime. As a consequence, such an approach is particularly well suited to modelling the very rapid pulse compression which occurs during the initial build-up of the pulsing solution, prior to the approach to steady-state pulse shape. This has been demonstrated by New[47]. However, since we are interested here in the time taken to establish SSP, the model due to New cannot be employed. Accordingly, an extensive survey is not undertaken concerning the comparison of our theoretical model and that due to New for parameters appropriate for flashlamp-pumped dye lasers. However, it does seem appropriate to compare the difference in mode-locking and pulse compression regions for this case (see Fig. 5-1) which, as can be seen, is very similar to Fig. 4-3 for low-gain CW dye lasers. On the other hand, it has been found that[86] for the high-gain dye lasers, the original full density matrix, radiation field coupled equations should be employed for the generation of SSP since the final pulse length tends towards the phase memory times of the gain and saturable loss, even for values of λ_o very close to threshold. This situation is very different from that of low gain CW dye lasers (Chapter 4) for which SSP can be generated within the

Fig. 5-1 Comparison of mode-locking and pulse compression regions for parameters appropriate to flashlamp-pumped dye lasers. The effect of finite recovery time of the absorber has been taken into account for the calculation of the pulse compression region using the composite medium model as described in Chapter 4. Note that the lower bound of the mode locking region is very close to the threshold given by $\lambda_o = 1$. Parameters: $T_1 = 5.5$ nsec., $T_2 = 0.05$ psec., $T_1' = 0.3$ nsec., $T_2' = 0.065$ psec., $\alpha_a L_a = 3.20$, $\gamma_g = 0.50$ and $m = 3$ ($s = m^2/(T_2/T_2') = 11.7$).

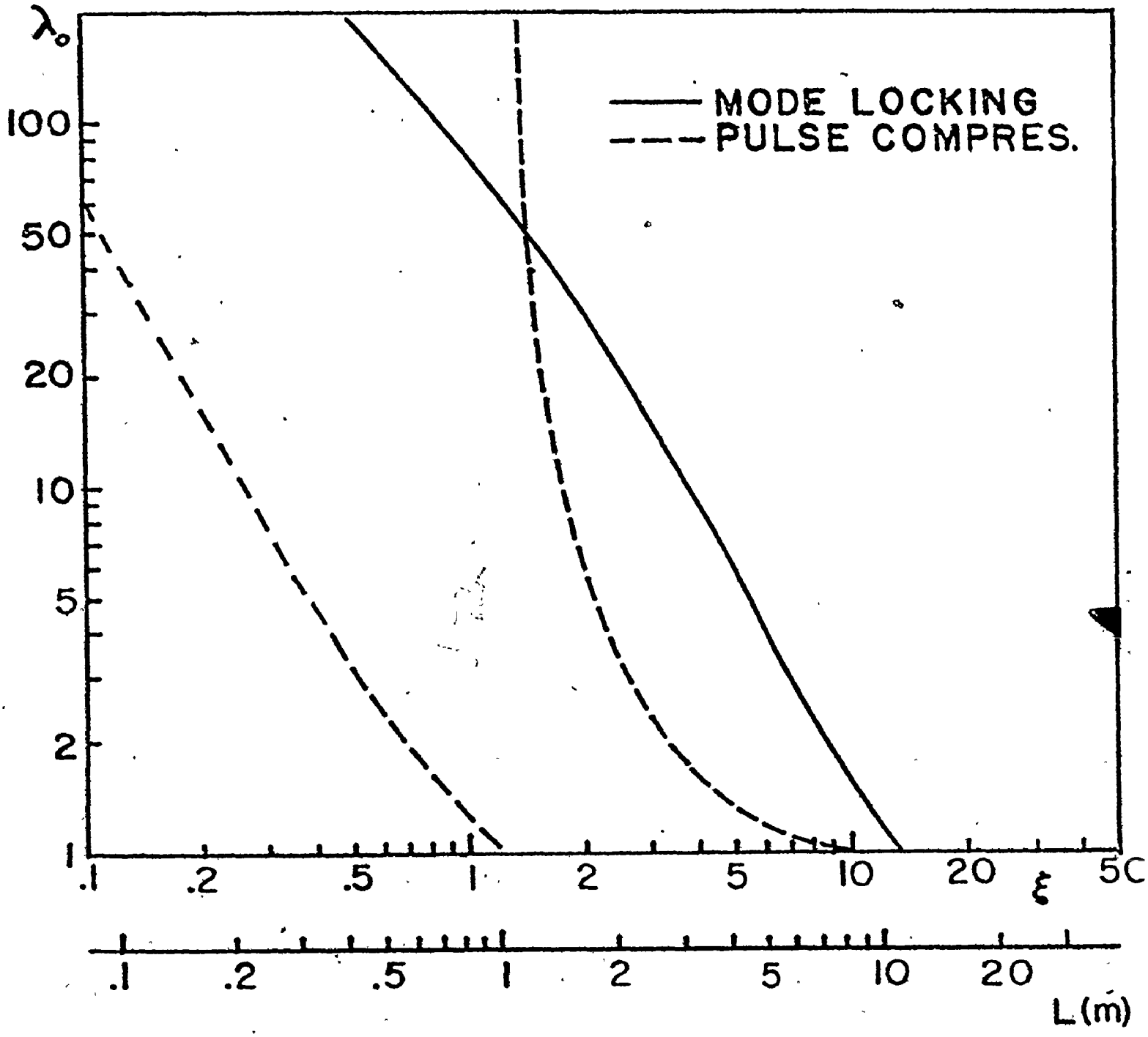
λ₀
100
50
20
10
5
2
1
MODE LOCKING
PULSE COMPRES.
.1
.2
.5
1
2
5
10
20
ξ
50
.1
.2
.5
1
2
5
10
20
L(m)

Fig. 5-1

rate equation approximation if the operating point is chosen to be sufficiently close to threshold.

5.3 Evolution of SSP in Flashlamp-pumped Dye Lasers:

5.3.1 Mode-locking Regions:

The mode-locking regions have been calculated for parameters appropriate to high-gain flashlamp-pumped dye lasers such as are reported by Bradley and his co-workers[5]. Figure 5-2 shows the range of mode-locking for one pulse propagating in the laser resonator as γ_g is varied for three different cavity lengths. In general, the range of values of λ_o over which mode-locking can be obtained is very large. Furthermore, the inclusion of solutions involving more than one pulse in the resonator leads to instability regions over a larger range of λ_o at a given γ_g than for only one pulse.

5.3.2 The Definition of an Establishment Time for the SSP

Having calculated the mode-locking regions, the next step is to investigate whether mode-locked pulses (SSP) occur within these regions, and then to study the time taken to establish the SSP solutions for suitably chosen laser parameter ranges. The idea of an "establishment time" for the SSP is intuitively clear, but for purposes of comparison, it is necessary to select some arbitrary defintion. Accordingly, the SSP build-up time is defined to be the time taken (or the number of round trips) for build-up of the solution to 90% of the SSP intensity from an initial field distribution which is very slowly varying in space with an average value of 1% of the

Fig. 5-2 Mode-locking regions as a function of γ_g for three different cavity lengths L = 1.08, 1.50 and 2.16 m, assuming one pulse propagating in the laser cavity. Other parameters: T_1, T_2, T_1' and T_2' the same as in Fig. 5-1, $\alpha_a L_a = 2.10$, m = 3.0. Only one line is drawn for the lower boundary ($\lambda_{o,min}$) since the variation with L is relatively small.

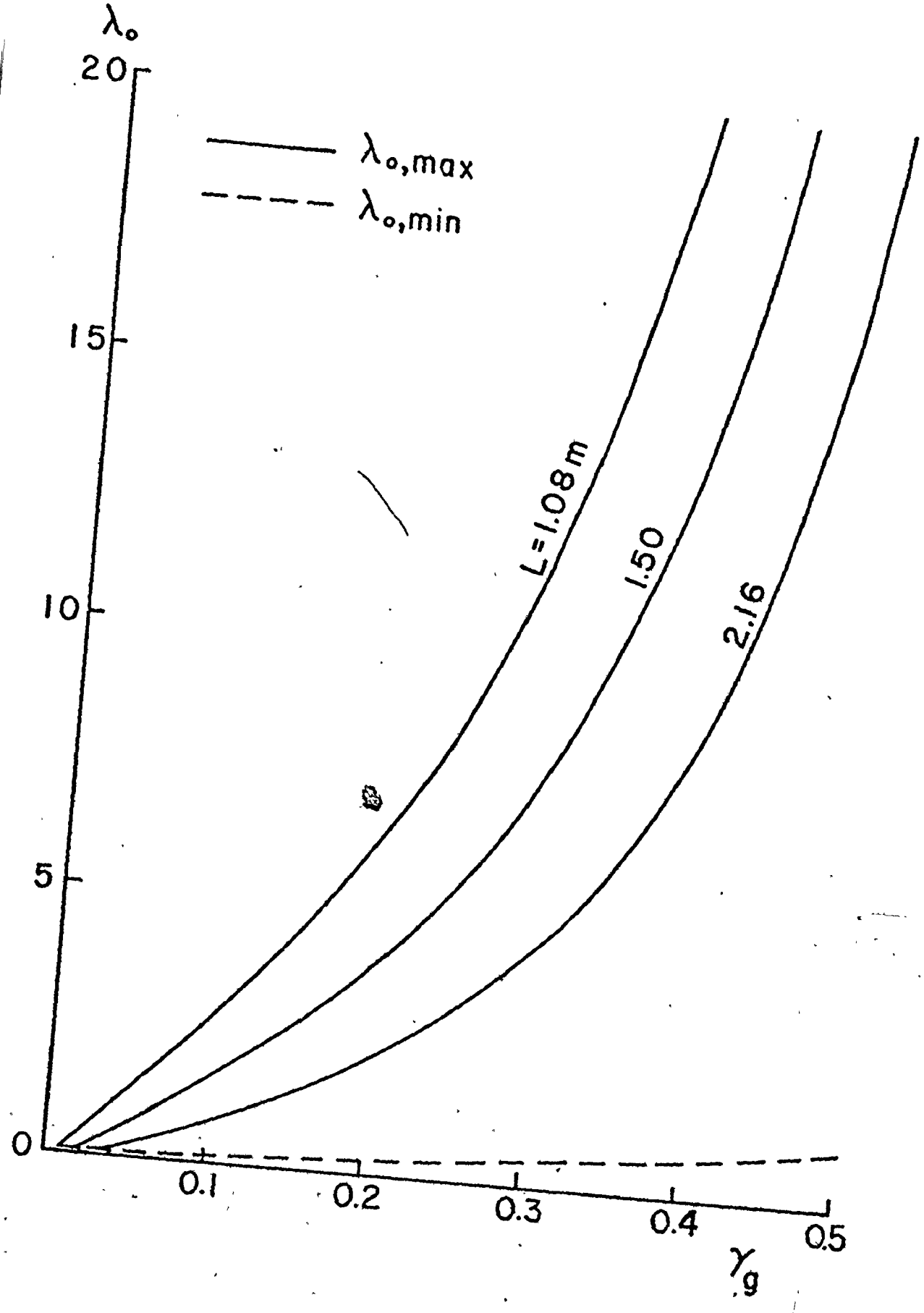

Fig. 5-2

intensity of the CW solution (the peak intensity of the SSP is typically 10^5 times that of the CW solution). In fact, this build-up or establishment time depends somewhat on the choice of initial field distribution. The above choice gives rather longer build-up times than are obtained with more realistic zero time intensity distributions including some regions of rapidly varying intensity in the laser cavity. Accordingly, the definition chosen represents a "worst case", at least among the initial distributions we have tested. However, since the laser operating time (typically $\sim$ 1 μsec) is much longer than the cavity round-trip time (a few nanoseconds), such a definition should be appropriate for our purpose.

5.3.3 Evolution of SSP (I) - Simulation of Photoisomer Formation:

The phase coherence times for the gain and loss media appropriate to dye lasers are extremely short ($\sim 10^{-13}$ sec). The use of finite difference equations for pulse propagation with increment sizes (in time) much less than T_2 would require the use of prohibitively large amounts of computer time, since the number of cavity round trips required to fully establish an SSP is typically in the region of one to two hundred. Accordingly, the following strategy is adopted. During the initial stages of the pulse build-up, the gain and loss media can be treated in the rate equation approximation (Appendix C) with the increment size in the numerical analysis being reduced as the pulse narrows. When the pulse length begins to approach

$\sim$ 1 picosecond ($\sim 10T_2$), the transition is made to the use of the full propagation equations (Appendix B) allowing for molecular coherence effects. As an example, Table 5-1 shows a record of a typical pulse propagation calculation, indicating the number of round trips, the calculational increment size, the normalized pulse peak and minimum intensities and the approximate value of the pulse width.

Observe that for the particular case shown in Table 5-1, the laser parameters chosen are typical of operation towards the long wavelength side of the mode-locking regimes obtained with a flashlamp-pumped Rhodamine 6G as described by Bradley[5]. The saturable absorption at such wavelengths is due partly to the formation of a photoisomer of DODCI during the build-up of the output pulses[76]. Detailed mechanisms of the photochemistry involved are still not very well understood. Further, an extensive investigation on this subject is not appropriate within the framework of our main concern. Accordingly, the effect of the photoisomer formation has been simulated in the calculation shown by supposing γ_g to be a function of time of the form:

$$\gamma_g(t) = \gamma_{go} + \gamma_{gi}(1-e^{-kt}) \qquad o \leq t \leq T \qquad (5-1)$$

where γ_{go}, γ_{gi}, k and T are chosen to fit the experimentally observed variation, and it is assumed that the build-up of γ_g ceases at t=T and is constant (γ_{gm}) thereafter*. The establish-

*Observe that, from N=35 up to N=80 (Table 5-1), the solution behaves not too differently from New's model in the sense that the pulse energy is approximately constant during the pulse propagation. The pulse narrows by a factor of 2 every 4 round trips and the peak intensity increases by approximately the same factor.

Evolution of the Steady-State Pulse from Quasi-CW Noise

Parameters: $T_1 = 5.5$ nsec, $T_2 = 0.05$ psec, $T_1' = 0.3$ nsec, $T_2' = 0.065$ psec, $L = 1.08$ m, $\alpha_a L_a = 2.10$, $m = 3.0$, $\lambda_o = 1.20$

No. of Round-trips N	Time-Step size Δt (psec)	Maximum Intensity[a] $\bar{I}_{max}$	Minimum Intensity[a] $\bar{I}_{min}$	Pulse Length $\Delta\tau_{1/2}$ (FWHM)
0	10	0.0269	0.0110	-
5	.	0.9256 (0.8338)[b]	0.6970	~ 1.80 nsec
10	.	1.0851 (0.9175)	0.6790	~ 1.14
15	.	0.9408 (0.8512)	0.4911	~ 0.96
20	.	0.8795 (0.8317)	0.3220	~ 1.30
25	.	1.0753 (0.6769)	0.1691	~ 1.11
30	.	1.7648 (0.4218)	0.0628	0.74
35	.	4.1207 (gone)	0.0134	0.42
40		11.07	0.0012	0.21
45	.	30.50	4.6×10^{-5}	0.08
50	.	76.69	$<10^{-6}$	0.03
52	2	116.3		20 psec
54	.	177.2		14
56	.	262.5		9
58	.	355.4		6
60	0.2	525.5		4.6
62	.	766.6		3.2
64	.	1150		2.2
66	.	1720		1.4
68	.	2561		0.9
70	0.02	3723		0.60
72	.	5572		0.42
74	.	8080		0.30
76	.	11150		0.23
78	.	14440		0.19
80	.	17720		0.16
84	.	22680		0.13
94	.	27220		0.12
104	.	28250		0.12
114	.	28380		0.12
134	.	28400		0.11
154	.	28400		0.11
174	.	28400		0.11

(a) Maximum and minimum intensity at the output section of the absorber, normalized to the CW intensity.

(b) The figure in brackets is the peak of a satellite pulse.

ment time of the SSP for the case illustrated in Table 5-1 is fairly long ($\sim$ 300 nsec). Cases more typical of operation towards the short wavelength side of the mode-locking regions for the Rhodamine 6G and DODCI combination have also been tested. The establishment of the SSP is much shorter ($\sim$ 100 nsec) as is expected since the gain is higher and the influence of the photoisomer dynamics is much less important.

Figure 5-3 shows the variation of the maxima and minima of the pulse as a function of the number of round trips in the laser resonator starting from a small, approximately constant intensity distribution, for the case given in Table 5-1. In addition, the figure shows a similar plot for a situation typical of operation at shorter wavelengths. This behaviour is qualitatively similar to that described by Bradley[5]. The output pulses at shorter wavelength are established very rapidly, whereas at longer wavelength there is a considerable period during which the output is close to a constant intensity before the onset of pulsing. The pulse peak intensity shown in the figure is much larger relative to the constant intensity than that shown in the oscillograms displayed experimentally. This is to be expected since these oscillograms are taken from a detection system which cannot respond fast enough to follow the light pulse intensity variations. Of course, the slow time-variation of the low signal gain has not been allowed for in the present calculations and so the output does not decay away. Nevertheless, in light of these

Fig. 5-3: Evolution of the steady-state pulse from quasi-CW noise. Plot of the maximum and minimum (normalized) intensities as a function of the number of round trips. Parameters: (a) $\alpha_a L_a = 2.10$, $\gamma_{go} = 0.12$, $\gamma_{gm} = 0.50$, $\lambda_o = 1.20$; (b) $\alpha_a L_a = 3.20$, $\gamma_{go} = 0.40$, $\gamma_{gm} = 0.50$, $\lambda_o = 0.80$. The cavity length used is L = 1.08 m (round-trip time = 3.6 nsec) and m = 3 for both cases. Values of T_1, T_2 T_1', T_2' are the same as in Fig. 5-1. The build-up of γ_g (Eq. (5-1)) is terminated at the end of the 50- and 30-th round trip for (a) and (b) respectively.

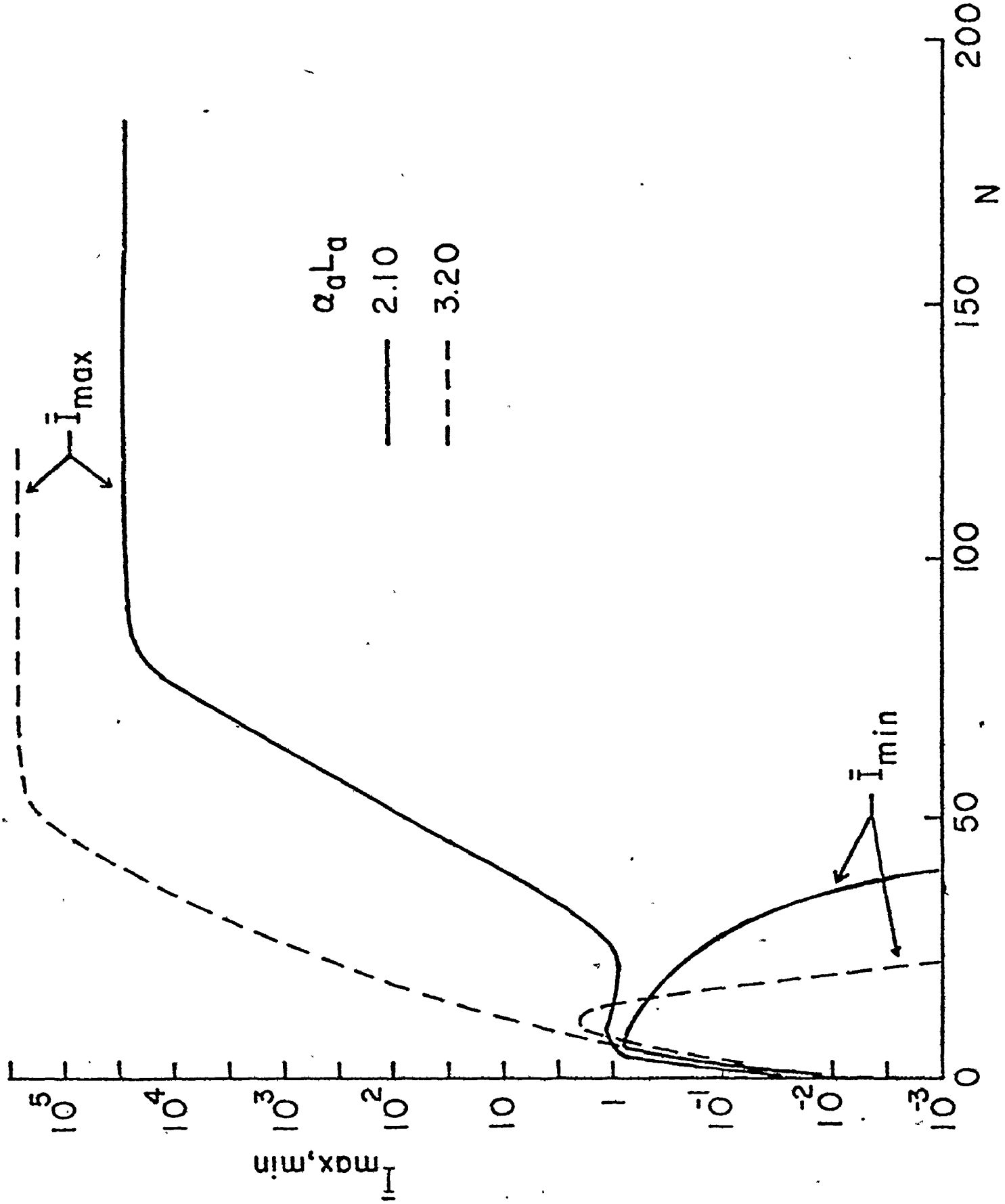
$\bar{I}_{max,min}$
10^{5}
10^{4}
10^{3}
10^{2}
10
1
10^{-1}
10^{-2}
10^{-3}
0
50
100
150
200
N
$\bar{I}_{max}$
$\bar{I}_{min}$
$\alpha_a L_a$
2.10
3.20

calculations, it seems probable that the high gain flashlamp-pumped mode-locked dye lasers described by Bradley and his co-workers[5] are operating in a quasi-continuous regime and the pulses close to being SSP. The time to establish an SSP is calculated to be in the region of 100-300 nsec, whereas the mode-locked laser output lasts for times in the region of one micro-second. One consequence of this is that a complete analysis of the dynamics of this type of laser necessarily requires an investigation of the generation of SSP. In this context, the approach due to New[46,47] can be regarded as a transient type of analysis since it can only account for the rapid pulse compression which occurs during the initial build-up of the pulse solution, prior to the approach to steady-state pulse shape.

5.3.4 Evolution of SSP (II) - Variation of Establishment Time with Laser Gain and Loss

Observe that the establishment time of the SSP calculated above are short because the gain and losses per round trip are very high. As the gain and loss are reduced, the establishment time is expected to increase until, at some point, this time exceeds the time over which laser oscillation takes place. Under these circumstances, a SSP solution will not be established and the laser will operate in a regime intermediate between the type I and tyep II mode-locking regimes. Figure 5-4 shows the variation of the SSP establishment time as $\alpha_a L_a$ and $\alpha_b L_b$ are simultaneously varied at constant linear loss and net low signal gain, i.e. both the values of R and

Fig. 5-4 Plot of the SSP peak intensity and establishment time for different values of $\alpha_a L_a$, and at constant cavity (linear) loss and net low signal gain. Parameters: L = 1.08 m, R = 0.40, λ = 0.10, m = 3, T_1, T_2, T_1' and T_2' the same as in Fig. 5-1. For the values of R and λ chosen, $(\alpha_a L_a - \alpha_b L_b) \simeq 1.01$ for all cases. The points plotted in this figure are the results obtained by computer simulations, assuming, for simplicity, γ_g does not change with time during the build-up of the SSP.

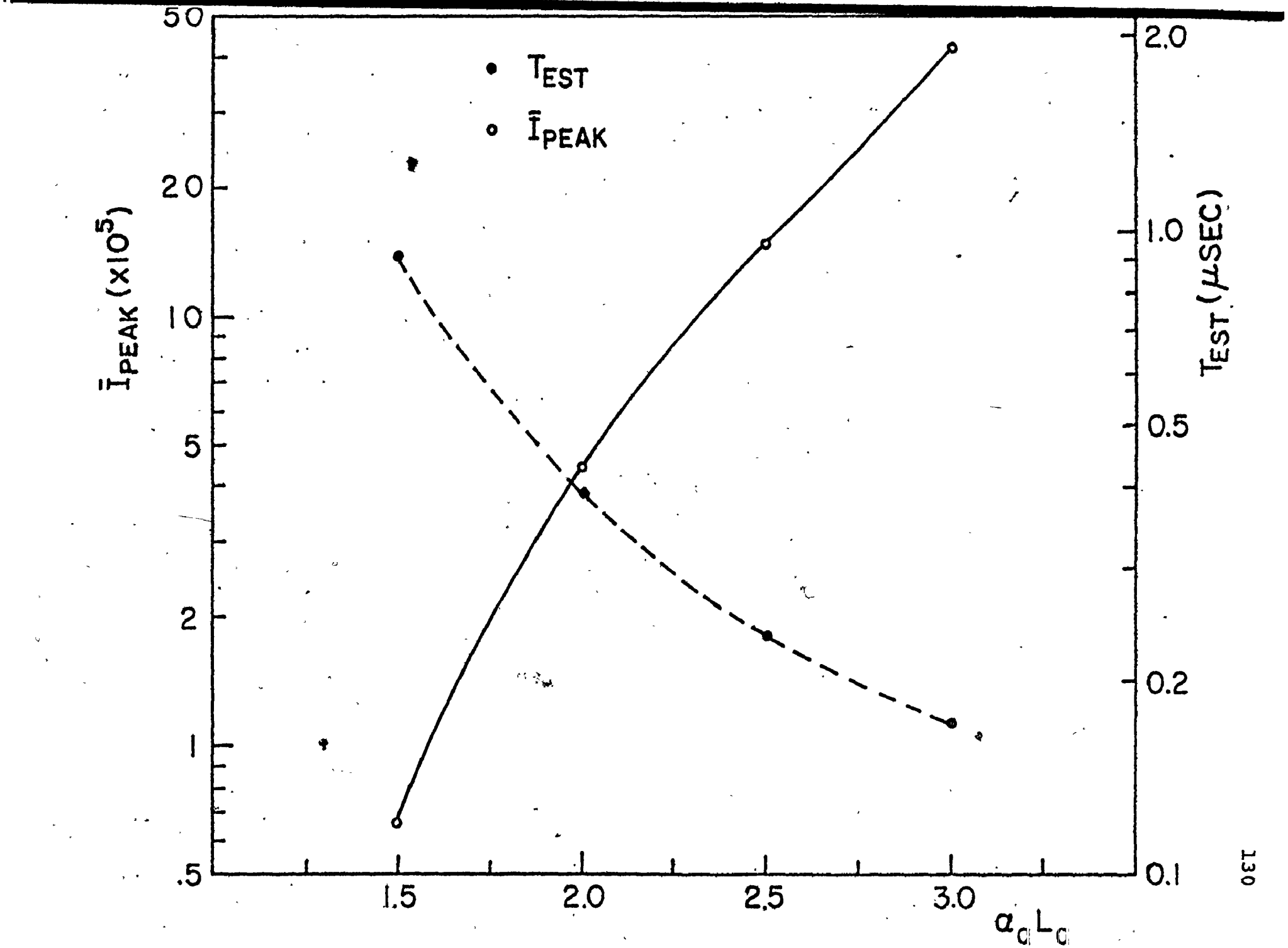
50
20
10
5
2
1
.5
$\bar{I}_{PEAK}$ (X10^5)
T_{EST}
$\bar{I}_{PEAK}$
2.0
1.0
0.5
0.2
0.1
T_{EST} (μSEC)
1.5
2.0
2.5
3.0
$\alpha_a L_a$

$\lambda[=(\alpha_a L_a - \alpha_b L_b)/\ell n(R^{-1})-1]$ are kept constant. For simplicity, the effect of the photoisomer formation of the absorber has not been incorporated in these calculations since it will not strongly affect our main conclusion. As anticipated, the establishment time increases as the laser gain and loss are reduced at least for the range of parameters investigated. This figure also shows how the values of the pulse peak intensity, normalized to the CW solution, varies over the same range of $\alpha_a L_a$. In addition, the evolution of the SSP's is also shown (Fig. 5-5) where the maximum and minimum (normalized) intensities are plotted as a function of the number of round trips. It can be seen that the period of approximately constant intensity before the onset of pulsing is relatively long for the case of lowest $\alpha_a L_a$.

Note that at the lowest value of $\alpha_a L_a$ investigated, the establishment time of the SSP is approximately equal to the time over which laser oscillation typically takes place[5]. For still lower values of $\alpha_a L_a$ the laser would turn off before a SSP could be established.

5.4 Remarks and Comments:

The calculations presented in this chapter indicate that, under typical experimental conditions, the high-gain flashlamp-pumped mode-locked dye lasers can be operated in a quasi-continuous regime where the output pulses are close to being SSP. As a consequence, a complete analysis of the dynamics of this type of laser necessarily requires an investi-

Fig. 5-5 Evolution of the SSP's corresponding to those described in Fig. 5-4. Plot of the maximum and minimum (normalized) intensities as a function of the number of round trips.

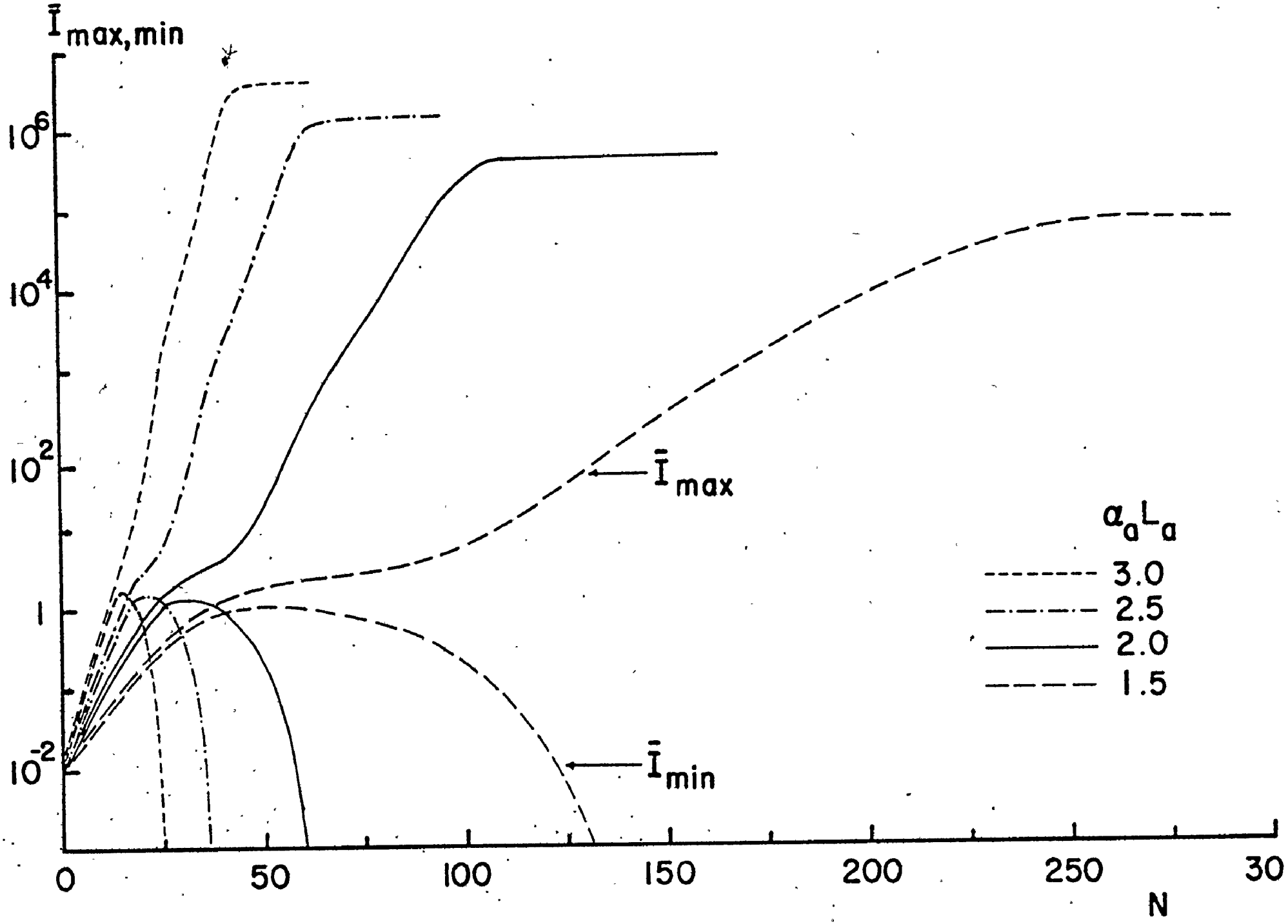
$\bar{I}_{max,min}$
10^6
10^4
10^2
1
10^{-2}
$\bar{I}_{max}$
$\bar{I}_{min}$
$\alpha_a L_a$
3.0
2.5
2.0
1.5
0
50
100
150
200
250
30
N

Fig. 5-5

gation of the generation of SSP. It is also shown that the establishment time of the SSP increases as the laser gain and loss are decreased, and the laser will be operating in a regime intermediate between the Type I and Type II mode-locking regime if the laser gain and loss are so low that the SSP cannot be established within the laser oscillation time.

In some calculations, the effect of the photoisomer formation of the absorber during the build-up of the SSP has been simulated by assuming a simple form of time dependence to the low-signal absorption. The results obtained show that the establishment of the SSP is much faster when the laser is operated at shorter wavelengths, which is in qualitative agreement with experimental observation.

The analysis summarized above suggests that our theoretical model can be applied to pulsed-gain laser systems provided that the laser operating time is not too different from the time taken for the establishment of the SSP.

Finally, observe that although the general behaviour of the solutions calculated here is in good agreement with observation, the calculated lengths of the SSP are generally a good deal shorter than experimental measurements indicate. It is possible that this discrepancy is due to the finite thermalization time of the upper and lower laser levels, which will tend to arrest the build-up (and hence the compression) of the laser pulse. This possibility requires further investigation, both because it is an important aspect of the dynamics of the pulse

build-up and also to see if there is some way to circumvent the consequences. Other possible causes for arresting the shortening of the pulse during build-up towards a SSP are the various dispersive effects within the laser cavity, and possibly the presence in the resonator of absorption which increases with radiation intensity[45].

CHAPTER 6

MODE-LOCKING AND RELAXATION OSCILLATIONS

6-1 Introduction:

It is well known that two basically different types of spontaneously pulsing laser output can be induced by the use of appropriate saturable absorbers[61,87-89]. For a suitable range of operating parameters, it is possible to produce mode-locked laser operation. However, under different circumstances, relaxation oscillations (also described as passive Q-switching) may occur in the laser output. Roughly speaking, the difference between these two modes of operation is characterized by the observation that, for mode-locking, the length of the output pulse is considerably less than the cavity round-trip time whereas the inverse of the relaxation oscillation frequency is longer than the cavity round-trip time in passive Q-switching. Physically, mode-locking involves the excitation of more than one cavity mode whereas passive Q-switching does not, and the relaxation oscillation period is not directly related to the cavity round-trip time.

Several treatments of passive Q-switching have been given in the literature[87-89]. Generally, the analysis has

been related to specific laser systems such as the CO_2 (low pressure) laser and double-cavity semiconductor laser. Restrictive assumptions concerning, for example, the relaxation times in the gain and absorber media are generally employed. Furthermore, in the theories presented thus far, it is invariably assumed that the spatial dependence of the photon density, the gain and loss may be neglected, and rate equations are employed to characterize the gain and loss media which are assumed to be homogeneously broadened two-level systems.

On the other hand, a theory of saturable absorber induced mode-locking has been given in the foregoing chapters of this thesis. Some of the results have also been reported[61,86,90,91]. In this theory, the rate equation formalism is not used to characterize the gain and absorber, but rather the density matrix formalism is employed, allowing for the incorporation of not only the gain and loss recovery times, but also the phase memory times of both media. In addition, the spatial dependences of the absorption, the gain and the laser field amplitudes are incorporated within this theory.

Despite the different approaches employed in the theories of saturable mode-locking and passive Q-switching as described above, there exist certain similarities concerning the mathematical treatments in a sense that both theories proceed in the following way. The CW (time-invariant) solutions for the radiation field, the gain and the saturable loss are determined and then the operational stability of these solu-

tions against small perturbations is examined. As a consequence, it appears to be possible that some sort of relationship can be established between these two theories although they describe two physically different types of laser operation. Accordingly, in the work to be described in this chapter, we consider the relation between the two types of instability described above, and show that the passive Q-switching solutions follow as a special case of the analysis given previously for the case of laser mode-locking using saturable absorbers. A method of differentiating between these instability regimes is given, and it is shown how the regions of mode-locking should be corrected, where necessary, by the subtraction of the relaxation oscillation regime. The analysis is employed to generate a method for investigating the relaxation oscillation regions when the spatial dependence of field and medium variables is incorporated. The model constitutes a generalization of previously published work, and the difference between the two approaches is tested for specific cases. Finally, the formalism is employed to study the transition from mode-locked regions of operation to relaxation oscillation regimes for several continuous or quasi-continuous laser systems. As a particular result, it is suggested that relaxation oscillations from flash-lamp-pumped dye lasers and mode-locking in suitable semiconductor lasers may be obtainable.

6.2 The Laser Dynamical Equations in the Rate Equation Approximation:

In this section, several stages of simplification to the laser dynamical equations developed in Chapter 2 and employed previously for the investigation of saturable absorber mode-locking are discussed. The analysis is first specialized to the case in which both the gain and absorption media can be described by rate equations (that is, when atomic coherence effects are negligible) but the spatial variation of the dynamical variables is retained. Finally, the equations describing the situation in which this spatial variation is also omitted are generated. This last situation has been treated by other authors[87-89] in the analysis of relaxation oscillations, generally with more restrictive assumptions concerning laser gain and absorption media parameters, and with a rather different mathematical approach.

6.2.1 Rate Equation Formalism, Including Spatial Variation of Dynamical Variables:

The laser dynamical equations describing the gain and absorber media developed in Chapter 2 (section 2.2) can be reduced to a rate equation formulation by employing the following approximations:

$$\left|\frac{\partial P_a}{\partial t'}\right| << \left|P_a\right| \quad ; \quad \left|\frac{\partial P_b}{\partial t'}\right| << \gamma_2 \left|P_b\right| . \qquad (6\text{-}1)$$

In this case, the dynamical equations (2-39) and (2-40) for the gain and absorber respectively reduce to the following sets:

$$(P_a = D_a E_a)$$

$$\frac{\partial D_a}{\partial t'} = -D_a I_a - \gamma(D_a - 1) \qquad (6\text{-}2)$$

$$\frac{\partial I_a}{\partial x'} + \frac{\partial I_a}{\partial t'} = 2G_a D_a I_a$$

and

$$(p_b = D_b E_b/\gamma_2)$$

$$\frac{\partial D_b}{\partial t'} = -D_b I_b/\gamma_2 - \gamma'(D_b + a_o) \qquad (6\text{-}3)$$

$$\frac{\partial I_b}{\partial x'} + \frac{\partial I_b}{\partial t'} = 2G_b D_b I_b/\gamma_2$$

where $I_a \equiv E_a^2$ and $I_b \equiv E_b^2$ are the radiation field intensities in the gain and absorber media respectively. All variables and other parameters* are as defined in section 2.2. Observe that the number of equations that must be solved has been reduced by the rate equation approximation to four from the previous six. However, as before, it is necessary to specify boundary conditions for the propagating field at the gain and loss cells and at the lossy reflector. It is easy to show from Eqs. (2-44) that the field intensities I_a and I_b must satisfy the following conditions:

$$m^2 I_a(x_2', t' - \Delta_{23}) = I_b(x_3', t')$$
$$m^2 I_a(x_1' + L', t') = R I_b(x_4', t' - \Delta_{41}) \qquad (6\text{-}4)$$

where all other quantities are as defined in section (2.2).

---

*Note that, in the rate equation approximation, the quantity $\gamma_2 = T_2/T_2$ is just a scaling factor which is related to the cross-sections of the gain and absorber media.

6.2.2 Rate Equation Formalism, Omitting Spatial Dependence of the Dynamical Variables:

In this simplest case, it is supposed that the gain medium, the loss medium and the linear cavity loss are all distributed uniformly throughout the laser resonator. Furthermore, the spatial dependence of the populations of the two media and the radiation field is omitted, and so boundary conditions for the propagating field are no longer required. Evidently, this analysis will only apply if the build-up time, and the length, of the relaxation oscillation pulses are much longer than the laser resonator round-trip time. In this approximation, the equations which the media and the radiation intensity must obey reduce to

$$\frac{dD_a}{dt'} = -D_a I - \gamma(D_a - 1)$$

$$\frac{dD_b}{dt'} = -D_b I/\gamma_2' - \gamma'(D_b + a_o) \qquad (6\text{-}5)$$

$$\frac{dI}{dt'} = \tilde{G}_a D_a I + \tilde{G}_b D_b I - \gamma_c' I$$

where $\tilde{G}_a = \alpha_a L_a / L'$, $\tilde{G}_b = \alpha_b L_b / a_o L'$ and $\gamma_c' = \ell n(R^{-1})/L'$ with $L' = L/cT_2$ being the reduced cavity parameter as defined before. Note that the parameter $\gamma_2' (=\gamma_2/m^2)$ which appears in the above equations is, in the simplest case, just the ratio of the cross-sections of the amplifying and absorbing media*. It can be seen, with this in mind, that the equations given above are equivalent to those given previously by Powell and Wolga[87] in their analysi

*See section 4.4.1, where we pointed out that the parameter s used by New[47] is equivalent to our parameter $(\gamma_2')^{-1} = m^2/\gamma_2$.

of passive Q-switching of low pressure CO_2 lasers.

6.3 Time-Invariant (CW) Solutions and Instability Analysis:

Exact time-invariant (CW) solutions of the laser dynamical equations can be found for the rate equation models given in the previous section. It can be shown that, as expected, the solutions for the rate equation approximation with proper allowance for spatial variations of the dynamical variables are identical to those that are found in section 2.3 for the model employing density matrix formalism. On the other hand, the case where the spatial dependence of the variables is omitted has somewhat different and simpler solutions. The relevant details are given in Appendix E for both cases. Furthermore, the stability of the time-invariant (CW) solutions is determined by investigating the response of the system to small perturbations. The basic approach is the same as that described in section 2.4 (and Appendix A) for the model appropriate to saturable absorber mode-locking; more details are given in Appendix E. In each case, dispersion equations for $\beta = \beta_r + i\beta_r$ are found, and the range of operating parameters over which β_r is positive is investigated. Observe that the functional form assumed for the perturbations naturally differs between the various cases.

In the following section, the instabilities which can be generated in the different models, including the one which has been employed in the previous chapters, are investigated, starting with the simplest situation.

6.4 Types of Laser Pulsation Regimes:

6.4.1 Relaxation Oscillations - The Rate Equation Models

(a) A Conventional Model - Omitting Spatial Dependence of Dynamical Variables

The rate equation formalism, without allowance for spatial variations of the system variables, has been treated previously by a number of authors[87-89] particularly for the case that the absorber and gain recovery times are equal. The derivation of the appropriate dispersion relations for β in the more general case of unequal response times can be found in Appendix E. Observe that in this case, no spatial variation of the perturbations is in order, and the functional form is taken as:

$$f(t') = f_o \exp(\beta t') \qquad (6\text{-}6)$$

where f_o is a constant. The equations to be satisfied by $\beta = \beta_r + i\beta_i$ are of the form:

$$\beta_i^2 = 3\beta_r^2 + 2(p+q)\beta_r + [pq+(u+v)\bar{I}]$$

$$\beta_r^3 + (p+q)\beta_r^2 + (1/4)[p^2+q^2+3pq+(u+v)\bar{I}]\beta_r \qquad (6\text{-}7)$$

$$+ (1/8)[pq(p+q)+(pu+qv)\bar{I}] = 0$$

where the values of p, q, u and v are functions of the laser parameters (Appendix E), and $\bar{I}$ is the time-invariant field intensity. For a given set of parameters, the second equation above can be solved for β_r and then substituted in the first to give the value of β_i. The boundary of the instability regions can be found by setting $\beta_r = o$ in the dispersion equa-

tions, and then solving for β_i and $\bar{I}$. It turns out that the second equation, with $\beta_r = 0$, can be written in the form of a cubic equation for the intensity $\bar{I}$, i.e.

$$\bar{I}^3 + a_2\bar{I}^2 + a_1\bar{I} + a_0 = 0 \qquad (6\text{-}8)$$

where the values of a_0, a_1 and a_2 depend only on the gain and loss media response times (Appendix E). This circumstance provides a convenient way of determining the instability regions of laser operation. The roots of the above equation can be determined analytically, and those corresponding to real, positive values of $\bar{I}$ selected. The corresponding values of β_i and the linear distributed cavity loss (γ_c') can then be calculated from the original dispersion relations with β_r taken as zero.

The analysis given above permits the determination of the range of laser parameters over which instabilities in the CW solutions occur. Of course, it requires direct generation of the solution to the differential equations to show that stable oscillatory behaviour results for any given CW instability. On the other hand, the fairly simple nature of the dispersion equations permits the extraction of some further analytical insight into the instability behaviour. It will become evident subsequently that the type of instability which comes about in a particular laser system depends in an important way on the relation between the gain and absorber recovery times and the laser resonator round-trip time. In fact, it can be shown (Appendix E) that there is a maximum value

for the cavity length beyond which relaxation oscillations will not occur in a particular, but important, situation. The analysis leads to the following expression:

$$\frac{cT_1}{L_{max}} = \left(\frac{27}{4}\right)\left[\frac{\gamma_1(1+\gamma_1)}{\alpha_a L_a(\gamma_g\gamma_1^2-1)}\right] \qquad (6\text{-}9)$$

where L_{max} is the maximum allowed value of the cavity length, and $\gamma_1 = T_1/T_1'$ and $\gamma_g = \alpha_b L_b/\alpha_a L_a$ are defined as before (Table 2-1). It has been assumed in the derivation of this expression that $\gamma_1\gamma_2' = (T_1T_2/T_1'T_2'm^2)$ is equal to unity, i.e. $m^2 = \gamma_1\gamma_2$. (This condition has been shown to be optimum for the production of mode-locking previously.) The above equation for L_{max} can be rewritten as

$$\frac{L_{max}}{cT_1\alpha_a L_a} = \left(\frac{4}{27}\right)\left[\left(\frac{\gamma_1}{1+\gamma_1}\right)\gamma_g - \frac{1}{\gamma_1(1+\gamma_1)}\right], \qquad (6\text{-}10)$$

which can be regarded as a linear relation between a normalized maximum cavity length $\ell = L_{max}/(cT_1\alpha_a L_a)$ and γ_g, with γ_1 treated as a variable parameter. Figure 6-1 shows a plot of the equation for a number of values of γ_1, ranging from unity to infinity. Observe that there is no passive Q-switching regions for $\gamma_1 = 1$. This is a consequence of the special assumption $\gamma_1\gamma_2' = 1$ under which the expression for L_{max} was developed. Thus, no relaxation oscillations will occur for $0 \leq \gamma_g \leq 1$ when $T_1 = T_1'$ and the saturation behaviour of the two media is arranged to be the same. In addition, Equation (6-10) indicates that for given values of γ_g and γ_1, L_{max} is proportional to the

Fig. 6-1 Plot of $\ell = L_{max}/cT_1\alpha_a L_a$ as a function of $\gamma_g = \alpha_b L_b/\alpha_a L_a$ (Eq. (6-10)). The quantity $\gamma_1 = T_1/T_1'$ is treated as a variable parameter. Observe that there is no passive Q-switching region for $\gamma_1 = 1$.

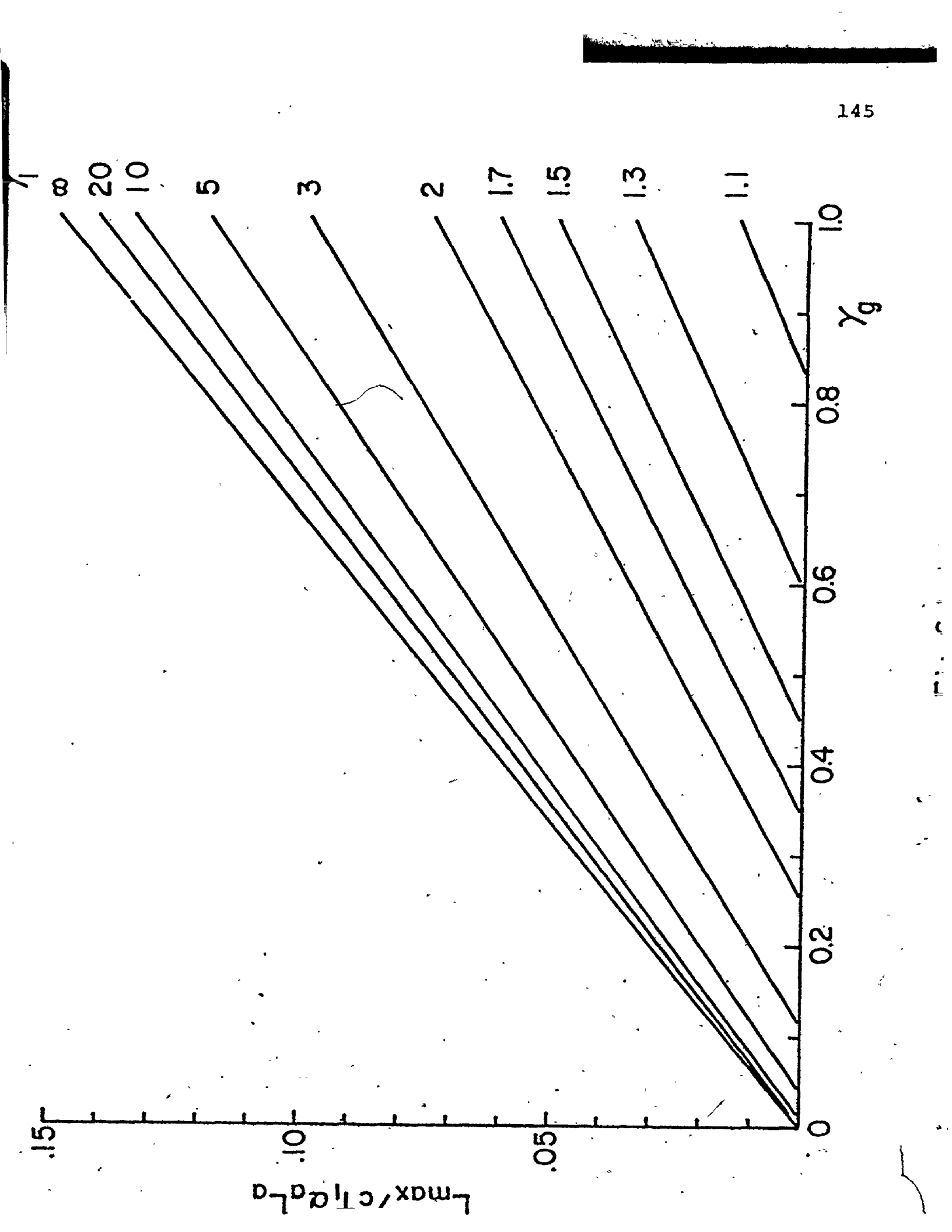
γ_l
8
20
10
5
3
2
1.7
1.5
1.3
1.1
γ_g
1.0
0.8
0.6
0.4
0.2
0
.15
.10
.05
$L_{max}/c\tau_l\alpha_L\alpha_L$

are allowed for if the laser gain and saturable loss are higher and/or the recovery times are longer. Further investigations reveal that this is a general property of the relaxation oscillation operation and the numerical value of L_{max} obtained from Eq. (6-10) usually gives a fairly good estimate for the maximum cavity length allowed when other models (as described subsequently) are employed, provided that the value of $\gamma_1\gamma_2'$ is not too different from unity.

(b) A Modified Model - Allowance for the Spatial Variations of the Dynamical Variables

In this subsection, brief consideration is given to pulsation conditions for the rate equation model in which spatial variations within the laser cavity are allowed for. The basic elements of the derivation of the characteristic equations for this case are given in Appendix E. The analytical form of the perturbations is taken as

$$f(x',t') = f_o(x')\exp(\beta t') \tag{6-11}$$

and the resulting dispersion equations are given by

$$\begin{aligned} &\ell n(R_2/R_1) - \ell n(R_3/R_4) + \beta_r L' = 0 \\ &(\phi_2-\phi_1)-(\phi_3-\phi_4) + \beta_i L' = 0 \end{aligned} \tag{6-12}$$

where R_j and ϕ_j are defined by

$$\begin{aligned} R_j\exp(i\phi_j) &= (\beta_r+\gamma+\bar{I}_j)+i\beta_i \ , \quad j = 1,2 \\ &= (\beta_r+\gamma'+\bar{I}_j/\gamma_2)+i\beta_i \ , \ j = 3,4. \end{aligned} \tag{6-13}$$

As expected, the dispersion equations (6-12) are rather more complicated than Eq. (6-7) for the case of no spatial dependence.

The above analysis constitutes a direct generalization of previously published work[87] on the subject of passive Q-switching by allowing for spatial variations of the gain, the loss and the radiation field. Figure 6-2 shows a comparison of the instability regions determined from the above analysis with those found by the method described in section (a). The laser parameters are chosen to be typical of a flashlamp-pumped dye laser system for which the behaviour of mode-locking operation has been investigated in Chapter 5. Evidently, for the laser system parameters considered, there are very significant differences between the two calculated instability regions. This is to be expected since the cavity round-trip time concerned is comparable to both the recovery times of the gain and the loss media and as a consequence the spatial dependence of the dynamical variables is important in describing the behaviour of laser operation.

As indicated earlier, the presence of instabilities does not prove that passive Q-switched relaxation oscillations will occur and recourse must be had to direct numerical testing of the temporal development of the laser output by computer simulation. The finite difference equations developed in Appendix C are employed for this purpose. It is found, for the cases investigated, that the existence of an instability in the time-invariant solution invariably leads to the occurrence of limit cycle behaviour. Figure 6-3 shows the result of two such numerical solutions; the relevant laser parameters are

Fig. 6-2 Comparison of the instability regions determined from the rate equation formalism with and without spatial dependence. Parameters: $T_1 = 5.5$ nsec., $T_2 = 0.05$ psec, $T_1' = 0.3$ nsec., $T_2' = 0.065$ psec., $\alpha_a L_a = 3.5$, $\gamma_g = 0.8$ and $m = 4$. The parameters chosen are typical of a flashlamp-pumped dye laser system. Note that the maximum cavity length as calculated from Eq.(6-10) is given by $L_{max} = 0.647$ m for $m = (\gamma_1 \gamma_2)^{1/2} = 3.77$.

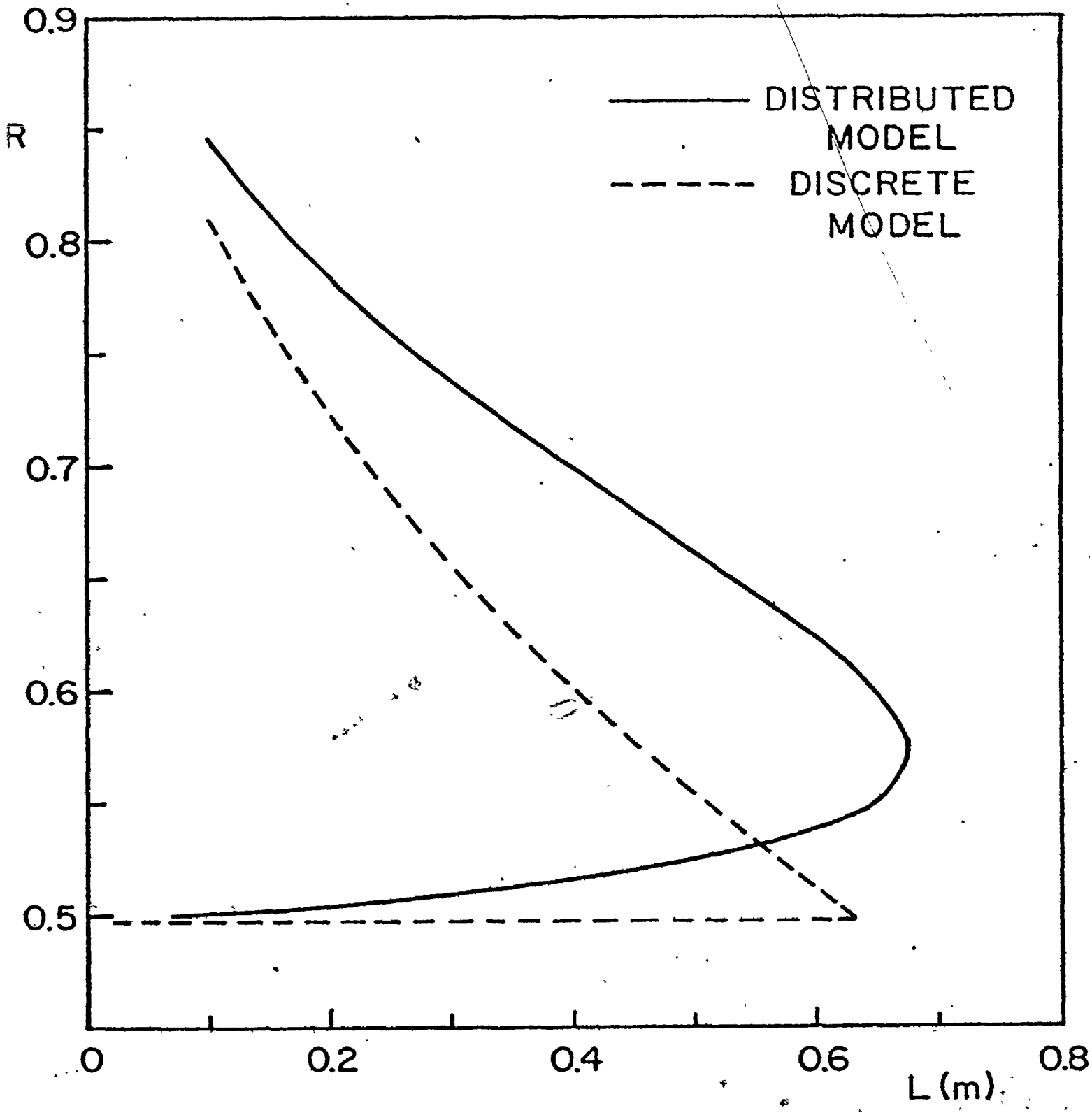
0.9
R
0.8
0.7
0.6
0.5
DISTRIBUTED MODEL
DISCRETE MODEL
0
0.2
0.4
0.6
0.8
L (m)

F[illegible]

Fig. 6-3 Relaxation oscillation pulses generated from the perturbed CW solutions by computer simulation. Parameters: L = 0.135 m, m = 3 and R = 0.80 and 0.61 for (a) and (b) respectively. Other parameters are the same as in Fig. 6-2. The normalized intensity (I/I_{CW}) is plotted as a function of the number of round trips N. For clarity, the temporal widths of the second and subsequent pulses plotted are, respectively, two and four times of the actual widths for (a) and (b). Observe the difference in the structure of the first pulse for the two cases. The envelope of the short spikes in (b) is shown by dashed line. For both cases, steady-state pulses have been established for the time period shown; the pulse widths (FWHM) are 1.87 and 1.42 nsec for (a) and (b) respectively.

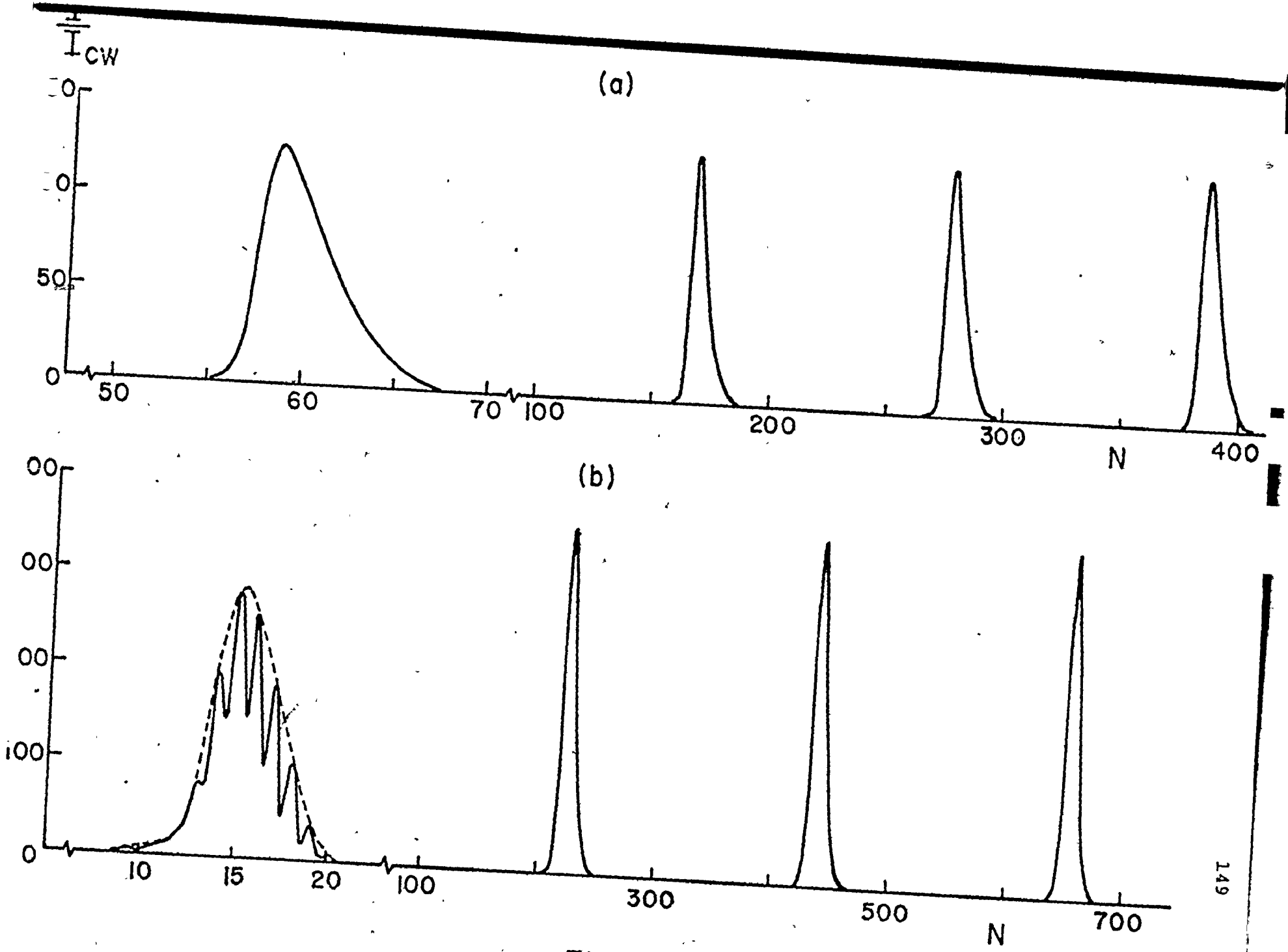
I_{CW}
(a)
0
0
50
0
50
60
70
100
200
300
N
400
(b)
00
00
00
100
0
10
15
20
100
300
500
N
700

Fig. 6-3

given in the caption. It can be seen that the pulsing output consists of quite short output spikes of high intensity relative to the CW solution. Furthermore, it is found that the value of β_i solved from the dispersion equations gives a reasonably good estimate for the relaxation oscillation period.

6.4.2 Mode-locking and Relaxation Oscillations - a General Model:

The generation of dispersion (characteristic) equations for $\beta = \beta_r + i\beta_i$ for the model (referred to as the "general model" hereafter) employed for the investigation of saturable absorber mode-locking has been discussed in Chapter 2 (section 2.4). Recall that, in this case, the rate equation approximation is not employed and the analytical form of the perturbation is taken to be

$$f(x',t') = f_o(x')\exp(i\frac{2\pi n x'}{L'} + \beta t') . \qquad (6\text{-}14)$$

Observe that when this model is applied to study mode-locking*, n is assumed to be a positive integer which corresponds to the number of mode-locked pulses circulating within the laser cavity. Now, if n is taken to be zero, the form of the perturbations is identical to that employed in section 6.4.1(b) (Eq. (6-11)). It follows that relaxation oscillation-type pulsation conditions can be generated as a special case of the general model. Furthermore, under certain circumstances,

*The rate equation formalism (including spatial dependence) with the same analytical form for the perturbation can also, but less generally, be used to study mode-locking. See Appendix E for further discussion.

instabilities found in the time-invariant solution for $n \geq 1$ may be nothing other than passive Q-switching instabilities. Evidently, if the system is unstable against relaxation oscillation, any perturbation will tend to grow. As a consequence, in an investigation of the mode-locking behaviour of lasers with intracavity absorbers, it is important to generate the instability regions for $n=0$ to exclude from the apparent mode-locking regime any part which is also unstable against passive Q-switching Besides this, the relaxation oscillation regions are of considerable intrinsic interest as is the region of transition between the two types of laser pulsation. Several numerical investigations directed towards the above issues are presented in the following section.

6.5 Mode-locking and Relaxation Oscillation Regimes:

For the calculations presented in this section, we have usually employed the general model. Comparison with the other models has been made where appropriate. In what follows, results are shown first for parameters appropriate to flashlamp-pumped dye lasers for which the mode-locking regime is of particular interest[46,47,86,91]. The dynamics of mode-locking of this type of pulsed gain lasers has been investigated in the previous chapter. Accordingly, in the first part of this section, we investigate the extent to which the predictions concerning the mode-locking regions for flashlamp-pumped dye lasers must be modified due to the presence of relaxation oscillation instability regions. In the second half of this section,

the situation of semiconductor lasers is analysed and the approach employed in the present calculation is related to previous analyses undertaken by other authors[88,89].

6.5.1 Flashlamp-pumped Dye Lasers:

The passive mode-locking of flashlamp-pumped dye laser is of particular importance in practice. This has been pointed out in the previous chapter. In addition, the dynamics of mode-locking operation has also been investigated therein. It has been shown that the laser operating time for this type of high-gain pulsed laser is sufficiently long for the establishment of the mode-locked steady-state pulses (SSP) and the laser operation mode can be regarded as quasi-continuous. Furthermore, it is found, by calculating the value of L_{max} from Eq. (6-10) that relaxation oscillation operation may occur for flashlamp-pumped dye lasers for parameter range of practical interest. This has been verified by the results shown in Fig. 6-2. Accordingly, it is important to investigate the extent to which the predictions concerning the mode-locking regions must be modified due to the presence of relaxation oscillation instability regions. In addition, it is also interesting to know whether relaxation oscillation pulses are observable within the laser operation time. Numerical results concerning these issues are presented below.

Figure 6-4 shows the regions of instability of the CW solutions for n=0 and n=1 (mode-locking with one pulse circulating within the resonator). These regions are calculated

Fig. 6-4 Regions of instability of the CW solutions for $n = 0$ (relaxation oscillation) and $n = 1$ (mode-locking) using parameters typical of the flash-lamp-pumped dye lasers: T_1, T_2, T_1' and T_2' the same as in Fig.6-2, $\alpha_a L_a = 3.20$, $m = 3$, $\gamma_g = 0.8$ and 0.2. The shaded areas are the relaxation oscillation regimes, and the solid lines are the boundaries of the mode-locking regions.

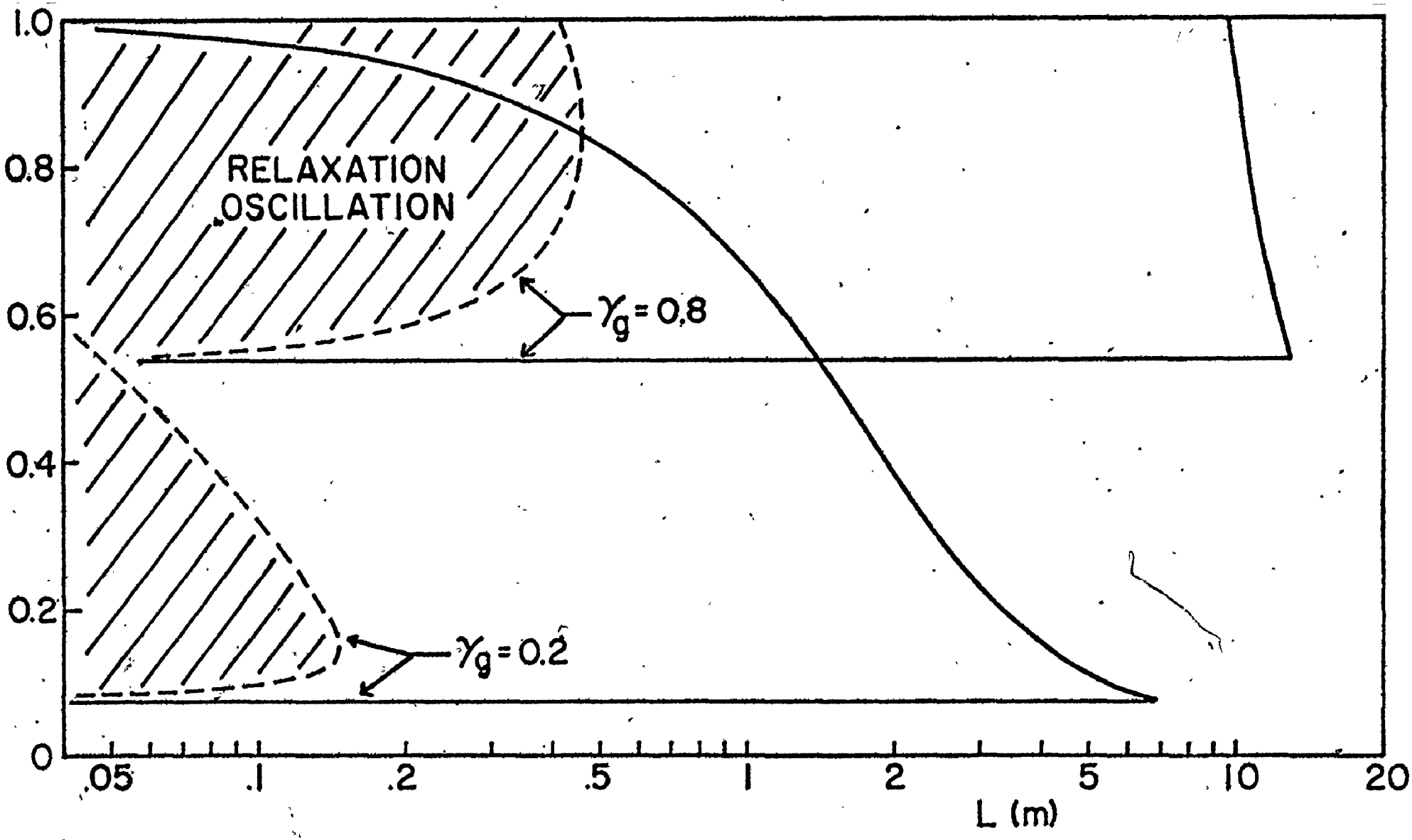
1.0
0.8
0.6
0.4
0.2
0
RELAXATION
OSCILLATION
$\gamma_g = 0.8$
$\gamma_g = 0.2$
.05
.1
.2
.5
1
2
5
10
20
L (m)

Fig. 6-4

for parameters typical of the flashlamp-pumped dye lasers reported by Bradley[5] and his co-workers. In this figure, two sets of instability regions are shown, where γ_g (the ratio $\alpha_b L_b/\alpha_a L_a$) has been employed as a variable parameter. Observe that in each case, a considerable portion of the apparent range of n=1 mode-locking at lower values of cavity length is actually due to an n=0 instability. In truth, this is an assertion which can only be verified by direct numerical testing of the build-up of the laser solution from an initial small value. Such investigations, over the range tested, show that the passive Q-switching solution invariably supercedes the mode-locking instability. However, there can be considerable noise structure retained within the envelope of the passive Q-switched laser output. Further investigations concerning the details of such laser operation are required, including build-up characteristics of the solutions and the dependence on laser gain and absorber properties.

Observe that, for a sufficiently long laser cavity, the system ceases to be unstable against single pulse mode-locking. However, the inclusion of solutions for n>1 (multiple pulse mode-locking) leads to instability regions at higher values of L. Note also that the (n=0) relaxation oscillation regime extends to sufficiently high values of L, particularly for high γ_g, that it lies within range of experimental investigation. This holds provided that the time taken for the onset of such a relaxation oscillation is sufficiently short that it be est[illegible] in the $\sim$ 1 μsec operating time of this

laser system. For the case shown in Fig. 6-3, the establishment time of the relaxation oscillation is approximately 200 nsec, and the time between successive pulses thereafter is $\sim$ 100 nsec*. Consequently, this operating regime is established sufficiently fast to permit it to be observed during a flash-lamp-pumped dye laser pulse. The situation illustrated in Fig. 6-3 is for a rather short resonator; a more practical case would require a resonator several times longer. However, the overall behaviour is not greatly changed for longer resonators at higher values of γ_g, and several cycles of relaxation oscillation should be observable at practical values of resonator length.

In Fig. 6-5, the variation of the mode-locking and passive Q-switching regimes are shown as a function of γ_g for a fixed cavity length. In this figure, the ranges of operation are characterized by the values of the equivalent reflectivity (R) and the variation of γ_g is accomplished by varying the absorption ($\alpha_b L_b$) at constant low signal gain. Observe that, similar to that in Fig. 6-4, at high values of γ_g, a very considerable fraction of the total instability region is due to passive Q-switching operation rather than mode-locking.

---

*The propagation equations developed in Appendix C within the rate equation approximations (including spatial dependence) are generally employed for the generation of the relaxation oscillation pulses since the steady-state pulse length is expected to be much longer than T_2 and T_2'. In addition, for the parameter range investigated, it is found that the relaxation oscillation instability regions calculated by using the rate equation model are in good agreement with those found from the general model.

Fig. 6-5 Variation of mode-locking and relaxation oscillation regions as a function of γ_g, for a fixed cavity length. Parameters: L = 0.36 m, $\alpha_a L_a$ = 3.50, m = 3, T_1, T_2, T_1' and T_2' the same as in Fig. 6-2.

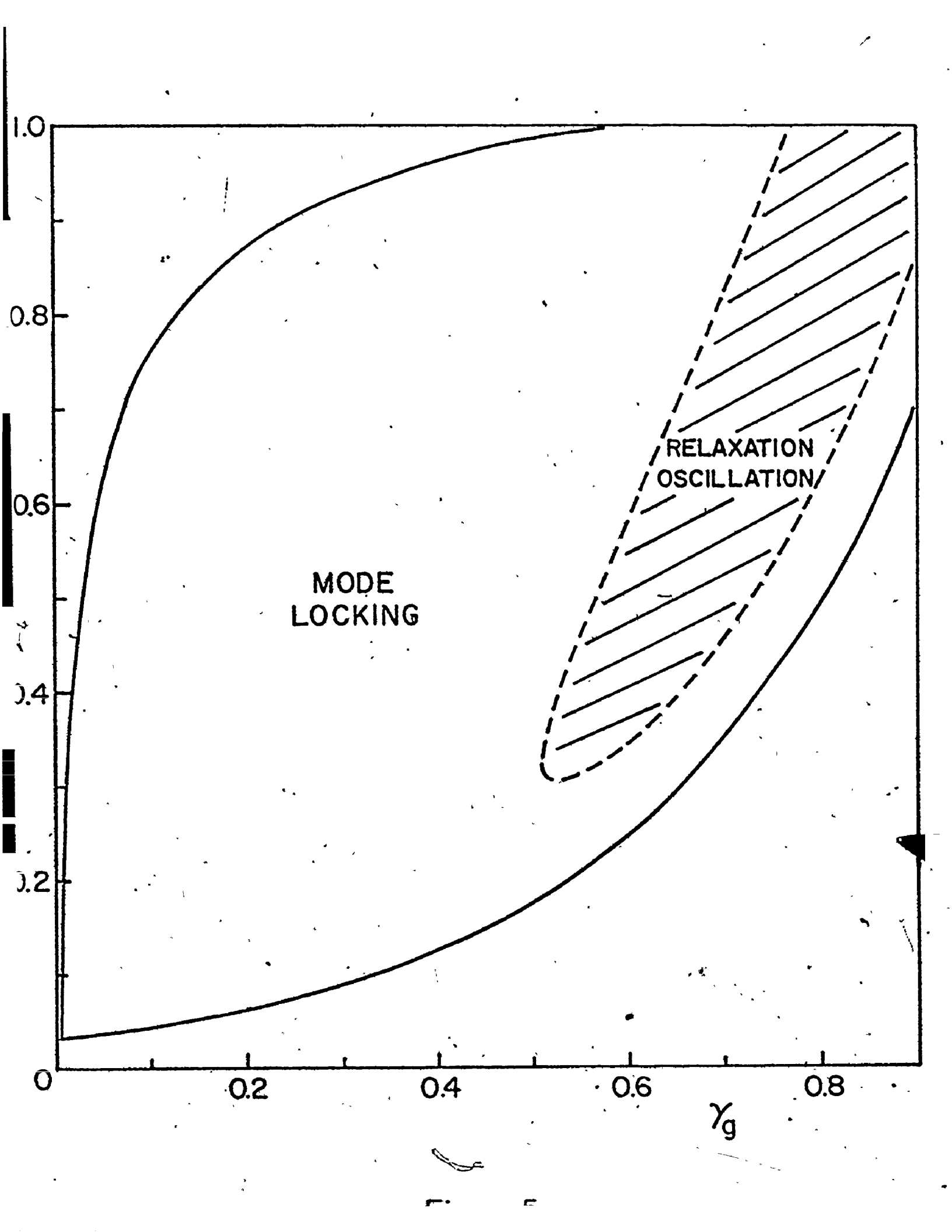
1.0
0.8
0.6
0.4
0.2
0
0.2
0.4
0.6
0.8
γ_g
RELAXATION
OSCILLATION
MODE
LOCKING

Note that the ranges of value of R over which both relaxation oscillations and mode-locking occur are strongly dependent on the value of m which is chosen. Generally speaking, the operating range for mode-locking is close to optimal when m is chosen to have the value of $\sim (\gamma_1\gamma_2)^{1/2}$, that is $\gamma_1\gamma_2' \approx 1$. Accordingly, this is normally employed as a general rule for choosing m in the previous investigations of mode-locking. However, it is of interest to reinvestigate this issue to determine how the passive Q-switching region changes as a function of m relative to the mode-locking regions. This is particularly important when $T_1 = T_1'$ and $T_2 = T_2'$ for which the choice of $m = (\gamma_1\gamma_2)^{1/2} = 1$ removes the passive Q-switching region in the distributed loss and gain model. This particular case will be considered in the following subsection when the situation of semiconductor lasers is investigated. At the moment, for the dye lasers, the variation of the instability regimes as a function of L for a given value of γ_g is shown in Fig. 6-6 for several values of m. Evidently, proper choice of the value of m permits considerable enhancement of either operating regime relative to the other. Furthermore, the maximum allowed cavity length depends rather strongly on the value of m for both the mode-locking and passive-Q switching operations.

6.5.2 Semiconductor Lasers:

So far, parameters appropriate to flashlamp-pumped dye lasers have been employed, primarily due to the importance of passive mode-locking in this system. Previously, a number of

Fig. 6-6 Variation of the instability regimes as a function of L for a given value of γ_g and several values of m. Parameters: $\alpha_a L_a = 3.20$, $\gamma_g = 0.5$, T_1, T_2, T_1' and T_2' the same as in Fig.6-2. The horizontal line denoted by R_{th} is the laser threshold defined by $\lambda_{th} = (\alpha_a L_a - \alpha_b L_b)/\ell n(R_{th}^{-1}) - 1 = 0$. This line serves as the lower boundaries for all the mode-locking regimes and also for the lower boundary of the m = 8 relaxation oscillation regimes.

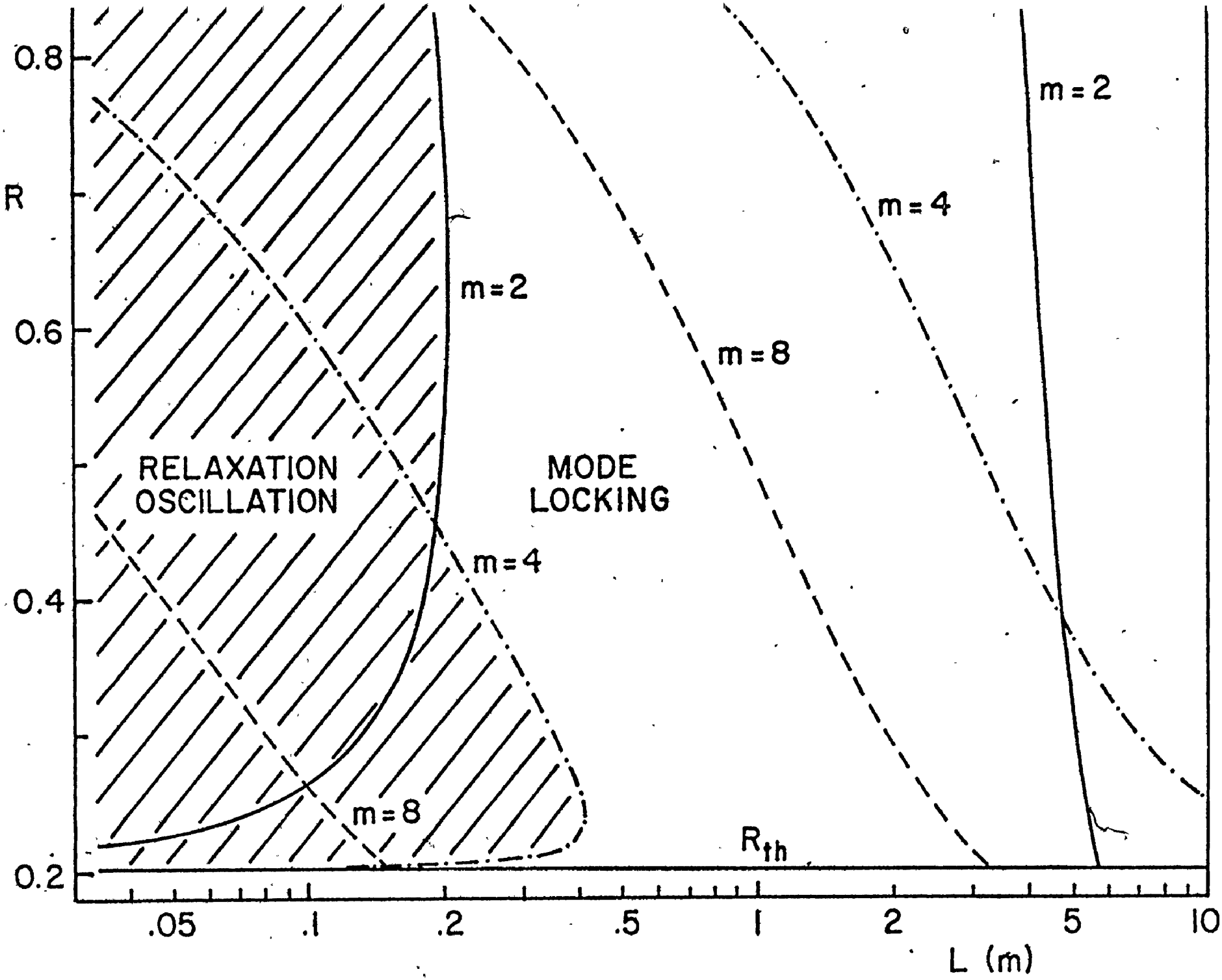
0.8
0.6
0.4
0.2
R
m=2
m=4
m=8
m=2
m=4
m=8
RELAXATION
OSCILLATION
MODE
LOCKING
R_{th}
.05
.1
.2
.5
1
2
5
10
L (m)

Fig. 6-6

authors have studied the case of passive Q-switching in semiconductor lasers[88,89]. In general, attention has been fixed upon a system in which both gain and absorption are obtained from diodes constructed of the same material but operated at different drive currents. The two diodes are electrically independent but optically closely-coupled, forming two parts of a laser resonator cleaved from the semiconductor material. In the analysis of this situation, it is generally supposed that $T_1 = T_1'$ and implicitly $T_2 = T_2'$ (since the optical cross-sections in the two media are taken to be the same). Furthermore, due to the structure of the optical cavity, there is no laser mode-size change between the two media and so $m = m_o m_d = 1$ as both m_o and m_d (ratio of μ_b/μ_a) are unity. For a model employing distributed loss and gain in a rate equation approximation, this situation precludes passive Q-switching operation over the whole operating regime (see Fig. 6-1). Consequently, in order to produce instability in the CW solutions, it is necessary to invoke some other effects such as that the gain (loss) depends in some nonlinear fashion on the "inversion"[88]. In the present analysis, a rather different approach is employed and the transition between the relaxation oscillation and mode-locking regions is investigated for parameters typical of semiconductor gain and loss media. Initially, it is supposed that T_1' may be chosen to be close to, but not equal to T_1. Practically, this could be brought about in several ways, such as the use of two somewhat different alloy compositions for a suitable semiconductor alloy system. A combination of direct bandgap transitions to produce

the gain and trapping levels for the absorption could also serve this purpose. In addition, we shall treat the resonator round-trip time as an independent variable. In practice, this may be accomplished by the use of the amplifier and absorber within an external resonator system. It will also be supposed that this system can be arranged so as to give different resonator mode diameters within the gain and absorption media if required.

The passive Q-switching and mode-locking regimes have been calculated as a function of the resonator length for parameters representative of semiconductor lasers* (see Fig. 6-7). Observe that, in this case, the mode-locking and relaxation oscillation regions do not overlap. Note that because T_1 is close, but not equal, to T_1', the value of m chosen is close to unity. Also, the value of L_{max} calculated from Eq. (6-10) is marked on the figure for comparison. The difference between this value and that found from the plotted curve is a measure of the deviation between the general model and its distributed variables counterpart. A curve marked n=1, $\gamma_g = 0.5$ is also shown on the figure. This indicates the shorter cavity length (lower) boundary of the n=1 mode-locking regions for a lower value of the saturable absorber loss. It can be seen

---

*The value for T_2 is not critical for investigation of the mode-locking instability regions provided that $T_2 = T_2'$. The value chosen here is reasonable for the laser level thermalisation time within the band and is of the right order of magnitude for the inverse of the operating bandwidth.

Fig. 6-7 Relaxation oscillation and mode-locking regimes as a function of the cavity length for parameters representative of semiconductor lasers. Parameters: $T_1 = 3$ nsec., $T_2 = 5$ psec., $T_1' = 2.5$ nsec., $T_2' = 5$ psec., $\alpha_a L_a = 1.0$, $\gamma_g = 0.8$, $m = 1.1$. The value of L_{max} calculated from Eq. (6-10) for the distributed rate equation formalism is also marked in for comparison with the general model since the value of $m = 1.1$ used here is very close to $m = (\gamma_1 \gamma_2)^{1/2}$. In addition, a curve marked $n = 1$, $\gamma_g = 0.5$ is also shown, which is the lower boundary of the mode-locking regime for $\gamma_g = 0.5$ and $m = 2$.

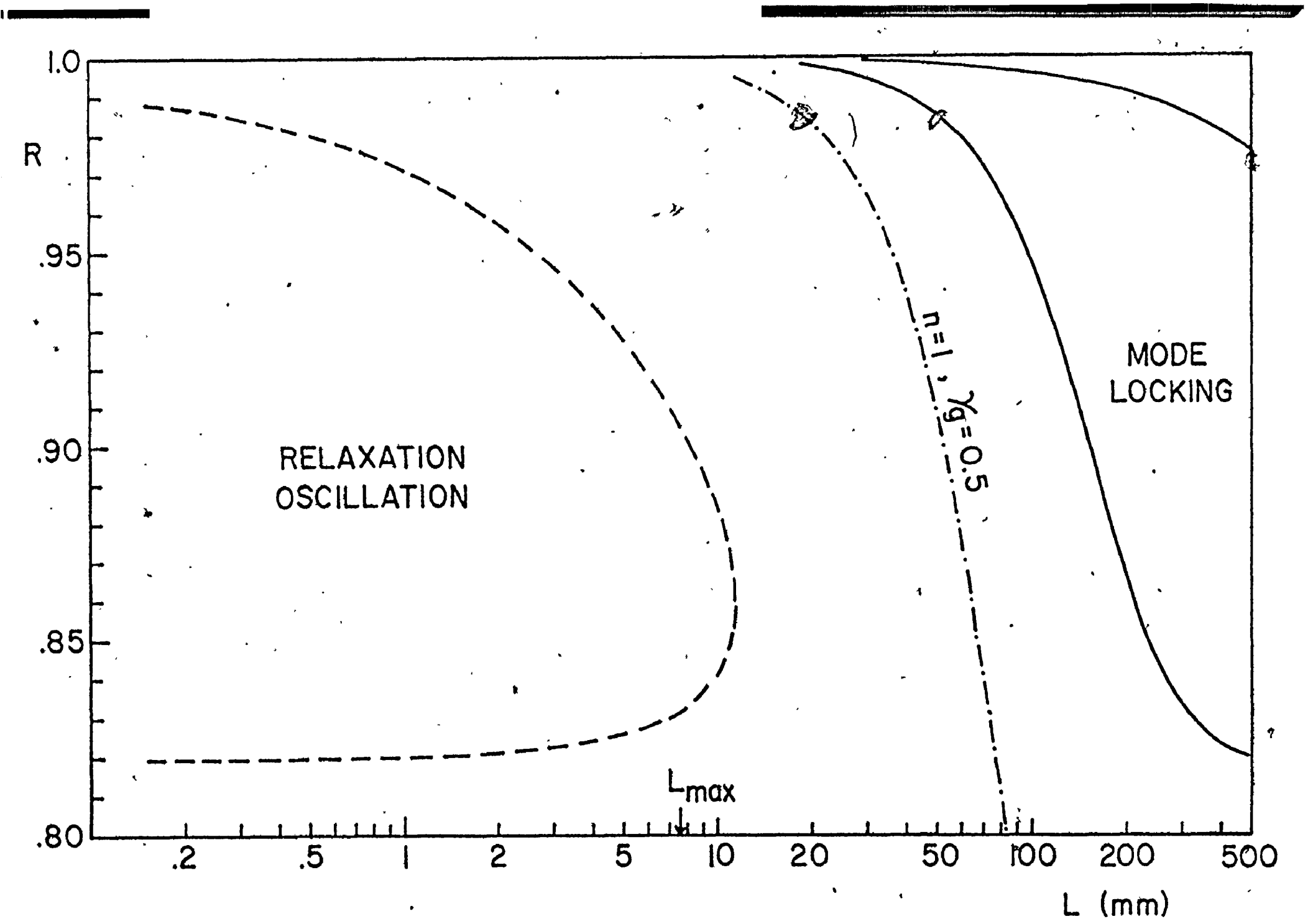
1.0
R
.95
.90
.85
.80
RELAXATION
OSCILLATION
MODE
LOCKING
n=1, l=1, γ=0.5
Lmax
.2
.5
1
2
5
10
20
50
100
200
500
L (mm)

Fig. 6-7

that mode-locked operation can be obtained within a resonator just a few centimeters long for practical values of the reflectivity. Note that the model employed for these calculations takes no account of dispersion due to the gain and loss media. Now, it is well-known that semiconductor media are strongly dispersive in the region where gain occurs. Nevertheless, if the mode-locked pulses are not very short (that is, the necessary oscillation bandwidth is restricted), the above model can represent a good approximation to the actual behaviour. Accordingly, it may be possible by operating fairly close to threshold to produce mode-locked operation of this system giving pulses with temporal lengths in the picosecond range at repetition rates considerably higher than 10^9 sec^{-1}.

Finally, an investigation has been made for the case $T_1 = T_1'$ with m treated as a variable parameter. Figure 6-8 shows the relaxation oscillation and the mode-locking regions as a function of the resonator length for several values of m. The values of m are chosen close to the value of $(\gamma_1\gamma_2)^{1/2}$ which for this system has the value of unity. Observe that the mode-locking regions are much less sensitive to the variation in m than the passive Q-switching regions. As a consequence, the above remarks concerning the possibility of mode-locking are not greatly dependent on the particular choice of T_1 and T_1'.

6.6 Summary:

The theoretical model previously employed to study saturable absorber mode-locking has been reexamined in this

It is shown that the type of instability generated

Fig. 6-8 Relaxation oscillation and mode-locking regimes as a function of L for several values of m. Parameters: $T_1 = T_1' = 3$ nsec., $T_2 = T_2' = 5$ psec., $\alpha_a L_a = 1.0$, $\gamma_g = 0.8$, m = 1.07, 1.1 and 1.3. Note that the values of m used are close to the value of $(\gamma_1 \gamma_2)^{1/2}$ which is unity in this case.

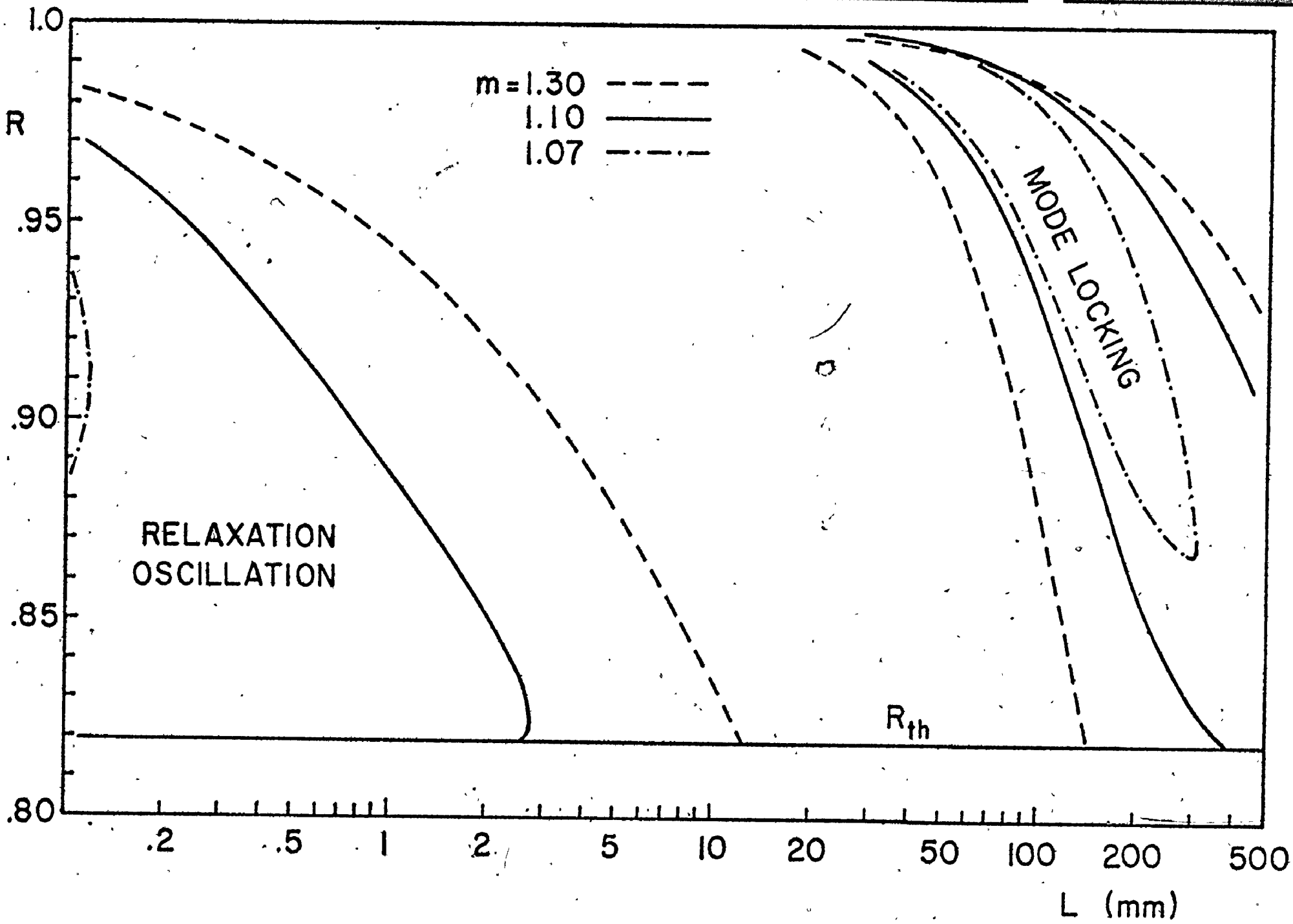
1.0
R
.95
.90
.85
.80
m=1.30
1.10
1.07
MODE LOCKING
RELAXATION
OSCILLATION
R_{th}
.2
.5
1
2
5
10
20
50
100
200
500
L (mm)

Fig. 6-8

from the characteristic equations depends on the functional form of the perturbations employed. Instabilities can be generated which, on the one hand, correspond to mode-locked laser operation (as already found previously), and on the other, to operation in a passive Q-switching mode. Accordingly, the applicability of the model has been extended in the present work in several directions. In the first place, it is employed to investigate certain aspects of the relaxation oscillation regime. The treatment of the model in this case has been studied in several approximations. It is shown that the present analysis constitutes a direct generalisation of previously presented models which make no allowance for the spatial dependence of the laser dynamical variables. A comparison has been presented, for certain specific cases, between the predictions of the present model and those due to the (suitably modified) models employing rate equations and a distributed gain and loss.

The impact of the existence of passive Q-switching instabilities on the prediction of mode-locking regions has been investigated for some specific laser parameters. It is found that, in some cases, instabilities in the CW solutions which appear at first sight to correspond to mode-locking can be due to relaxation oscillation-type instabilities. Accordingly, when the analysis is employed for the determination of the mode-locking range of operating parameters, it is very important to generate the relaxation oscillation operating region and, if necessary, exclude it from the mode-locking range.

The augmented model of saturable absorber induced laser pulsation has also been employed to study the transition from laser mode-locking to passive Q-switching regimes in two particular cases. Predictions are made of the circumstances under which either mode-locking or relaxation oscillation may be obtained in presently available systems. It is suggested that a relaxation oscillation regime could be observed in flashlamp-pumped dye lasers. Furthermore, a range of laser parameters is determined within which mode-locked operation of a semiconductor system may be obtained. These, as yet unachieved, laser operating regimes are of interest in their own right. Practical realisation could also provide sources with potentially useful characteristics.

CHAPTER 7

CONCLUSIONS AND SUGGESTIONS FOR FURTHER RESEARCH

In this thesis, a theoretical model for mode-locked CW and quasi-CW lasers using a suitable saturable absorber has been developed and applied to a number of important laser systems. In particular, the mode-locked CW and flashlamp-pumped dye lasers have been studied. A comparison between our model and the so-called pulse compression model has also been made. In addition, the mode-locked regime of operation has been related to passively Q-switched pulsations. In this chapter, the work described in the foregoing chapters is summarized and suggestions for further research are proposed.

In the development of the theoretical model, both the gain and the loss media are assumed to consist of two-level atoms with homogeneously broadened line. A density matrix formalism together with the Maxwell's equations is employed to describe the interaction of the media and the radiation. The time-invariant solutions of the laser coupled equations, in conjunction with appropriate boundary conditions, are deduced exactly, and the operating stability of the system against small perturbations in the laser dynamical variables is determined. In addition, a finite difference approximation is

employed as a means of solving the non-linear dynamical equations and the finite difference equations so developed facilitate the generation of steady-state pulses for mode-locked operations.

It is shown that the present model represents a more general approach to saturable absorber mode-locking than those previously presented in several ways. In the first place, an analysis employing density matrix formalism rather than rate equation approach allows for the incorporation of not only the recovery times but also the phase memory times of the active media. It has been demonstrated with this model that atomic coherence effects are important for certain combinations of gain and absorber media. Obviously, an analysis based on rate equations cannot be employed to investigate such phenomena. Furthermore, in our analysis, no assumption concerning the temporal width of the laser pulse relative to the recovery times of the gain and loss media and the cavity round-trip time has been made. This, in conjunction with taking coherence effects into account, allows the generation of the steady-state mode-locked pulses and the determination of the actual pulse widths. Accordingly, our model can be applied to both low-gain and high-gain laser systems. Typical examples are the CW and flashlamp-pumped dye lasers which have been investigated in this thesis. The important conclusions resulting from these investigations are given below.

The analysis of the low-gain CW dye lasers shows explicitly that this mode-locking situation (Type I mode-locking) is basically different from the mode-locking (Type II mode-locking) of Nd:glass, ruby or other similar gain-pulse laser systems, and can be distinguished from the latter by the characteristics of the laser output. It has been shown that a true steady-state solution of the dynamical equations governing the laser operation can be obtained for Type I mode-locking. In contrast, the Type II mode-locking is characterized by transient dynamical solution which never attains a steady-state[40-45]. Furthermore, the output pulses from a Type I mode-locked laser can be very much shorter than the recovery times of either the gain or the absorber since the dynamics of both media play an important role in the production of the mode-locked pulses. In fact, we have shown that picosecond pulses can be generated from a mode-locked CW dye laser with an absorber whose recovery time is several hundred picoseconds. This is very different from the situation of Type II mode-locking for which the pulse length is usually limited to times no shorter than the recovery time of the absorber and the dynamics of the laser gain do not play a major role in the pulse development process.

Investigations on the dynamics of mode-locking in pulsed gain lasers indicate that under typical experimental conditions, the high-gain flashlamp-pumped dye lasers can be operated in a quasi-continuous regime where the output pulses are close to

being SSP. As a consequence, a complete analysis of the dynamics of this type of laser necessarily requires an investigation of the generation of SSP. In this context, the pulse compression approach[46,47] can be regarded as a transient type of analysis since it can only account for the rapid pulse narrowing which occurs during the initial build-up of the pulse solution, prior to the onset of a steady-state pulse shape. More importantly, the analysis presented in this thesis suggests that our model can be applied to other pulsed-gain lasers provided that the laser operating time is longer than the time taken for the establishment of the steady-state solution.

In the last part of this thesis, it is shown that our theoretical model for saturable absorber mode-locking incorporates the analysis of passive Q-switching (relaxation oscillations) as a special case. In particular, it is found that, in some laser systems, instabilities in the CW solutions which appear at first sight to correspond to mode-locking can be due to relaxation-oscillation type instabilities. In this situation, the regions of mode-locking must be corrected by the subtraction of the relaxation oscillation regime. Such a correction is particularly important when the recovery time of the laser gain is much longer than the cavity round-trip and the absorber recovery times. In fact, a study of the transition from laser mode-locking to passive Q-switching regimes predicts that a relaxation oscillation regime could be observed in flashlamp-pumped dye lasers if the laser cavity is sufficiently short. On the other

hand, it is suggested that mode-locking operation of a semiconductor system may be obtained by using an external resonator with a round-trip time comparable to the gain recovery time.

The general behaviour of mode-locked CW or quasi-CW lasers using saturable absorbers has been reasonably well accounted for using the theoretical investigations presented in this thesis. In particular, numerical results calculated for parameters appropriate to CW and flashlamp-pumped dye lasers are in substantial agreement with experimental observations although the detailed mechanisms controlling and limiting the pulsewidth still remain to be explored. However, for a better understanding on the dynamics of the mode-locking process, certain modifications and generalisations of the theoretical model are required. Accordingly, some suggestions appropriate for further research are in order.

As pointed out previously, the calculated length of the SSP for flashlamp-pumped dye lasers are generally a good deal shorter than experimental measurements indicate. It is possible that this discrepancy is due to the finite thermalization time of the upper and lower levels, which will tend to arrest the build-up of the laser pulse. This possibility requires further investigation, both because it is an important aspect of the dynamics of the pulse build-up and also to see if there is some way to circumvent the consequences. As a direct modification of our present model, the effects of the finite thermalization time may be accounted for by assuming additional

levels which are connected with, and act as, population reservoirs for the upper and lower levels respectively. Such a modification should also prove very useful for other types of systems having degenerate or near-degenerate atomic levels.

Up to date, the CW Nd:YAG lasers have been usually mode-locked by internal loss or phase modulation[1,2,6]. According to the analysis of active mode-locking[6], it is shown that picosecond pulses cannot be generated from this kind of mode-locked laser although the gain medium does possess such a potential. As the approximation of homogeneously broadened gain line applies to CW Nd:YAG lasers, it is potentially useful to employ our theoretical model for the analysis of these systems to see whether a suitable saturable absorber for the production of picosecond pulses can be found. Furthermore, the transition between passive mode-locking and Q-switching can also be investigated since the recovery time of the gain medium is much longer than the cavity round-trip time in practical systems.

Finally, for some laser systems, such as the He-Ne laser mode-locked by a Ne absorber, the inhomogeneous broadening of the active media should be taken into account. Accordingly, our model could also be generalized in this direction, although the analysis is extremely, and probably prohibitively, complex.

APPENDIX A

DERIVATION OF THE CHARACTERISTIC EQUATIONS (2-65)

The two sets of linearized equations (2-62) and (2-63) are

$$\begin{aligned}(\beta+1)p_o &= \bar{E}\,\delta_o + \bar{D}e_o \\ (\beta+\gamma)\delta_o &= -\bar{E}\,p_o - \bar{P}e_o \quad (x_1' \le x' \le x_2') \\ (i\alpha+\beta)e_o &+ \frac{de_o}{dx'} = G_a p_o\end{aligned} \tag{A-1}$$

and

$$\begin{aligned}(\beta+\gamma_2)p_o &= \bar{E}\,\delta_o + \bar{D}e_o \\ (\beta+\gamma')\delta_o &= -\bar{E}\,p_o - \bar{P}e_o \quad (x_3' \le x' \le x_4') \\ (i\alpha+\beta)e_o &+ \frac{de_o}{dx'} = G_b p_o\end{aligned} \tag{A-2}$$

Solving for δ_o from the second equation of (A-1) and substituting the result into the first we obtain

$$p_o = \frac{\bar{D}[(\beta+\gamma)-\bar{I}]}{(\beta+1)(\beta+\gamma)+\bar{I}}\, e_o . \tag{A-3}$$

Inserting this expression into the third equation and separating the variables gives

$$\frac{de_o}{e_o} = \frac{G_a\bar{D}(\beta+\gamma-\bar{I})}{(\beta+1)(\beta+\gamma)+\bar{I}}\, dx' - (i\alpha+\beta)dx' . \tag{A-4}$$

Using the relation (the third equation of (2-49) in section 2.3),

$$\frac{d\bar{I}}{dx'} = 2\,G_a\gamma\bar{I}/(\gamma+\bar{I}) = 2G_a\bar{I}\,\bar{D} \tag{A-5}$$

for the first term on the right hand side of (A-4) enables us to perform the integration exactly

$$\int_{e_o(x_1')}^{e_o(x')} \frac{de_o}{e_o} = \int_{\bar{I}(x_1')}^{\bar{I}(x')} \frac{(\beta+\gamma-\bar{I})d\bar{I}}{2\bar{I}[(\beta+1)(\beta+\gamma)+\bar{I}]} - \int_{x_1'}^{x'} (i\alpha+\beta)dx' \quad (A-6)$$

which turns out to be, after multiplying both sides by $2(\beta+1)$

$$2(\beta+1)\ln\left[\frac{e_o(x')}{e_o(x_1')}\right] = \ln\left[\frac{\bar{I}(x')}{\bar{I}_1}\right] - (\beta+2)\ln\left[\frac{(\beta+1)(\beta+\gamma)+\bar{I}(x')}{(\beta+1)(\beta+\gamma)+\bar{I}_1}\right]$$

$$-2(i\alpha+\beta)(\beta+1)(x'-x_1'). \quad (A-7)$$

An identical procedure yields the following solutions to (A-2),

$$p_o = \frac{\bar{D}(\beta+\gamma'-\bar{I}/\gamma_2)}{(\beta+\gamma')(\beta+\gamma_2)+\bar{I}} e_o \quad (A-8)$$

$$2(\beta+\gamma_2)\ln\left[\frac{e_o(x')}{e_o(x_1')}\right] = \gamma_2 \ln\left[\frac{\bar{I}(x')}{\bar{I}_3}\right] - (\beta+2\gamma_2)\ln\left[\frac{(\beta+\gamma')(\beta+\gamma_2)+\bar{I}(x')}{(\beta+\gamma')(\beta+\gamma_2)+\bar{I}_3}\right]$$

$$-2(i\alpha+\beta)(\beta+\gamma_2)(x'-x_3'). \quad (A-9)$$

Multiplying (A-7) by $(\beta+\gamma_2)$ and (A-9) by $(\beta+1)$, adding the two and applying the boundary conditions (2-64) gives

$$2[(\beta+i\alpha)L' - \ln r](\beta+1)(\beta+\gamma_2)+2\gamma_2(\beta+1)\ln r-(1-\gamma_2)\beta\ln(\bar{I}_2/\bar{I}_1)$$

$$+(\beta+2)(\beta+\gamma_2)\ln(C_2/C_1)+(\beta+2\gamma_2)(\beta+1)\ln(C_4/C_3) = 0 . \quad (A-10)$$

Performing the multiplications and grouping terms with respect to β, we obtained

$$\beta^3+(q+i\alpha)\beta^2+(u+iv\alpha)\beta+i\alpha\gamma_2+[(\beta^2+(2+\gamma_2)\beta+2\gamma_2)\ln(C_2/C_1)$$

$$+(\beta^2+(1+2\gamma_2)\beta+2\gamma_2)\ln(C_4/C_3)]/2L' = 0 \quad (A-11)$$

with

$$
\begin{aligned}
v &= 1+\gamma_2 \\
q &= v-\ell n(R)/2L' \\
u &= q-1-(1-\gamma_2)\ell n(\bar{I}_2/\bar{I}_1)/2L' \\
C_j &= (\beta+1)(\beta+\gamma)+\bar{I}_j, \quad j=1,2 \\
&= (\beta+\gamma')(\beta+\gamma_2)+\bar{I}_j, \quad j=3,4.
\end{aligned}
\tag{A-12}
$$

Substitution of $\beta=\beta_r+i\beta_i$ into Eq. (A-11) and grouping the real and imaginary parts separately, we obtain the following equations

$$
\begin{aligned}
&\beta_r^3 - 3\beta_i^2\beta_r+q(\beta_r^2-\beta_i^2)-2\alpha\beta_i\beta_r+u\beta_r-\alpha v\beta_i \\
&\quad +[(b_1A_1-b_2A_2)+\beta_i(s_1B_1-s_2B_2)]/2L' = 0 \\
&2\beta_i\beta_r^2-\beta_i^3+\alpha(\beta_r^2-\beta_i^2)+2q\beta_i\beta_r+v\beta_r+u\beta_i+\alpha\gamma_2 \\
&\quad +\beta_i(s_1A_1-s_2A_2)-(b_1B_1-b_2B_2)]/2L' = 0
\end{aligned}
\tag{A-13}
$$

where

$$
\begin{aligned}
b_1 &= \beta_r^2-\beta_i^2+(2+\gamma_2)\beta_r+2\gamma_2 \\
b_2 &= \beta_r^2-\beta_i^2+(1+2\gamma_2)\beta_r+2\gamma_2 \\
s_1 &= 2\beta_r+2+\gamma_2 \\
s_2 &= 2\beta_r+1+2\gamma_2 \\
A_1 &= \ell n(R_2/R_1) \\
A_2 &= \ell n(R_3/R_4) \\
B_1 &= \phi_2-\phi_1 \\
B_2 &= \phi_3-\phi_4.
\end{aligned}
\tag{A-14}
$$

Here, R_j and ϕ_j are defined by

$$R_j \exp(i\phi_j) \equiv C_j = (b+\bar{I}_j) + i(\beta_i s) \quad , \quad j=1,2$$
$$= (b' + \bar{I}_j) + i(\beta_i s') , \quad j=3,4 \qquad \text{(A-15)}$$

with

$$b = \beta_r^2 - \beta_i^2 + (1+\gamma)\beta_r + \gamma$$
$$b' = \beta_r^2 - \beta_i^2 + (\gamma' + \gamma_2)\beta_r + \gamma'\gamma_2 \qquad \text{(A-16)}$$
$$s = 2\beta_r + 1 + \gamma$$
$$s' = 2\beta_r + \gamma' + \gamma_2 .$$

Equations (A-13) are the characteristic equations (2-65) in section 2.4 .

APPENDIX B

FINITE DIFFERENCE APPROXIMATION (I) - FULL COUPLED EQUATIONS

A finite difference approximation is applied to the coupled equations (2-39) and (2-40) to facilitate the generation of the steady-state pulse by computer simulation. For convenience, we transform (2-39) and (2-40) into the ordinary (x,t) co-ordinates, namely

$$\frac{\partial P}{\partial t} = -\gamma_\perp P + \gamma_\perp DE$$

$$\frac{\partial D}{\partial t} = -\gamma_\perp EP - \gamma_{||}(D - 1) \quad (x_1 \le x \le x_2) \quad \text{(B-1)}$$

$$c\frac{\partial E}{\partial x} + \frac{\partial E}{\partial t} = G_a \gamma_\perp P$$

and

$$\frac{\partial P}{\partial t} = -\gamma_\perp' P + \gamma_\perp DE$$

$$\frac{\partial D}{\partial t} = -\gamma_\perp EP - \gamma_{||}'(D + a_o) \quad (x_3 \le x \le x_4) \quad \text{(B-2)}$$

$$c\frac{\partial E}{\partial x} + \frac{\partial E}{\partial t} = G_b \gamma_\perp P$$

where $\gamma_{||} = T_1^{-1}$, $\gamma_\perp = T_2^{-1}$, $\gamma_{||}' = (T_1')^{-1}$, $\gamma_\perp' = (T_2')^{-1}$ and we drop the subscripts a and b in E, D, P as before. Other parameters are as defined in section 2.2.3.

In the finite difference approximation, first of all, the x-t plane is divided into a grid of points with spacings Δx and Δt as shown in Fig. B-1(a). A Taylor expansion is then carried out about an arbitrary point (m,n) for each differen-

Fig. B-1 (a) A mesh which divides the x-t plane into a grid of points with spacings Δx and Δt. The point (m,n) corresponds to an arbitrary point (x,t). In order to get stable difference equations, it is chosen that $\Delta x = c\Delta t$ where c is the phase velocity of the radiation that propagates in the laser cavity. The vertical arrow parallel to the time axis indicates the direction of the forward iteration employed in the pulse propagation simulation.

(b) A periodic optical system (the same as that shown in Fig. 2-1(b)) for a ring laser cavity. The spatial coordinates x_1, x_2, x_3, x_4 and x_L corresponding to the points A, B, C, D and E are shown. The indices defined by Eq. (B-13) for these points are also shown in this figure.

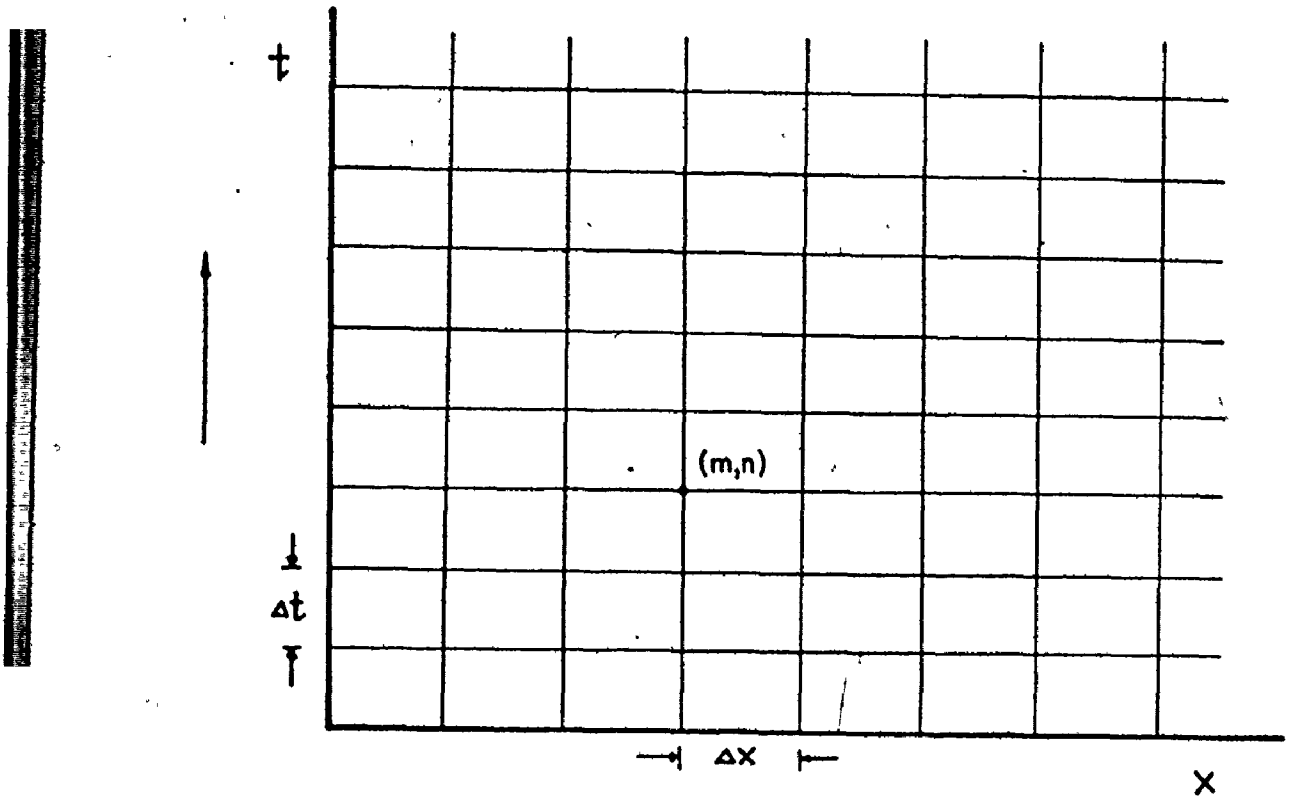
t
(m,n)
Δt
Δx
x

(a)

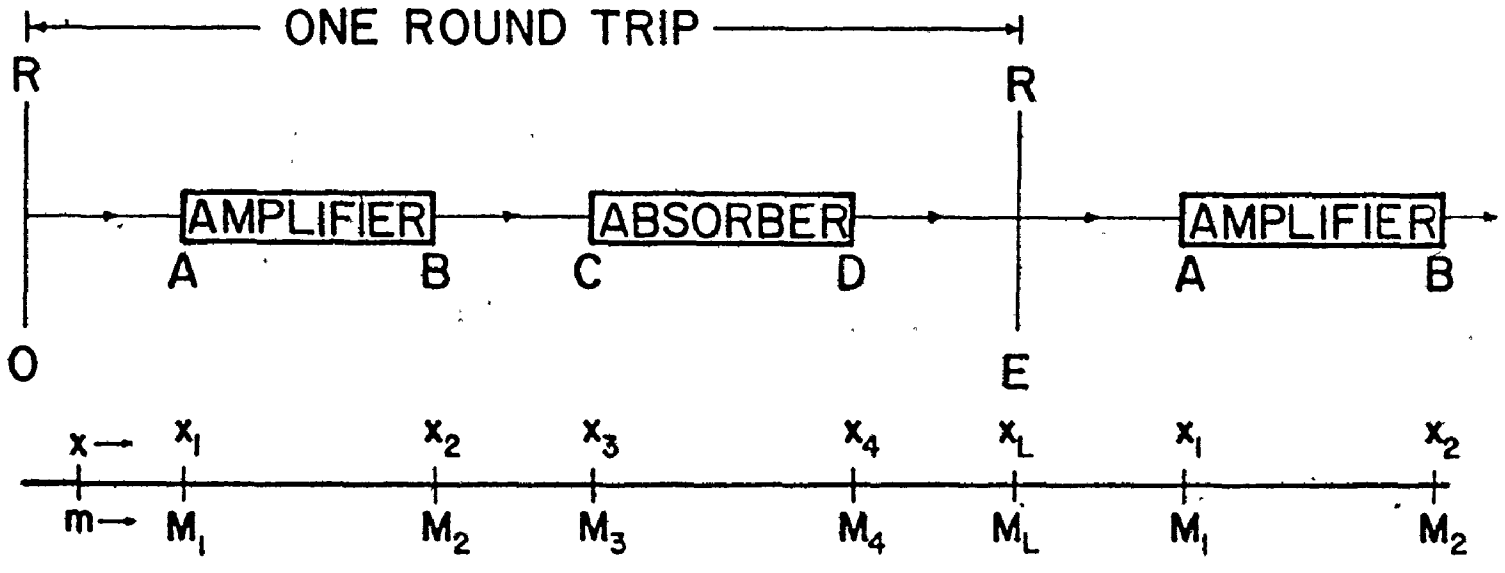
ONE ROUND TRIP
R
R
AMPLIFIER
ABSORBER
AMPLIFIER
A
B
C
D
A
B
O
E
x
x1
x2
x3
x4
xL
x1
x2
m
M1
M2
M3
M4
ML
M1
M2

(b)

Fig. B-1

tial equation concerned. In order to obtain stable difference equations for the coupled nonlinear partial differential equations (B-1) and (B-2), we choose, for both media, $\Delta x = c\Delta t$ and the partial derivatives as follows

$$\frac{\partial E(m,n)}{\partial t} = \frac{E(m,n+1)-E(m,n)}{\Delta t} - \frac{1}{2}\Delta t \frac{\partial^2 E(m,n)}{\partial t^2} \qquad \text{(B-3)}$$

$$\frac{\partial E(m,n)}{\partial x} = \frac{E(m,n)-E(m-1,n)}{\Delta x} + \frac{1}{2}\Delta x \frac{\partial^2 E(m,n)}{\partial x^2} \qquad \text{(B-4)}$$

with expressions for $\partial P(m,n)/\partial t$ and $\partial D(m,n)/\partial t$ identical to (B-3). The second order derivatives are calculated by differentiating the coupled equations once and substituting the first order approximation from (B-3) and (B-4) leading to a truncation errors of order $(\Delta t)^2$ in the derivatives.

For the gain medium, the following finite difference equation is obtained to the third equation of (B-1) by adding (B-3) and (B-4) and using the calculated expressions for $\partial^2 E(m,n)/\partial t^2 - c^2\,\partial^2 E(m,n)/\partial x^2$,

$$E(m,n+1)=c_1E(m-1,n)+c_2P(m,n)+c_3D(m,n)E(m,n)+c_4P(m-1,n) \qquad \text{(B-5)}$$

with

$$\begin{aligned} c_1 &= 1 \\ c_2 &= \tfrac{1}{2} G_a \gamma_\perp \Delta t(1-\gamma_\perp \Delta t) \\ c_3 &= \tfrac{1}{2} G_a (\gamma_\perp \Delta t)^2 \\ c_4 &= \tfrac{1}{2} G_a \gamma_\perp \Delta t . \end{aligned} \qquad \text{(B-6a)}$$

A similar procedure leads to the following equations for the two equations of (B-1),

$$P(m,n+1)=a_1P(m,n)+a_2E(m,n)+a_3D(m,n)E(m,n)+a_4D(m,n)E(m-1,n)$$
$$+ a_5P(m,n)[E(m,n)]^2 + a_6D(m,n)P(m,n) \qquad \text{(B-7)}$$

with

$$\begin{aligned} a_1 &= 1 - \gamma_\perp \Delta t + \tfrac{1}{2}(\gamma_\perp \Delta t)^2 \\ a_2 &= \tfrac{1}{2}\gamma_{\parallel}\gamma_\perp(\Delta t)^2 \\ a_3 &= \tfrac{1}{2}\gamma_\perp \Delta t[1 - (\gamma_{\parallel} + \gamma_\perp)\Delta t] \\ a_4 &= \tfrac{1}{2}\gamma_\perp \Delta t \\ a_5 &= -\tfrac{1}{2}(\gamma_\perp \Delta t)^2 \\ a_6 &= \tfrac{1}{2}G_a(\gamma_\perp \Delta t)^2 \end{aligned} \qquad \text{(B-8a)}$$

and

$$D(m,n+1) = b_1D(m,n) + b_2P(m,n)E(m,n) + b_3[P(m,n)]^2 + b_4P(m,n)$$
$$\times E(m-1,n) + b_5D(m,n)[E(m,n)]^2 + b_6 \qquad \text{(B-9)}$$

with

$$\begin{aligned} b_1 &= 1 - \gamma_{\parallel} \Delta t + \tfrac{1}{2}(\gamma_{\parallel} \Delta t)^2 \\ b_2 &= -\tfrac{1}{2}\gamma_\perp \Delta t[1 - (\gamma_{\parallel} + \gamma_\perp)\Delta t] \\ b_3 &= -\tfrac{1}{2}G_a(\gamma_\perp \Delta t)^2 \\ b_5 &= -\tfrac{1}{2}\gamma_\perp \Delta t \\ b_5 &= -\tfrac{1}{2}(\gamma_\perp \Delta t)^2 \\ b_6 &= \gamma_{\parallel} \Delta t(1 - \tfrac{1}{2}\gamma_{\parallel} \Delta t) . \end{aligned} \qquad \text{(B-10a)}$$

For the loss medium, following the same procedure, we obtain expressions identical to (B-5), (B-7) and (B-9) for Eqs.(B-2), except that the coefficients are now given by

$$
\begin{aligned}
c_1 &= 1 \\
c_2 &= \tfrac{1}{2} G_b \gamma_\perp \Delta t(1 - \gamma_\perp' \Delta t) \\
c_3 &= \tfrac{1}{2} G_b(\gamma_\perp \Delta t)^2 \\
c_4 &= \tfrac{1}{2} G_b(\gamma_\perp \Delta t) ,
\end{aligned}
\qquad \text{(B-6b)}
$$

$$
\begin{aligned}
a_1 &= 1 - \gamma_\perp' \Delta t + \tfrac{1}{2}(\gamma_\perp' t)^2 \\
a_2 &= -\tfrac{1}{2} a_o \gamma_{||}' \gamma_\perp (\Delta t)^2 \\
a_3 &= \tfrac{1}{2} \gamma_\perp \Delta t[1 - (\gamma_{||}' + \gamma_\perp')\Delta t] \\
a_4 &= \tfrac{1}{2} \gamma_\perp \Delta t \\
a_5 &= -\tfrac{1}{2} (\gamma_\perp \Delta t)^2 \\
a_6 &= \tfrac{1}{2} G_b(\gamma_\perp \Delta t)^2
\end{aligned}
\qquad \text{(B-8b)}
$$

and

$$
\begin{aligned}
b_1 &= 1 - \gamma_{||}' \Delta t + \tfrac{1}{2}(\gamma_{||}' \Delta t)^2 \\
b_2 &= -\tfrac{1}{2} \gamma_\perp \Delta t[1 - (\gamma_{||}' + \gamma_\perp')\Delta t] \\
b_3 &= -\tfrac{1}{2} G_b (\gamma_\perp \Delta t)^2 \\
b_4 &= -\tfrac{1}{2} \gamma_\perp \Delta t \\
b_5 &= -\tfrac{1}{2} (\gamma_\perp \Delta t)^2 \\
b_6 &= -a_o \gamma_{||}' \Delta t(1 - \tfrac{1}{2} \gamma_{||}' \Delta t)
\end{aligned}
\qquad \text{(B-10b)}
$$

instead of those defined by (B-6a), (B-8a) and B(10-a).

It should be pointed out that we have used the approximation

$$
\frac{\partial E(m,n)}{\partial t} = G_{a,b} \gamma_\perp P(m,n) - c\frac{E(m,n) - E(m-1,n)}{\Delta x} \qquad \text{(B-11)}
$$

in the derivations of (B-7) and (B-9). However, at the input sections of the gain and loss cells, this is not appropriate due to the discontinuity of the medium. In this case, we should use

$$\frac{\partial E(m,n)}{\partial t} = \frac{E(m,n+1)-E(m,n)}{\Delta t} \tag{B-12}$$

which leads to the following two equations,

$$P(m,n+1) = a_1 P(m,n)+a_2 E(m,n)+a_3 D(m,n)E(m,n)+a_4 D(m,n)E(m,n+1) + a_5 P(m,n)[E(m,n)]^2 \tag{B-7'}$$

and

$$D(m,n+1) = b_1 D(m,n)+b_2 P(m,n)E(m,n)+b_4 P(m,n)E(m,n+1) + b_5 D(m,n)[E(m,n)]^2 + b_6 \tag{B-9'}$$

where the definitions of the coefficients a's and b's are as given in Eqs. (B-8a) and (B-10a) (for the amplifier), or (B-8b) and (B-10b) (for the absorber). Note also that the value of $E(m,n+1)$ can be calculated simply by

$$E(m,n+1) = E(m-1,n) \tag{B-5'}$$

other than using (B-5) which is <u>not</u> relevant for the input sections of the media. Obviously, equation (B-5') describes the propagation of the radiation field in free space. Accordingly, if we define the following indices

$$M_i = x_i/\Delta x \qquad i = 1,2,3,4$$
$$M_L = x_L/\Delta x \tag{B-13}$$

which corresponds to the space coordinates x_i ($i = 1,2,3,4$) of the end points (A,B,C and D) of the amplifier and absorber ,

and the point E (see Fig. B-1(b)), then the boundary conditions (2-44) can be represented by

$$\begin{aligned} m_s E(M_2, n-\Delta M_{23}) &= E(M_3, n) \\ m_s E(M_1+M_L, n) &= rE(M_4, n-\Delta M_{41}) \end{aligned} \tag{B-14}$$

where

$$\begin{aligned} \Delta M_{23} &= M_3-M_2, \\ \Delta M_{41} &= M_L-M_4+M_1 \end{aligned} \tag{B-15}$$

and we have used m_s instead of $m(= m_d m_o)$ to avoid confusion with the index m which appears in the definition of the space-time grid point (m,n).

Observe that the form of the FDE's developed above permits a step-by-step forward iteration in the time domain once appropriate initial conditions for the laser dynamical variables are specified. Generally, the accuracy of the numerical simulation depends on the size of the time increment (Δt) employed, and the value of Δt that is applicable is in turn dictated by the relaxation times of the active media. To obtain reliable results, the size of Δt is usually chosen to be several times less than that of the shortest relaxation time. Consequently, the problem of the consumption of computer time could be very serious in practice. Fortunately, as pointed out in section 2.5, the amount of computations needed can be reduced sizeably by assuming relatively thin gain and loss cells so that the number of steps within the amplifier (M_2-M_1) and absorber (M_4-M_3) are much less than the total steps for the whole cavity (M_L). In

those cases for which very short and intense pulses are accounted for, further reduction of the computational labor can be achieved by the scheme of "pulse truncation". In this scheme, for each point in the active media, calculations employing the FDE's are only performed within that interval of local time where the radiation intensity is appreciably different from zero. Outside this region, the intensity is so small that the interactions between the active media and the field can be neglected and only the atomic recovery of the media together with the effects of pumping should be accounted for. This is done by assuming EP = 0 in the second equations of (B-1) and (B-2) and performing the integrations. This technique of pulse truncation is most useful in those systems for which the phase memory times T_2 and T_2' are much shorter than the cavity round-trip time and the temporal width of the SSP is expected to be very narrow, such as the situation of dye lasers.

Finally, for future reference, all the FDE's derived in this appendix are summarized in Table B-1.

Table B-1

Finite Difference Equations (FDE) Employed for Pulse Propagation (I) (Full Coupled Equations)

	Space Coordinate Concerned	Corresponding Space Index[a]	FDE(s) Employed	Coefficients of FDE(s) Defined by Eq(s).
Amplifier	x_1	M_1	(B-5') (B-7') (B-9')	none (B-8a) (B 10a)
	$x_1 < x \leq x_2$	$M_1 < m \leq M_2$	(B-5) (B-7) (B-9)	(B-6a) (B-8a) (B-10a)
Absorber	x_3	M_3	(B-5') (B-7') (B-9')	none (B-8b) (B-10b)
	$x_3 < x \leq x_4$	$M_3 < m \leq M_4$	(B-5) (B-7) (B-9)	(B-6b) (B-8b) (B-10b)
Boundary Conditions	x_1, x_2, x_3 x_4 and x_L	M_1, M_2, M_3 M_4 and M_L	(B-14)	$m_s = m_d m_o$ $r = \sqrt{R}$[b]

(a) Definition: $M_i = x_i/\Delta x$, $i = 1,2,3,4$; $M_L = x_L/\Delta x$ (see Eq. (B-13)).

(b) See Table 2-1 for the definitions and physical significance of m_s and r.

APPENDIX C

FINITE DIFFERENCE APPROXIMATION (II) - RATE EQUATION APPROXIMATION

In this appendix, a finite difference approximation is employed to develop a number of finite difference equations (FDE) within the rate equation approximation. The general procedure is the same as that used in Appendix B, and, as will be shown, the number of FDE's is less than that obtained in Appendix B since the polarization is directly related to the product of the field amplitude and the population inversion in the rate equation approximation.

Let us start with the two sets of laser coupled equations (B-1) and (B-2). In the rate equation formulation, we have the following conditions on the polarizations of the gain and loss media

$$\left|\frac{\partial P_a}{\partial t}\right| << \left|\frac{P_a}{T_2}\right| , \quad \left|\frac{\partial P_b}{\partial t}\right| << \left|\frac{P_b}{T_2'}\right| \qquad \text{(C-1)}$$

which means that the temporal width of the laser pulse is much longer than the phase memory times of the amplifier (T_2) and absorber (T_2') so that the pulse coherence effects are not important. Applying these conditions to Eqs. (B-1) and (B-2), we obtain

$$(P = DE)$$

$$\frac{\partial D}{\partial t} = - \gamma_{\perp} DI - \gamma_{\parallel} \quad \text{(D-1)} \qquad (x_1 \leq x \leq x_2) \qquad \text{(C-2)}$$

$$c \frac{\partial I}{\partial x} + \frac{\partial I}{\partial t} = g_a DI$$

and

$$(P = DE/\gamma_2)$$

$$\frac{\partial D}{\partial t} = -\gamma_e DI - \gamma'_{||}(D+a_o) \quad (x_3 \leq x \leq x_4) \qquad \text{(C-3)}$$

$$c\frac{\partial I}{\partial x} + \frac{\partial I}{\partial t} = g_b DI$$

where $\gamma_e = \gamma_\perp/\gamma_2 = T'_2/T_2^2$, $g_a = 2\gamma_\perp G_a$, $g_b = 2\gamma_e G_b$, $I = E^2$ and other parameters are as defined previously.

Observe that, in this case, the number of equations that must be solved has been reduced to four from the previous six. Further, the boundary conditions (2-44) becomes

$$\begin{aligned} m^2 I(x_2, t-\Delta_{23}T_2) &= I(x_3,t) \\ m^2 I(x_1+L,t) &= RI(x_4, t-\Delta_{41}T_2) \end{aligned} \qquad \text{(C-4)}$$

in the notation of ordinary (x,t) coordinates and $m = m_d m_o$ as before.

The derivation of the finite difference equations appropriate to Eqs. (C-2) and (C-3) now proceeds much as in Appendix B. First of all, we choose the partial derivatives for I as

$$\frac{\partial I(m,n)}{\partial x} = \frac{I(m,n)-I(m-1,n)}{\Delta x} + \frac{1}{2}\Delta x \frac{\partial^2 I(m,n)}{\partial x^2} \qquad \text{(C-5)}$$

$$\frac{\partial I(m,n)}{\partial t} = \frac{I(m,n+1)-I(m,n)}{\Delta t} - \frac{1}{2}\Delta t \frac{\partial^2 I(m,n)}{\partial t^2} \qquad \text{(C-6)}$$

with expression for $\partial D(m,n)/\partial t$ identical to (C-6).

Following the same procedure described in Appendix B, we obtain

$$I(m,n+1)=c_1 I(m-1,n)+c_2 I(m,n)+c_3 D(m-1,n) I(m,n)+c_4 D(m,n) I(m-1,n)$$

$$+ c_5 D(m,n) I(m,n)+c_6 D(m,n)[I(m,n)]^2+c_7[D(m,n)]^2 I(m,n) \quad (C-7)$$

$$D(m,n+1)=b_1 D(m,n)+b_2 I(m,n)+b_3 D(m,n) I(m-1,n)+b_4 D(m,n) I(m,n)$$

$$+ b_5 D(m,n)[I(m,n)]^2+b_6[D(m,n)]^2 I(m,n)+b_7 \quad (C-8)$$

where the coefficients c's and b's are defined below.

For the gain medium, we have

$$c_1 = 1$$

$$c_2 = \frac{1}{2}\gamma_{||} g_a (\Delta t)^2$$

$$c_3 = \frac{1}{2} g_a \Delta t$$

$$c_4 = g_a \Delta t \quad (C-9a)$$

$$c_5 = -\frac{1}{2} g_a \Delta t(1+\gamma_{||} \Delta t)$$

$$c_6 = -\frac{1}{2} g_a \gamma_{\perp} (\Delta t)^2$$

$$c_7 = \frac{1}{2}(g_a \Delta t)^2$$

and

$$b_1 = 1-\gamma_{||} \Delta t(1 - \frac{1}{2}\gamma_{||} \Delta t)$$

$$b_2 = -\frac{1}{2}\gamma_{||}\gamma_{\perp}(\Delta t)^2$$

$$b_3 = -\frac{1}{2}\gamma_{\perp} \Delta t$$

$$b_4 = -\gamma_{\perp} \Delta t(\frac{1}{2} - \gamma_{||} \Delta t) \quad (C-10a)$$

$$b_5 = \frac{1}{2}(\gamma_{\perp} \Delta t)^2$$

$$b_6 = -\frac{1}{2} g_a \gamma_{\perp} (\Delta t)^2$$

$$b_7 = \gamma_{||} \Delta t(1 - \frac{1}{2}\gamma_{||} \Delta t).$$

For the loss medium, we have

$$
\begin{aligned}
c_1 &= 1 \\
c_2 &= -\tfrac{1}{2}\, a_o \gamma'_{||} g_b (\Delta t)^2 \\
c_3 &= \tfrac{1}{2}\, g_b\, \Delta t \\
c_4 &= g_b\, \Delta t \\
c_5 &= -\tfrac{1}{2}\, g_b\, \Delta t (1 + \gamma'_{||}\, \Delta t) \\
c_6 &= \tfrac{1}{2}\, \gamma_e g_b (\Delta t)^2 \\
c_7 &= \tfrac{1}{2}\, (g_b \Delta t)^2
\end{aligned}
\qquad \text{(C-9b)}
$$

and

$$
\begin{aligned}
b_1 &= 1 - \gamma'_{||}\, \Delta t (1 - \tfrac{1}{2}\, \gamma'_{||}\, \Delta t) \\
b_2 &= \tfrac{1}{2}\, \gamma'_{||} \gamma_e a_o (\Delta t)^2 \\
b_3 &= -\tfrac{1}{2}\, \gamma_e \Delta t \\
b_4 &= -\gamma_e \Delta t (\tfrac{1}{2} - \gamma'_{||}\, \Delta t) \\
b_5 &= \tfrac{1}{2} (\gamma_e \Delta t)^2 \\
b_6 &= -\tfrac{1}{2}\, g_b\, \gamma_e (\Delta t)^2 \\
b_7 &= -a_o (\gamma'_{||} \Delta t)(1 - \tfrac{1}{2}\, \gamma'_{||} \Delta t).
\end{aligned}
\qquad \text{(C-10b)}
$$

Furthermore, as pointed out in Appendix B, the input sections of both media have to be treated differently from that of the bulk medium. In this case, equation (C-8) should be replaced by

$$
\begin{aligned}
D(m,n+1) = {} & b_1 D(m,n) + b_2 I(m,n) + b_3 D(m,n) I(m+1,n) + b_4 D(m,n) I(m,n) \\
& + b_5 D(m,n) [I(m,n)]^2 + b_7
\end{aligned}
\qquad \text{(C-8')}
$$

and instead of Eq. (C-7), we use

$$
I(m,n+1) = I(m-1,n) \qquad \text{(C-7')}
$$

which describes the propagation of the radiation field in free space. Using this equation, it can be shown that the boundary conditions (C-4) are described by

$$m_s^2 I(M_2, n-\Delta M_{23}) = I(M_3, n)$$
$$m_s^2 I(M_1+M_L, n) = RI(M_4, n-\Delta M_{41}) \qquad \text{(C-11)}$$

which are similar to Eqs. (B-14). The indices M_i (i = 1,2,3,4), M_L and the quantities ΔM_{23} and ΔM_{41} are as defined in Eqs. (B-13) and (B-15). Also, the parameter $m = m_d m_o$ has been changed to m_s as before to avoid confusion with the notation of the grid point (m,n) (see Fig. B-1(a)).

Note that in the rate equation approximation, no finite difference equation is needed for the calculations of the polarization since in this case it is directly related to the field and the inversion by the first equation of either (C-2) (amplifier) or (C-3) (absorber). Further, the phase coherence times (T_2 and T_2') enter the laser dynamical equations (C-2) and (C-3) just as proportionality constants which are related to the cross sections of the active media. As a consequence, the size of the time increment (Δt) to be used in the pulse propagation simulation is no longer restricted by the values of T_2 and T_2'. Accordingly, by employing the FDE's developed here, a large amount of computer time can be saved especially when T_2, $T_2' << L/c$ and the spatial extent of the field distributions is comparable to the cavity length (L). Therefore, these propagation equations are most useful when the steady-state pulse solutions are generated from CW or quasi-CW field distributions as is the

situation assumed in Chapter 5, where the relationship of the establishment time of the SSP with the laser gain and absorber characteristics in flashlamp-pumped dye lasers is investigated.

Finally, for some laser systems, the low signal gain and/or saturable loss may be time-dependent. The pulsed-gain lasers are good examples for which the laser gain usually follows the intensity variation of the pumping pulse. Another typical example is the Rhodamine 6G dye laser for which the saturable loss of the absorber (DODCI) is varying during the build-up of the mode-locked pulses due to the formation of a photoisomer. Accordingly, it is useful to incorporate the effects of time-dependence in the laser gain and loss into the propagation equations. For the case of time-varying loss (as discussed in Chapter 5), it can be shown that an extra term given by

$$b_8 = -\frac{1}{2}\gamma_{||}^{*}(\Delta t)^2\left(\frac{\Delta a_o}{\Delta t}\right) \qquad \text{(C-12)}$$

should be added to Eqs. (C-8) and (C-8') and those coefficients in the FDE's which involve the quantity a_o are no more constants as a_o (proportional to the low signal loss) is a function of time in this case. The quantity $(\Delta a_o/\Delta t)$ in Eq. (C-12) can be calculated by

$$\frac{\Delta a_o}{\Delta t} \approx \frac{a_o(t+\Delta t)-a_o(t)}{\Delta t} \qquad \text{(C-13)}$$

at any instant of time t provided that Δt is sufficiently small. Obviously, such a treatment can be generalized to the situation for which both the saturable gain and loss are time-dependent and can also be employed in the propagation equations of Appendix B. However, such a generalization is not attempted here since it is

of

APPENDIX D

THE PULSE COMPRESSION MODEL

The pulse compression model due to New[46,47] has been introduced in Chapter 4. In this appendix, the essence of the analysis will be described in somewhat more detail, starting with the general formulation, followed by the composite medium model and ending up with the discrete model for which propagation equations appropriate for a ring cavity are given.

(1) General Formulation:

Consider pulse propagation in an amplifying medium. The general rate equations are*

$$\left(\frac{\partial}{\partial x} + \frac{1}{c}\frac{\partial}{\partial t}\right)\rho = n_a \sigma_a \rho$$
$$\frac{\partial n_a}{\partial t} = \frac{n_{ao} - n_a}{T_{1a}} - n_a \sigma_a \rho \qquad \text{(D-1)}$$

where ρ is the photon flux, c the phase velocity of light, n_a the population inversion, σ_a the stimulated emission cross-section, n_{ao} is the value of n_a when $\rho = 0$ and T_{1a} is the recovery time of the medium.

Define the new coordinates

$$x' = x \quad \text{and} \quad \tau = t - x/c \ , \qquad \text{(D-2)}$$

where τ is known as the local time. Equation (D-1) can then be

*The factor of 2 that should be included in the final term of the second equation for a two-level system has been omitted for simplicity since it can be regarded as a scaling factor for the photon flux ρ. In other words, for a two-level system, the value of ρ in (D-1) is twice of the actual photon flux.

transformed to

$$\frac{\partial \rho}{\partial \xi} = n_a \sigma_a \rho$$
$$\frac{\partial n_a}{\partial \tau} = \frac{n_{ao} - n_a}{T_{1a}} - n_a \sigma_a \rho. \qquad \text{(D-3)}$$

Further, assume that T_{1a} >> pulse duration, or more precisely that $|(n_{ao}-n_a)/T_{1a}| << |n_a \sigma_a \rho|$, then the second equation of (D-3) can be solved to give

$$n_a(\tau,x') = n_{ai}(x') \exp(-\sigma_a J(\tau,x')) \qquad \text{(D-4)}$$

where

$$J(\tau,x') = \int_{-\infty}^{\tau} \rho(\tilde{t},x') d\tilde{t} \qquad \text{(D-5)}$$

and

$$n_{ai}(x') = n_a(-\infty,x') \qquad \text{(D-6)}$$

with $\tau = -\infty$ denoting the leading edge of the pulse. From (D-5), it is obvious that $J(-\infty,x') = 0$. Now, using (D-4) in the first equation of (D-3), we have

$$\frac{1}{\rho} \frac{\partial \rho}{\partial x'} = n_{ai}(x') \sigma_a \exp(-\sigma_a J(\tau,x')). \qquad \text{(D-7)}$$

and in particular, for the leading edge

$$\frac{1}{\rho(-\infty)} \frac{\partial \rho(-\infty)}{\partial x'} = n_{ai}(x') \sigma_a \qquad \text{(D-8)}$$

since $J(-\infty) = 0$; similarly, for the trailing edge

$$\frac{1}{\rho(\infty)} \frac{\partial \rho(\infty)}{\partial x'} = n_{ai}(x') \sigma_a \exp(-\sigma_a J_\infty(x')) \qquad \text{(D-9)}$$

with $J_\infty(x') \equiv J(+\infty,x')$.

By definition, the gain factors at the leading (g_L) and trailing (g_T) edges for a medium of thickness d are thus given by

$$g_L \equiv \frac{\rho(-\infty,d)}{\rho(-\infty,o)} = \exp(n_{ai}\sigma_a d) \qquad \text{(D-10)}$$

$$g_T \equiv \frac{\rho(\infty,d)}{\rho(\infty,o)} = \exp\left[n_{ai}\sigma_a \int_o^d \exp(-\sigma_a J_\infty(x'))dx'\right] \qquad \text{(D-11)}$$

where it has been assumed that n_{ai} is not a function of x'. Consequently, if we can solve for the pulse energy $J_\infty(x')$, we are able to calculate g_T, the gain for the trailing edge.

Using the definition of $J(\tau,x')$ (Eq. (D-5)), Eq. (D-7) can be transformed to

$$\left(\frac{\partial j}{\partial x}_\tau\right) = \int_o^j G(j)\, dj \qquad \text{(D-12)}$$

where

$$j(\tau,x') = \sigma_a J(\tau,x') \qquad \text{(D-13)}$$

$$G(j) = \sigma_a n_{ai} \exp(-j). \qquad \text{(D-14)}$$

The solution of Eq. (D-12) can be shown to be

$$j(\tau,x') = \ln\{1+\exp(n_{ai}\sigma_a x')[\exp(j(\tau,o))-1]\}. \qquad \text{(D-15)}$$

where as before n_{ai} is assumed to be independent of x'. The gain factor g_T can now be calculated by using (D-15) (with $\tau=\infty$) in (D-11) and performing the integration. The final result is given by

$$g_T = g_L \exp[j_i(\infty)-j_f(\infty)] \qquad \text{(D-16)}$$

where j_i and j_f are defined by

$$j_i(\tau) = j(\tau,o) \tag{D-17}$$

$$j_f(\tau) = j(\tau,d) = \ell n[1+g_L[\exp(j_i(\tau))-1]]. \tag{D-18}$$

In general, for any local time τ, the gain factor is

$$g(\tau) = g_L \exp[j_i(\tau)-j_f(\tau)] \tag{D-19}$$

from which the values of the gain factors for the leading and trailing edges follow as $g_L = g(\tau = -\infty)$ and $g_T = g(\tau = \infty)$.

Equations (D-10), (D-16) (or more generally (D-19)), (D-17) and (D-18) are the main results of the analysis. Clearly, the above analysis applies to the loss medium as well provided that we employ n_b, n_{bo}, σ_b ahd n_{bi} instead of the corresponding variables for the gain medium and also assume T_{1b} >> pulse duration. Furthermore, by the definition of $j(\tau,x')$ (Eq. (D-13)), the corresponding pulse energy for the loss medium should be defined as

$$j_b(\tau,x') = sj(\tau,x') \tag{D-20}$$

where the parameter $s = \sigma_b/\sigma_a$ is just the ratio of the cross-sections. However, the definition of s can be generalised to include other effects such as that due to the change of laser beam sizes in the gain and loss media. Consequently, we have a general expression

$$s = k\left(\frac{\sigma_b}{\sigma_a}\right)\left(\frac{A_a}{A_b}\right) \tag{D-21}$$

where k is a parameter depending on the relative positions of the gain and loss cells in the cavity and A_a/A_b is the ratio

of the beam areas. For a normal-type cavity with the gain cell sitting at the center and the loss cell in contact with one mirror, k = 2. On the other hand, for a ring laser, k = 1 always since in this case the relative positions of the two cells do not affect the ratio of the effective cross-sections of the active media. Accordingly, the parameter s can be related to the parameter m (Table 2-1) employed in our model by

$$s = m^2/\gamma_2 \qquad \text{(D-22)}$$

since $\sigma_b/\sigma_a = \mu_b^2 T_2'/\mu_a^2 T_2 = m_d^2/\gamma_2$ and $A_a/A_b = m_o^2$.

For clarity, from now on, the gain factor $g(\tau)$ will be written as $\alpha(\tau)$ and $\beta(\tau)$ for the gain and loss media respectively. Accordingly, $\alpha(-\infty)$ or $\beta(-\infty)$ means g_L, and $\alpha(\infty)$ or $\beta(\infty)$ means g_T. The symbol g will be used for the overall gain factor per round trip.

(2) The Composite Medium Model:

In this simple model, the gain and the loss media as well as the linear losses are all assumed to be uniformly distributed in a single cell of thickness d, situated at the center of the cavity formed by two 100%-reflecting mirrors (Fig. D-1(a)). In this case, the propagation of the pulse in the composite medium is described by the equation

$$\left(\frac{\partial \rho}{\partial x}\right)_\tau = (A-B-\Gamma)\rho \equiv G\rho \qquad \text{(D-23)}$$

where $A = n_a\sigma_a$, $B = -n_b\sigma_b$ and Γ is an absorption coefficient associated with the linear losses (γ). The overall unsaturated

Fig. D-1. (a) The composite medium model with the composite medium situated at the center of a normal resonator formed by two 100%-reflecting mirrors M_1 and M_2. The low signal gain and loss coefficients per pass are, respectively, A_o and B_o for the composite medium and the linear loss coefficient is Γ (Eq. (D-24)). The optical length of the resonator is $L_n = (1/2)cT_{RT}$.

(b) The composite medium model employing a ring cavity formed by three 100%-reflecting mirrors M_1, M_2 and M_3. In this case, the low signal gain and loss coefficients of the composite medium are $2A_o$ and $2B_o$ respectively, and the linear loss coefficient is 2Γ. The cavity length $L = cT_{RT}$ which is twice of L_n in case (a).

(c) The discrete model employing a ring cavity formed by three partially reflecting mirrors M_1, M_2 and M_3 which can be represented by a single mirror M with an equivalent reflectivity R in theoretical analysis. The amplifier and absorber are assumed to be infinitesmally thin slabs with low signal gain and loss coefficients $2A_o$ and $2B_o$ respectively which are equivalent to the quantities $\alpha_a L_a$ and $\alpha_b L_b$ (see Table 2-1) employed in our model of saturable absorber mode-locking. The points marked by 1 and 2 (2 and 3) denote respectively the input and output sections of the amplifier (absorber). The output section of the amplifier and the input section of the absorber have been labelled by the same letter 2 since no ambiguity can arise in the

of

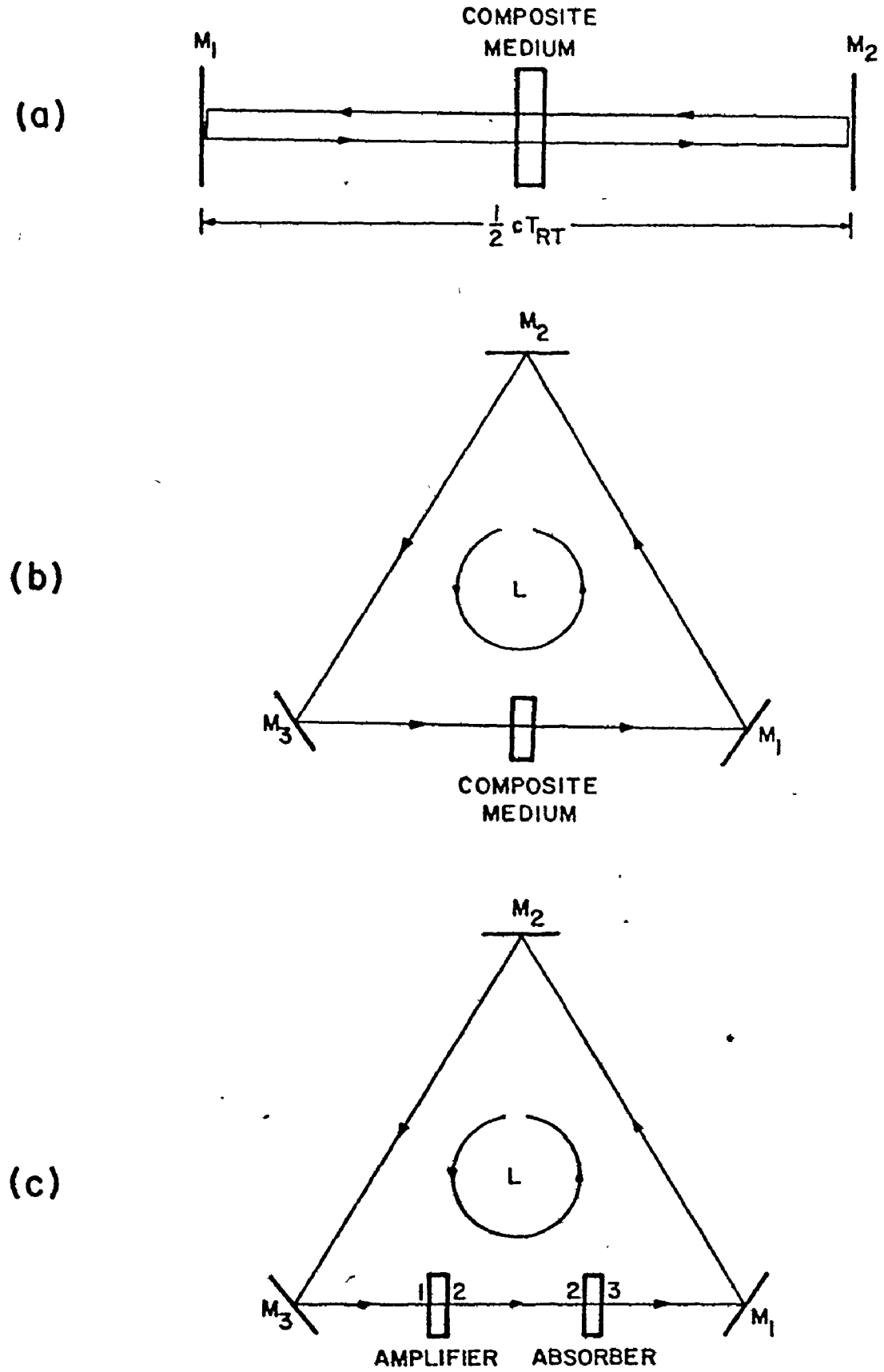
(a)
COMPOSITE
MEDIUM
M1
M2
½ cTRT
(b)
M2
L
M3
M1
COMPOSITE
MEDIUM
(c)
M2
L
M3
1
2
2
3
M1
AMPLIFIER
ABSORBER

Fig. D-1

gain factor per round trip is given by

$$g_o = \alpha_o \beta_o \gamma = \exp[2(A_o - B_o - \Gamma)] \qquad \text{(D-24)}$$

where d has been set to unity and the subscript zero denotes low signal values. Note that the laser threshold is defined by

$$g_{o,th} = 1. \qquad \text{(D-25)}$$

Following the same procedure used in the transformation of Eq. (D-7) into (D-12), we obtain an equation of motion for the pulse energy from Eq. (D-23), namely

$$\left(\frac{\partial j}{\partial x'}\right)_\tau = \int_o^{j(\tau)} G(j')dj' \equiv I(j) \qquad \text{(D-26)}$$

with G(j) given by

$$G(j) = A_i \exp(-j) - B_o \exp(-sj) - \Gamma. \qquad \text{(D-27)}$$

Here, $A_i = A(\tau = -\infty)$ which is assumed to be less than A_o as a result of the incomplete recovery of the gain medium between successive pulse transits. On the other hand, the absorption coefficient at the leading edge is taken to be just the low signal value B_o which follows from the assumption that $T_{1b} << \frac{1}{2} T_{RT}$.

The equilibrium state in which the total pulse energy j_∞ maintains the same value everywhere in the cavity is defined by the following two conditions:

(i) The amplification coefficient A_i must be the same before every pulse transit, that is, the final value $A_i \exp(-j_\infty)$ should recover to exactly A_i in the time interval $(1/2)T_{RT}$ according to the configuration of Fig. D-1(a).

(ii) The total pulse energy j_∞ must remain constant as the pulse propagates through the composite medium.

From the first condition, the equilibrium value of A_i can be found by solving the second equation of (D-3) with $\rho = 0$ and imposing the assumption that $T_{RT} >>$ pulse duration. The result is given by

$$A_{ie}(j_\infty) = \frac{A_o(1-E)}{1-E\exp(-j_\infty)} \qquad \text{(D-28)}$$

where

$$E = \exp(-\frac{1}{2}\xi) \qquad \text{(D-29)}$$

with $\xi = T_{RT}/T_{la}$ for a normal cavity as shown in Fig. D-1(a).

From equation (D-26), it is evident that the second requirement for the equilibrium state is just $I(j_\infty) = 0$. Therefore, by performing the integration in (D-26) with A_{ie} substituted for A_i in the expression of $G(j')$, we obtain

$$A_{ie}(j_\infty) - H(j_\infty) = 0 \qquad \text{(D-30)}$$

where

$$H(j_\infty) = \frac{B_o s^{-1}[1-\exp(-sj_\infty)]+\Gamma j_\infty}{[1-\exp(-j_\infty)]} . \qquad \text{(D-31)}$$

The value of j_∞ can be solved from (D-30) for a given set of laser parameters and the gain factor per round trip $g(j)=\exp(2G(j$ can be calculated from the value of $G(j)$ given by

$$G(j) = A_{ie}(j_\infty)\exp(-j)-B_o\exp(-sj)-\Gamma. \qquad \text{(D-32)}$$

Clearly, the gain factors on the leading and trailing edges per round trip can be computed from

$$g_L = \exp[2G(0)] \qquad \text{(D-33)}$$

$$g_T = \exp[2G(j_\infty)]. \qquad \text{(D-34)}$$

In particular, the boundaries of the pulse compression region are defined by $g_L = 1$ and $g_T = 1$. Consequently, it follows from (D-30) and (D-32) that the pulse compression region can be determined by solving the following two equations, with $H(j_\infty)$ defined by (D-31),

$$H(j_\infty) - B_o - \Gamma = 0 \qquad \text{(D-35)}$$

$$H(j_\infty)\exp(-j_\infty) - B_o\exp(-sj_\infty) - \Gamma = 0. \qquad \text{(D-36)}$$

Furthermore, the overall unsaturated gain factor (g_o) can be calculated from

$$\ell n\, g_o = 2\{\frac{H(j_\infty)[1-E\exp(-j_\infty)]}{(1-E)} - B_o - \Gamma\} \qquad \text{(D-37)}$$

which follows from (D-24), (D-28) and (D-30).

Observe that Eqs. (D-35) and (D-36) are suitable for the determination of pulse compression regions for given values of B_o, Γ, ξ and s with A_o (and hence g_o) treated as a variable parameter. To make comparison with our theory (Chapter 2), it is preferable to permit the linear cavity loss (Γ) to vary at given values of A_o, B_o, ξ and s. Therefore, it is necessary to rewrite Eqs. (D-35) and (D-36).

For the condition $g_L = 1$, it can be shown by solving Γ from (D-32) (with j=0) and substituting back into (D-30), that the following equation must hold

$$F_L(j_\infty) = [1-j_\infty-\exp(-j_\infty)]A_{ie}(j_\infty)-B_o s^{-1}[1-sj_\infty-\exp(-sj_\infty)] = 0 \qquad \text{(D-38}$$

which is Eq. (4-4). Similarly, for unity gain on the trailing ed (g_T=1), it follows by solving Γ from (D-32) (with $j = j_\infty$ this tim

and substituting into (D-30) that

$$F_T(j_\infty) = [1-(1+j_\infty)\exp(-j_\infty)]A_{ie}(j_\infty)-B_o S^{-1}[1-(1+sj_\infty)\exp(-sj_\infty)]=0 \quad (D-$$

which is Eq. (4-6).

Furthermore, for a ring laser cavity (Fig. D-1(b)), all the equations derived in this section are still valid except that the time interval between successive transits of the pulse through the composite medium is T_{RT} rather than $(1/2)T_{RT}$. Accordingly, $E = \exp(-T_{RT}/T_{1a})$ for ring cavity and ξ should be given by $\xi = 2T_{RT}/T_{1a}$ if we retain the definition of $E = \exp(-\xi/2)$ given by (D-29).

In addition, the assumption that $T_{1b} << T_{RT}$ for the recovery time T_{1b} of the absorber can be omitted by substituting

$$B_{ie}(j_\infty) = \frac{B_o(1-E')}{1-E'\exp(-sj_\infty)} \qquad (D-40)$$

for B_o in all relevant equations with E' given by

$$E' = \exp(-T_{RT}/T_{1b}) \qquad (D-41)$$

for a ring cavity (or $E' = \exp(-T_{RT}/2T_{1b})$ for a normal cavity). Note that Eq. (D-40) is the counterpart of (D-28) for the absorbe

(3) The Discrete Model:

In this model, discrete components are assumed for the gain and loss cells and also for the linear losses. In the original analysis given by New[47], a normal laser resonator is employed. For convenience, a ring cavity is used here as shown in Fig. D-1(c), which is the same as that employed in our model (see Fig. 2-1) except that the gain and loss cells are assumed (implicitly) to be infinitesmally thin slabs in the present situation.

The analysis presented in the first part of this appendix can be applied directly to describe the response of the gain and loss media to a propagating pulse. Accordingly, the equations of motion for a pulse circulating around inside the cavity and with constant (normalized) energy can be written down immediately by using Eqs.(D-18) and (D-19) and noting that the gain (or loss) factor of an active medium is defined as the ratio of the photon flux at the output and input sections. According to the configuration of Fig. D-1(c), the complete set of equations for one round trip are given below:

A. Transit 1-2 (gain cell): Amplification

Energy increase: $j_2(\tau) = \ell n\{1+\alpha_{12}(-\infty)[\exp(j_1(\tau))-1]\}$ (D-42)

Profile amplification: $\rho_2(\tau) = \rho_1(\tau)\alpha_{12}(-\infty)\exp[j_1(\tau)-j_2(\tau)]$ (D-

B. Transit 2-3 (loss cell): Absorption

Energy decrease: $sj_3(\tau) = \ell n\{1+\beta_o[\exp(sj_2(\tau))-1]\}$ (D-44)

Profile absorption: $\rho_3(\tau) = \rho_2(\tau)\beta_o\exp[sj_2(\tau)-sj_3(\tau)]$ (D-45)

C. Transit 3-1 (cavity mirrors): Linear Losses

Energy decrease: $j_1(\tau) = Rj_3(\tau)$ (D-46)

Profile absorption: $\rho_1(\tau) = R\rho_3(\tau)$. (D-47)

Note that in (D-42) and (D-43), $\alpha_{12}(-\infty)$ is the amplification factor of the gain medium on the leading edge ($\tau = -\infty$) of the pulse. On the other hand, for simplicity, we have used β_o (the low signal absorption factor) instead of $\beta_{23}(-\infty)$ by assuming that $T_{1b} << T_{RT}$ for the absorber.

In addition to Eqs. (D-42) to (D-47), the recovery of the gain medium in the time interval between successive pulse

transits can be represented by the following equation:

$$\ell n[\alpha_{12}(-\infty)] = \ell n(\alpha_o)(1-E) + E\,\ell n[\alpha_{12}(+\infty)] \qquad \text{(D-48)}$$

with $E = \exp(-T_{RT}/T_{1a})$ and $\alpha_{12}(+\infty) = \rho_2(\infty)/\rho_1(\infty)$ (Eqs. (D-43) with $\tau = \infty$). Note that (D-48) is obtained by solving the second equation of (D-3) with $\rho = 0$ and assuming that the quantities $\ell n[\alpha_{12}(-\infty)]$ and $\ell n[\alpha_{12}(+\infty)]$ are, respectively, proportional to the <u>average</u> population inversions in the slab before and after the pulse transit 1-2. Accordingly, equation (D-48) is analogous to (D-28) which describes the recovery of the gain in the composite medium. However, it should be noted that the averaging processes involved in these two equations are quite different since only the <u>average</u> pulse energy j_∞ is accounted for in the composite medium model whereas pulse energies at the input ($j_1(\infty)$) and output ($j_2(\infty)$) sections are involved in the discrete model. As a consequence, although the difference in the overall gain factors per round trip found by these two models may not be very significant, the pulse compression regions so determined could be very different, particularly in low-gain and low-loss systems operated close to threshold for which the overall gain factor is always close to unity.

In the present model, it can be shown from (D-43), (D-45) and (D-47) that the overall gain factor per round trip is given

$$g(\tau) = \alpha_{12}(-\infty)\beta_o R \exp[j_1(\tau)+(s-1)j_2(\tau)-sj_3(\tau)] \qquad \text{(D-49)}$$

where we have used the relation $g(\tau) = \alpha(\tau)\beta(\tau)R$. From this

equation the gain factors on the leading (g_L) and trailing (g_T) edges can be calculated from

$$g_L = g(-\infty) = \alpha_{12}(-\infty)\beta_o R \qquad \text{(D-50)}$$

$$g_T = g(+\infty) = g_L \exp[j_1(\infty)+(s-1)j_2(\infty)-sj_3(\infty)] \qquad \text{(D-51)}$$

and the boundaries of the pulse compression region can be determined by solving these two equations with $g_L = 1$ and $g_T = 1$. Note that the second equation is a generalization of (D-16) which is for a single medium.

In actual calculations, for a given set of laser parameters, the values of $j_1(\infty)$ and $\alpha_{12}(-\infty)$ (and hence $j_2(\infty)$ and $j_3(\infty)$) can be solved iteratively from the system of equations (D-42)-(D-48) with $\tau = \infty$. The overall gain factors g_L and g_T are then calculated from (D-50) and (D-51) respectively, and the region over which both g_L and g_T are less than unity defines the pulse compression region. Such a procedure is, in a sense, analogous to that in solving the characteristic equations (2-65) for which the region of $\beta_r > 0$ defines the mode-locking regime. Furthermore, once $j_1(\infty)$ and $\alpha_{12}(-\infty)$ have been determined, the propagation equations (D-42) to (D-47) can be employed to investigate the evolution of the pulse profile starting with an initial pulse envelope such that the total area under the envelope in τ-space is just equal to $j_1(\infty)$ at the input section of the amplifier. Observe that, in this way, only the <u>relative</u> narrowing or broadening of the pulse shape with respect to the temporal width of the initial envelope can be studied and <u>no</u> steady-state pulse solution can be generated. This is a natural consequence of

using the integrated photon flux (pulse energy) in the analysis of pulse propagation because in this type of approach the dependence of the interactions between the active media and the radiation on the structure (shape) of the laser pulse has been implicitly neglected.

APPENDIX E

THE RATE EQUATION APPROACH TO LASER PULSATION

In this appendix, the time-invariant solutions and the dispersion equations for the rate equation models described in Chapter 6 are derived.

(I) Rate Equation Formalism, including Spatial Variation of the Dynamical Variables:

(1) Time-Invariant (CW) Solutions:

For the time-invariant solutions, we have

$$\frac{\partial \bar{D}}{\partial t'} = 0 \quad \text{and} \quad \frac{\partial \bar{I}}{\partial t'} = 0 \tag{E-1}$$

for both the gain and the loss media. The CW intensities must satisfy the boundary conditions

$$\begin{aligned} \bar{I}_1 &= R\bar{I}_4/m^2 \\ \bar{I}_2 &= \bar{I}_3/m^2 \end{aligned} \tag{E-2}$$

where we have abbreviated $\bar{I}(x_i')$ by $\bar{I}_i$, $i = 1,2,3,4$. Note that the bar on top of the variables $\bar{D}$ and $\bar{I}$ denotes that they are time independent.

Substitution of Eq. (E-1) into Eqs. (6-2) and (6-3) gives

$$(\bar{P} = \bar{D}\,\bar{E})$$

$$\begin{aligned} \bar{D} &= \gamma/(\gamma + \bar{I}) \ , \quad x_1' \le x' \le x_2' \\ \frac{d\bar{I}}{dx'} &= \frac{2G_a\gamma\bar{I}}{\gamma + \bar{I}} \end{aligned} \tag{E-3}$$

$$(\bar{P} = \bar{D}\,\bar{E}/\gamma_2)$$

$$\bar{D} = -\gamma' a_o/(\gamma' + \bar{I}/\gamma_2)\ ,\quad x_3' \le x' \le x_4' \qquad \text{(E-4)}$$

$$\frac{d\bar{I}}{dx'} = \frac{2G_b\gamma_b a_o \bar{I}}{\gamma' + \bar{I}/\gamma_2}$$

where $\gamma_b = T_2'/T_1'$. For simplicity, the subscripts a and b for the variables D, P and I have been dropped.

It is straightforward to show that the solutions to the third equations of (E-3) and (E-4) can be put into the final forms

$$\ell n(\bar{I}_2/\bar{I}_1) + (\bar{I}_2-\bar{I}_1)/\gamma = \alpha_a L_a$$
$$\ell n(\bar{I}_4/\bar{I}_3) + (\bar{I}_4-\bar{I}_3)/\gamma'\gamma_2 = -\alpha_b L_b \qquad \text{(E-5)}$$

where $\alpha_a L_a = 2G_a L_a/cT_2$ and $\alpha_b L_b = 2G_b a_o L_b/\gamma_2 cT_2$ are, respectively, the low-signal intensity gain and loss per round trip in the two media.

Solving for $\bar{I}_2$ from (E-5), using the boundary conditions (E-2), we obtain

$$\bar{I}_2 = [(1/R\gamma_2'-\gamma_1)\bar{I}_1+\gamma'\lambda\ell n(R)]/(1/\gamma_2'-\gamma_1) \qquad \text{(E-6)}$$

where $\gamma_1' = T_1/T_1'$ and λ is defined by (see Table 2-1)

$$\lambda = (\alpha_a L_a - \alpha_b L_b)/\ell n(R^{-1}) - 1 \qquad \text{(E-7)}$$

which is known as the pump parameter. Observe that the CW solutions given here are identical with those given for the general model (see section 2.3).

(2) Perturbation Analysis - The Dispersion Equations:

As in the treatment of the general model, we assume small variations in the variables I and D about the CW solutions namely

$$I = \bar{I} + i \quad , \quad D = \bar{D} + \delta. \tag{E-8}$$

Substitution of Eq. (E-8) into Eqs. (6-2) and (6-3), and omission of second order terms in the small variations gives

$$\frac{\partial \delta}{\partial t'} = -(\bar{I} + \gamma)\delta - \bar{D}i \qquad (x_1' \le x' \le x_2') \tag{E-9}$$

$$\frac{\partial i}{\partial x'} + \frac{\partial i}{\partial t'} = 2G_a(\bar{D}i + \bar{I}\delta)$$

and

$$\frac{\partial \delta}{\partial t'} = -(\gamma' + \bar{I}/\gamma_2)\delta - \bar{D}i/\gamma_2 \qquad (x_3' \le x' \le x_4') \tag{E-10}$$

$$\frac{\partial i}{\partial x'} + \frac{\partial i}{\partial t'} = \frac{2G_b}{\gamma_2}(\bar{D}i + \bar{I}\delta).$$

To solve these equations, we assume that the time and spatial dependences of the small variations can be separated an represented in the form

$$f(x',t') = f_o(x')\exp(\beta t') \tag{E-11}$$

with f standing for i or δ, and $\beta = \beta_r + i\beta_i$ is to be determine It can be shown that the amplitude $i_o(x')$ must satisfy

$$\begin{aligned} m^2 i_o(x_2') &= i_o(x_3')\exp(\beta\Delta_{23}) \\ m^2 i_o(x_1') &= R\, i_o(x_4')\exp(-\beta\Delta_{41}) \end{aligned} \tag{E-12}$$

which are similar to Eqs. (2-64).

Equations (E-9) and (E-10) with the aid of (E-11) can be solved exactly for $i_o(x')$. The dispersion equations for β are then derived when the boundary conditions (E-12) are applied. It can be shown that β must satisfy

$$\ell n\left[\frac{\beta+\gamma+\bar{I}_2}{\beta+\gamma+\bar{I}_1}\right] + \ell n\left[\frac{\beta+\gamma'+\bar{I}_4/\gamma_2}{\beta+\gamma'+\bar{I}_3/\gamma_2}\right] + \beta L' = 0. \qquad \text{(E-13)}$$

Substitution of $\beta = \beta_r + i\beta_i$ into (E-13) and grouping the real and imaginary parts, we obtain Eqs. (6-12) of the main text.

It is appropriate to point out here that if the functional form of the perturbations is taken to be

$$f(x',t') = f_o(x')\exp(i\alpha x'+\beta t') \qquad \text{(E-11')}$$

rather than that of Eq. (E-11) and with $\alpha = \alpha_n = 2n\pi/L'$ as in the case of the general model (see Eq. (2-61)), the rate equation model can also be employed, although less generally, to study the mode-locking-type instabilities. In this case, an extra term $i\alpha L'$ will appear in (E-13) and consequently, a term $\alpha L'$ should be included in the second equation of (6-12).

A necessary condition under which the rate equation approach can be used to investigate mode-locking-type instability is that <u>both</u> T_2 and T_2' should be much less than the cavity length. Under this circumstance, the instability regions generated in this case are expected to be in close agreement with those found from the general model.

(II) Rate Equation Formalism, omitting Spatial Dependence of the Dynamical Variables

(1) Time-Invariant Solutions:

In this case, we have both $\partial\bar{D}/\partial t'$ and $\partial\bar{I}/\partial t'$ equal to zero. However, no boundary condition is required since the spatial dependence of the dynamical variables has been omitted. Consequently, it follows from Eq. (6-5) that the CW solutions are given by

$$\begin{aligned} \bar{D}_a &= \gamma/(\gamma + \bar{I}) \\ \bar{D}_b &= -a_o\gamma'/(\gamma'+\bar{I}/\gamma_2') \\ (\tilde{G}_a\bar{D}_a &+ \tilde{G}_b\bar{D}_b - \gamma_c')\,\bar{I} = 0. \end{aligned} \qquad \text{(E-14)}$$

Observe that the third equation of (E-14) has a trivial solution $\bar{I} = 0$. For non-zero intensity, which is of interest to us, we have

$$\tilde{G}_a\bar{D}_a + \tilde{G}_b\bar{D}_b - \gamma_c' = 0 \qquad \text{(E-15)}$$

which can be solved analytically for $\bar{I}$ when the laser parameters are given.

(2) Stability of the CW Solutions:

Following the procedure in the previous section, we assume that

$$D_a = \bar{D}_a + \delta_a, \quad D_b = \bar{D}_b + \delta_b \text{ and } I = \bar{I} + i. \qquad \text{(E-16)}$$

Substitution of (E-16) into Eq. (6-5) and retaining only the linear terms on the small perturbations, we obtain

$$\begin{aligned} \frac{d\delta_a}{dt'} &= -(\bar{I}+\gamma)\delta_a - \bar{D}_a i \\ \frac{d\delta_b}{dt'} &= -(\gamma'+I/\gamma_2')\delta_b - D_b i/\gamma_2' \end{aligned} \qquad \text{(E-17)}$$

$$\frac{di}{dt} = \tilde{G}_a \bar{I}\delta_a + \tilde{G}_b \bar{I}\delta_b \,.$$

Assume the functional form

$$f(t') = f_o \exp(\beta t') \qquad \text{(E-18)}$$

for δ_a, δ_b and i with f_o being a constant and $\beta = \beta_r + i\beta_i$ as before. Using (E-18) in (E-17) we have the following equations

$$\begin{aligned} &(\beta + \gamma + \bar{I})\delta_{ao} + \bar{D}_a i_o = 0 \\ &(\beta + \gamma' + \bar{I}/\gamma_2')\delta_{bo} + \bar{D}_b i_o = 0 \qquad \text{(E-19)} \\ &\tilde{G}_a \bar{I}\delta_{ao} + \tilde{G}_b \bar{I}\delta_{bo} - \beta i_o = 0. \end{aligned}$$

The determinant condition on the coefficients of (E-19) for non-zero solutions of δ_{ao}, δ_{bo} and i_o yields a cubic equation for β

$$\beta^3 + (p+q)\beta^2 + [pq + (u+v)\bar{I}]\beta + (uq+vp)\bar{I} = 0 \qquad \text{(E-20)}$$

where

$$\begin{aligned} &p = \gamma/\bar{D}_a \,, \quad q = -a_o\gamma'/\bar{D}_b, \\ &u = \tilde{G}_a\bar{D}_a \,, \quad v = \tilde{G}_b\bar{D}_b/\gamma_2' \,. \end{aligned} \qquad \text{(E-21)}$$

Equations (6-7) follow from (E-20) when $\beta = \beta_r + i\beta_i$ is substituded and the real and imaginary parts are grouped separately.

In particular, for $\beta_r = 0$, which defines the boundary of the instability regions, we have

$$\begin{aligned} &\beta_i^2 = pq + (u + v)\,\bar{I} \qquad \text{(E-22)} \\ &pq\,(p + q) + (pu + qv)\bar{I} = 0. \end{aligned}$$

A careful examination of the second equation above reveals that the value of $\bar{I}$ can be solved analytically since it is a cubic equation in $\bar{I}$, namely

$$\bar{I}^3 + a_2\bar{I}^2 + a_1\bar{I} + a_o = 0 \qquad \text{(E-23)}$$

where

$$\begin{aligned} a_o &= v_1 v_2 v_4 \\ a_1 &= v_1 + v_2 v_3 v_4 + (\tilde{G}_a v_o - \tilde{G}_b a_o v_1 / v_o) v_4 \\ a_2 &= v_3 + v_2 v_4 \end{aligned} \qquad \text{(E-24)}$$

with

$$\begin{aligned} v_o &= \gamma\gamma_2' \,, \quad v_1 = \gamma\gamma'\gamma_2' \,, \quad v_2 = \gamma + \gamma' \\ v_3 &= \gamma + \gamma'\gamma_2' \,, \quad v_4 = \gamma_2'/(1 + \gamma_2') \,. \end{aligned} \qquad \text{(E-25)}$$

Observe that for a positive and real solution of $\bar{I}$ to Eq. (E-23), a necessary condition is

$$w = (y^3 + z^2) \leq 0 \qquad \text{(E-26)}$$

where

$$\begin{aligned} y &= \frac{1}{3} a_1 - \frac{1}{9} a_2^2 \,, \\ z &= \frac{1}{6} (a_1 a_2 - 3a_o) - \frac{1}{27} a_2^3 . \end{aligned} \qquad \text{(E-27)}$$

Equation (E-26) with the equaltiy sign can be solved for a_1 in terms of a_o and a_2. The solution for the particular case of $\gamma_1\gamma_2' = 1$ can be shown to be

$$a_1 = -\frac{15}{4}\gamma^2 = \gamma^2 \left[3 + \frac{\alpha_a L_a}{\gamma_1(1+\gamma_1)} (1 - \gamma_g\gamma_1^2) T_L\right] \qquad \text{(E-28)}$$

where $T_L = cT_1/L_{max}$. Equation (6-9) then follows from this relation.

REFERENCES

1. P. W. Smith, Proc. IEEE, 58, 1342 (1970), and references cited therein.
2. P. W. Smith, M. A. Duguay and E. P. Ippen, "Mode-Locking of Lasers", in Progress of Quantum Electronics, edited by J. H. Sanders and S. Stenholm (Pergamon, Oxford, 1974), vol. 3.
3. C.V. Shank and E. P. Ippen, "Mode-locking of Dye Lasers", in Dye Lasers edited by F. P. Schäfer (Springer-Verlag, Berlin, 1974), Chapter 3.
4. D. von der Linde, Appl. Phys. 2, 281 (1973).
5. D. J. Bradley, Opto-Elect., 6, 25 (1974), and references cited therein.
6. A. E. Siegman and D.J. Kuizenga, Opto-Elect., 6, 43 (1974).
7. A. Dienes, Opto-Elect., 6, 99 (1974).
8. H. Kogelnik and T. Li, Appl. Opt., 5, 1550 (1966).
9. S. E. Harris, Proc. IEEE, 54, 1401 (1966), and references cited therein.
10. V. I. Malyshev, A. S. Markin, A. V. Masalov and A. A. Sychev, Sov. Phys. JETP, 30, 453 (1970).
11. M. A. Duguay, J.W. Hansen and S. L. Shapiro, IEEE J. Quant. Elec., QE-6, 725 (1970).
12. V. S. Letokhov, Sov. Phys. JETP, 28, 1026 (1969).
13. P. W. Smith, IEEE J. Quant. Elect., QE-3, 627 (1967).
14. R. E. McClure, Appl. Phys. Lett., 7, 148 (1965).

15. T. Uchida and A. Ueki, IEEE J. Quan. Elect., QE-3, 17 (1967).

16. F. R. Nash, IEEE J. Quant. Elect., QE-3, 189 (1967).

17. J. Hirano and T. Kumura, Appl. Phys. Lett., 12, 196 (1968), also, IEEE J. Quant. Elect., QE-5, 219 (1969).

18. L. E. Hargrove, R. L. Fork and M. A. Pollack, Appl. Phys. Lett. 5, 4 (1964).

19. B. Ellis and A. K. Walton, "A Bibliography on Optical Modulators", Infrared Phys. E, 11, 85 (1971).

20. R. Targ and J. M. Yarborough, Appl. Phys. Lett. 12, 3 (1968).

21. T. Uchida, IEEE J. Quant. Elect., QE-1, 336 (1965).

22. A. Dienes, E. P. Ippen and C. V. Shank, Appl. Phys. Lett., 19, 258 (1971).

23. D. J. Kuizenga, Appl. Phys. Lett., 19, 260 (1971).

24. E. P. Ippen, C. V. Shank and A. Dienes, Appl. Phys. Lett., 21, 348 (1972).

25. F. O'Neill, Opt. Comm., 6, 360 (1972).

26. W. E. Lamb, Jr., Phys. Rev., 134, A1429 (1964).

27. (a) M. Sargent III, IEEE J. Quant. Elect., QE-4, 346 (1968); (b) L. Allen and D.G.C. Jones, in Progress in Optics, edited by E. Wolf, (North-Holland, Amsterdam, 1971), vol. 9, and references cited therein.

28. O.P.McDuff and S. E. Harris, IEEE J. Quant. Elect., QE-3, 101 (1967).

29. A. G. Fox and P. W. Smith, Phys. Rev. Lett. 18, 826 (1967).

30. S. L. McCall and E. L. Hahn, Phys. Rev., 183, 457 (1969).

31. H. Risken and K. Nummedal, J. Appl. Phys., 39, 4662 (1968).

32. T. K. Lim and B. K. Garside, IEEE J. Quant. Elect., QE-8, 454 (1972).

33. J. A. Carruthers and T. Bieber, J. Appl. Phys., 40, 426 (1969).

34. B. K. Garside, IEEE J. Quant. Elect., QE-6, 471 (1970).

35. A. E. Siegman and D. J. Kuizenga, Appl. Phys. Lett., 14, 181 (1969).

36. D.J.Kuizenga and A. E. Siegman, IEEE J. Quant. Elect., QE-6, 694 (1970).

37. D.J. Kuizenga and A. E. Siegman, IEEE J. Quant. Elect., QE-6, 709 (1970).

38. (a) Ya. I. Khanin, Sov. Phys. JETP, 33, 694 (1971);
(b) J. Hobart, Coherent Radiation Inc., (unpublished).

39. P. W. Smith, T. J. Bridges, E. G. Burkhardt and O. R. Wood, Appl. Phys. Lett., 21, 470 (1972).

40. B. Ya. Zeldovich and T. I. Kuznetosva, Sov. Phys. Usp., 15, 25 (1972) and references cited therein.

41. V. S. Letokhov, Sov. Phys. JETP, 28, 562 (1969).

42. P.G. Kryukov and V. S. Letokhov, IEEE J. Quant. Elect., QE-8, 766 (1972).

43. J. A. Fleck, Phys. Rev. B, 1, 84 (1970).

44. B. Hausherr, E. Mathieu and H. Weber, IEEE J. Quant. Elect., QE-9, 445 (1973).

45. A. Caruso, R. Gratton and W. Seka, IEEE J. Quant. Elect., QE-9, 1039 (1973).

46. G. H. C. New, Opt. Comm., 6, 188 (1972).

47. G. H. C. New, IEEE J. Quant. Elect., QE-10,115 (1974).

48. E. G. Arthurs,D. J. Bradley and A. G. Roddie, Appl. Phys. Lett., 23, 88 (1973).

49. R. P. Feynman, F. L. Vernon and R. W. Hellwarth, J. Appl. Phys., 28, 49 (1957).

50. A. A. Vuylsteke, Elements of Maser Theory (D. Van Norstrand, Princeton, 1960), Chapters 4 and 5.

51. J. P. Wittke and P. J. Warter, J. Appl. Phys., 35, 1668 (1964).

52. M. Sargent III and M. O. Scully, in Laser Handbook, edited by F. T. Arecchi and E. O. Schultz-DuBois (North-Holland, Amsterdam, 1972), vol. I, Chapter A2.

53. W. E. Lamb, Jr., in Impact of Basic Research on Technology, edited by B. Kursunoglu and A. Perlmutter (Plenum, New York, 1973).

54. See, for example, C. P. Slichter, Principles of Paramagnetic Resonance, (Harper and Row, New York, 1963).

55. F. T. Arecchi and R. Bonifacio, IEEE J. Quant. Elect., QE-1, 169 (1965).

56. B. K. Garside, IEEE J. Quant. Elect., 4, 940 (1968).

57. T. K. Lim and B. K. Garside (unpublished).

58. J. A. Armstrong and E. Courtens, IEEE J. Quant. Elect., QE-4, 411 (1968).

59. R. A. Marth, D. A. Holmes and J. H. Eberly, Phys. Rev. A,9, 2733 (1974).

60. See, for example, A. Yariv, Quantum Electronics, (Wiley, New York, 1967).

61. B. K. Garside and T. K. Lim, J. Appl. Phys., 44, 2335 (1973).

62. See, for example, W. F. Ames, Nonlinear Partial Differential Equations in Engineering (Academic, New York, 1965).

63. A. G. Fox, S. E. Schwarz and P. W. Smith, Appl. Phys. Lett., 12, 371 (1968).

64. A. Frova, M. A. Duguay, C.G.B. Garrett and S. L. McCall, J. Appl., Phys. 40, 3968 (1969).

65. P. W. Smith, Opt. Comm., 2, 292 (1970).

66. P. W. Smith, J. Appl. Phys., 37, 2089 (1966).

67. P. K. Runge, Opt. Comm., 3, 434 (1971).

68. F. P. Schäfer, in Dye Lasers, edited by F. P. Schäfer (Springer-Verlag, Berlin, 1973).

69. O. G. Peterson, S. A. Tuccio and B. B. Snavely, Appl. Phys. Lett., 17, 245 (1970).

70. M. Herscher and H. A. Pike, Opt. Comm., 3, 65 (1971).

71. A. Dienes, E. P. Ippen and C. V. Shank, IEEE J. Quant. Elect., QE-8,388 (1972).

72. A. Dienes, E. P. Ippen and C. V. Shank (unpublished).

73. P. K. Runge, Opt. Comm., 4, 195 (1971).

74. P. K. Runge, Opt. Comm., 5, 311 (1972).

75. D. N. Dempster, T. Morrow, R. Rankie and G. F. Thompson, J. Chem. Soc. Faraday II, 68, 1479 (1972).

76. E. G. Arthurs, D. J. Bradley and A. G. Roddie, Chem. Phys. Lett., 22, 230 (1973).

77. E. G. Arthurs, D. J. Bradley and A. G. Roddie, Opt. Comm., 8, 118 (1973).

78. M. E. Mack, J. Appl. Phys., 39, 2483 (1968).

79. M. J. Weber and M. Bass, IEEE J. Quant. Elect., QE-5, 175 (1969).

80. M. Hercher, Appl. Opt., 6, 947 (1967).

81. J. P. Webb, W. C. McColgin, O. G. Peterson, D. L. Stockman and J. H. Eberly, J. Chem. Phys., 53, 4227 (1970).

82. M. Bass, T. F. Deutsch and M. J. Weber, in Lasers, edited by A. K. Levine and A. J. DeMaria (Marcel and Dekker, New York, 1971), vol. 3.

83. A. Yariv and J. P. Gordon, Proc. IEEE, 51, 4 (1963).

84. R. Bellman, G. Birnbaum and W. G. Wagner, J. Appl. Phys., 34, 780 (1963).

85. L. M. Frantz and J. S. Nodvik, J. Appl. Phys., 34, 2346 (1963).

86. T. K. Lim and B. K. Garside, Opt. Comm. (in press).

87. H. T. Powell and G.J. Wolga, IEEE J. Quant. Elect., QE-7, 213 (1971).

88. T. Ohmi and S. Yamazaki, IEEE J. Quant. Elect., QE-9, 366 (1973).

89. T. P. Lee and R.H.R. Roldan, IEEE J.Quant. Elect., QE-6, 339 (1970).

90. B. K. Garside and T. K. Lim, Opt. Comm., 8, 297 (1973).

91. B. K. Garside and T. K. Lim, Opt. Comm. (in press).